MODELING AND CONTROL OF WEB TRANSPORT IN THE PRESENCE OF NON-IDEAL ROLLERS

By

CARLO BRANCA

Laurea degree in Computer Engineering
Università di Roma "Tor Vergata"
Rome, Italy
2003

Master of Science in Electrical Engineering
Oklahoma State University
Stillwater, Oklahoma, USA
2005

Submitted to the Faculty of the
Graduate College of the
Oklahoma State University
in partial fulfillment of
the requirements for
the Degree of
DOCTOR OF PHILOSOPHY
MAY 2013

MODELING AND CONTROL OF WEB TRANSPORT
IN THE PRESENCE OF NON-IDEAL ROLLERS

Dissertation Approved:

Dr. Prabhakar R. Pagilla

Dissertation Adviser

Dr. Karl N. Reid

Dr. Gary E. Young

Dr. Martin Hagan

Name: CARLO BRANCA

Date of Degree: MAY 2013

Title of Study: MODELING AND CONTROL OF WEB TRANSPORT IN THE PRESENCE OF NON-IDEAL ROLLERS

Major Field: MECHANICAL AND AEROSPACE ENGINEERING

Abstract: In roll-to-roll processes the presence of non-ideal elements, such us out-of-round or eccentric rollers is fairly common. Periodic oscillations in web tension and web velocity are observed because of the presence of such non-ideal elements. Models of web transport on rollers based on the ideal behavior of various machine elements are not able to reproduce these oscillations in model simulations but can only follow the average of the measured tension and velocity signals. In order to reproduce the tension oscillations the models have to be modified to include the mechanism that creates the oscillations. The first part of this dissertation discusses the necessary modification of the governing equations of web velocity and web tension in the presence of an eccentric roller and an out-of-round roll. It was found that two aspects need to be included in the model: (i) the web span length adjacent to the non-ideal roller is varying with time and must be included in the governing equation for web span tension and (ii) the material flow rate in the web span, which is needed for deriving the governing equation for web tension, is not proportional to the peripheral velocity of the roller as in the ideal case and must be explicitly computed. An extensive set of experiments is presented to validate the proposed governing equations for web transport. The second part of the dissertation addresses the problem of designing a control algorithm for the attenuation of oscillations in the presence of a non-ideal roller. Besides stability, the controller needs to guarantee robustness to changing configurations and simplicity for real time implementation. An adaptive feed-forward control algorithm is identified as a suitable control algorithm for the attenuation of tension and velocity oscillations. The algorithm estimates amplitude and phase of the oscillations and generates a control input which compensates for the oscillations. Extensive experiments are conducted on a large web platform with different scenarios and by transporting two different web materials at various speeds. Experimental results show the effectiveness of the proposed algorithm to attenuate tension and velocity oscillations due to non-ideal rollers.

TABLE OF CONTENTS

LIST OF TABLES

Table Page

LIST OF FIGURES

Chapter 1

Introduction

Web processing is an important manufacturing activity because of its ability to mass produce products made from flexible materials in a fast, convenient and reliable manner. Any flexible, continuous material is referred to as a web. Examples of web include paper, aluminum foil, plastic film, composite polymers, etc. Any time a web needs to be altered in any way a web process is involved. Examples of web processes are printing, coating, lamination, heating, slitting, etc. Along with the problems related to web processing, the problem of how to properly transport the web on rollers through processing machinery is important. In fact, the web is commonly available in the form of rolls of raw material which need to be unwound, transported through processing machinery on rollers and rewound into finished rolls.

A web machine consists of a variety of mechanical and electrical devices assembled in a specific manner to process the web. Typically, a web machine is divided into specific sections. In the most general sense, every web machine consists of an unwind section, a master speed section, process sections, and a rewind section. More specifically, the unwind section contains the roll of raw material and other mechanical components such as guides, accumulators and driven rollers; the

master speed section contains driven rollers which are typically under pure speed control mode and is the primary section setting up transport or line speed; the processing of the material takes place in the various process sections; and finally the rewind section is where the finished web gets rewound on a roll. A web line is composed of several elements that support and control the movement of the web, such as driven rollers, idle rollers, dancers, load cells, etc. Every element in the line serves a specific purpose. A driven roller can be used to control the speed of the line or web tension or both. Idle rollers are used to support the web and achieve the desired web path through processing machinery. Dancers are devices that contain rollers whose axis of rotation is allowed to move in a specific manner based on their construction: linear dancers move in a straight path; pendulum dancers rotate on an arm around a pivot point. Dancers can be used as a means to either modify web tension or infer variations in web tension based on dancer displacement. A roller supported on the ends by load cells has the ability to sense roller reaction forces which can be assumed to be proportional to the tension in the web wrapping the roller. An example of a web machine, the Euclid Web Line (EWL) at the Web Handling Research Center at Oklahoma State University, is shown in Fig. 1.1.

Web handling is the field in which the transport behavior of the web in the web machine is studied. Research in web handling covers a variety of topics, such as: mechanics of winding and unwinding, wrinkling, out-of-plane dynamics, air-web interaction, longitudinal dynamics and tension control, lateral dynamics and control, guiding and tracking, etc. The two main areas of interest from a control system point of view are: lateral and longitudinal dynamics. Web guiding focuses on the problem of keeping the web at the desired position on the roller. Because of disturbances, roller imperfections or misalignments, the web can shift laterally

Figure 1.1: The Euclid Web Line (EWL), Web Handling Research Center.

on the surface of the roller if a mechanism to control the lateral position of the web is not used. On the other hand, the research in longitudinal behavior of the web during transport concentrates on the longitudinal movement of the web, specifically the transport velocity of the web and the tension in the web. Web tension and velocity are two key variables in web handling because they affect both quality and quantity of the final product. For example, in a printing process, in order to have the machine print exactly the desired image, the web needs to be transported through the line at a very specific velocity. Tension variations may also cause imperfections such as wrinkling, which affects the quality of the final product. Moreover, undesired decrease in tension may also cause loss of traction on the roller which will affect transport as well as guiding. And finally, the velocity of the web directly influences the production rate of the finished material, and therefore, there is always a desire to achieve the highest possible velocity without sacrificing product quality.

As highlighted earlier, in web handling processes there is a clear need for controlling web velocity and tension. As for any control problem, the best results are achieved when there is a clear understanding of the controlled process. Thus, the need for accurate models which can predict the behavior of the web during transport through processing machinery is evident. Having good models can help in many different ways: at the design stage to forecast achievable performances; to develop simulations tools; or to achieve better control performances by designing control systems based on the understanding gained by studying the models.

Driven by this necessity, several researchers have been studying the physics associated with web handling processes and the related control problems. Examples can be found in [1, 2, 3, 4, 5, 6]. In particular, the Web Handling Research Center at Oklahoma State University has been particularly active in this field, and fundamental work has been undertaken over the years. Specifically, models for general web handling machines and its components have been proposed. The basic idea is to divide the web handling machine into primitive elements, such as driven roller, idle roller, free web span, etc. First principles are then used to derive the governing equation for each primitive element. In this way the primitive elements can be used as building blocks that can be composed together to describe the behavior of any complex web handling machine. A simulation tool, called WTS (Web Transport System), has also been developed based on these ideas. The software allows to reproduce the structure of any web handling machine and can be used to study the effects of changes in the layout of the line, type of controllers or the behavior of the system under a variety of circumstances. Fig. 1.2 shows the implementation of the EWL model using WTS.

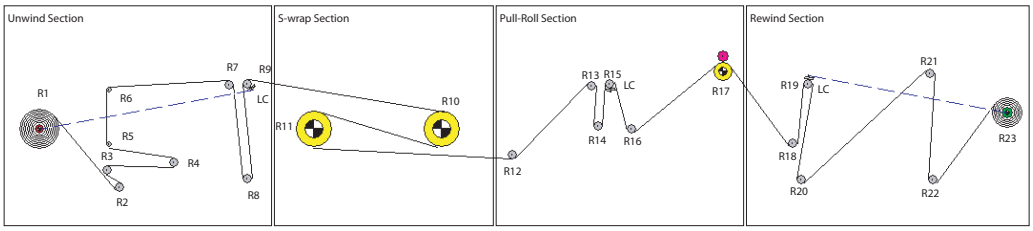

Figure 1.2: Schematics of the EWL in WTS.

1.1 Motivation and Objectives

Although there has been much work in dynamic modeling of different web handling elements and web longitudinal behavior, efforts to systematically validate models by experimentation on a web platform are non-existent. Existing literature has extensively used dynamic models for numerical analysis and/or design of control systems without adequate experimental validation of the models. Since the dynamic models for some of the primitive elements are nonlinear, designing experiments for web line model validation is a difficult task. There are a few known model validation techniques for nonlinear systems but these do not provide any clear procedures that can be applied to the web line. The only viable alternative is to compare experimental and model simulation data on a set of experiments that mimic typical web line operations in the industry, such as acceleration/deceleration of the line and running the line at a constant speed.

Most of the existing models assume ideal behavior of all the primitive elements found in the web line. As a consequence these models do not reproduce the tension oscillations that are commonly observed in experimental data. Since rollers and rotating machinery are primarily involved in transport of webs, the measured web tension signal often contains oscillations of periodic nature. These

periodic oscillations (disturbances) are typically generated by non-ideal effects and resonances. Some non-ideal effects that deteriorate web tension regulation performance include the presence of eccentric or out-of-round idle rollers and material rolls, backlash in mechanical transmission systems, and compliance in machine components or shafts transmitting power. A clear explanation of the source of the tension oscillations would be a valuable contribution to the web handling literature.

Moreover, despite the ability to machine roller surfaces with great accuracy, the occurrence of eccentric rollers is common due to the difficulty of aligning the rollers properly in harsh industrial environments. Also, it is common to find out-of-round unwind material rolls due to many reasons: (1) an improperly wound roll from the previous process, (2) laying of material rolls on the ground which creates a flat spot, (3) holding a heavy roll on mandrels for a long time causes the bottom portion of the material to bulge due to gravity, etc. Therefore, incorporation of these non-ideal effects into models and their subsequent analysis are important to provide a better understanding of the behavior of the web during transport.

Once accurate models are developed to describe the effects of the presence of a non-ideal roll or roller, it is possible to design better control systems to attenuate the tension oscillations. Design of control strategies that prevent tension oscillations to propagate through the web handling process is also important for those situations where oscillations in tension must be kept as small as possible in certain processes.

The goal of this dissertation is to fulfill these needs. In particular: provide experimental validation of the theoretical models available in the literature; identify the source of the tension oscillations in the tension signal; explain the mechanism that causes the tension oscillations when non-ideal elements such as eccentric

rollers or rolls are present in the web line; provide analytical models for web tension and web velocity in the presence of non-ideal rollers and rolls; propose control strategies to improve tension regulation and attenuate tension oscillations.

1.2 Experimental Model Validation

The first part of this work will focus on validation of the web handling models. To validate the models, data collected from the experimental testbed (the Euclid Web Line) are compared with data obtained from computer simulations based on the theoretical model. Also refinements to the models are proposed to improve correlation between experimental and simulation data whenever necessary.

Two sets of experiments are presented. The first set consists of experiments conducted with a stationary web. These experiments show that data from the computer model simulations closely match the experimental data. The second set of experiments is done with a moving web. These experiments and model simulations show that the data from model simulations follow the experimental data in an average sense, but the data from model simulations do not show tension oscillations around the reference value that are found in the measured data. These results demonstrate the need for refinements of the models to reproduce these tension oscillations. The fact that the macroscopic response of tension is reproduced in the model data proves that first order effects are included in the model. Therefore, the reason for the mismatch must be due to some second order effects. In deriving the dynamic equations for the primitive elements, it is assumed that they exhibit ideal behavior. In real situations many primitive elements are not ideal, and hence, their non-ideal characteristics will affect tension response. Therefore, non-ideal effects must be systematically included in the models since

it is unclear which non-ideal effects are causing discrepancies between the model and experimental data. Further, once it is known that a non-ideal component is causing these tension oscillations, a modeling mechanism must be determined to appropriately include that particular non-ideal effect into the model. One of the objectives is to study the non-ideal components and include their effects into the web line model and verify whether their inclusion makes the data from model simulations correlate closely with the experimental data.

It is well known that the presence of play between moving parts (backlash) will deteriorate system performance by inducing oscillations, limit cycles and even instability. Backlash is commonly found in the mechanical transmission between motor and roll shafts. In addition to backlash, compliance of shafts/belts will also reduce performance. An extensive discussion on backlash and compliance can be found in [7]. These two effects are incorporated into the web line models and simulations are conducted with different values of backlash and compliance. Comparison of simulation and experimental data showed that the inclusion of this non-ideal effect did not adequately capture the tension oscillations in the measured data.

It is also known that non-ideal components, such as out-of-round material rolls and eccentric rollers, induce tension disturbances. One of the objectives is to find a mechanism through which the model can be refined to include these non-ideal effects. The analysis of the frequency content of the measured data reveals that the tension oscillations can, in fact, be attributed to non-ideal rotating elements, such us eccentric rollers or out-of-round roll. In particular, by running experiments at different line speeds and with different unwind roll radii one can pinpoint the source of most of the disturbance frequencies found in the tension signal. This is an important result because the knowledge of sources of tension oscillations is the

basic step to design control systems for their attenuation.

1.3 Effect of an Eccentric Roller

A roller is considered to be eccentric when its center of gravity does not coincide with its center of rotation; in this study an eccentric roller is considered to be perfectly circular.

Once it is evident that the tension oscillations can be attributed to the presence of eccentric rollers, the question that needs to be addressed is how does an eccentric roller affect web tension. From experimental observations of the machine and web transport it is clear that because of the presence of eccentric rollers the length of the spans adjacent to the roller are time varying. One of the assumptions used to derive the governing equation for tension in a web span is that the span length is not varying with time. Clearly, in the presence of an eccentric roller, such an assumption does not hold, therefore, the governing equation for tension needs to be modified where span length changes are encountered. The modified governing equation for tension should take into account the effects of the span length variations. To numerically solve the modified governing equation of tension it is necessary to find an expression for the span length as a function of the angular displacement of the eccentric roller. To find the span length between two idle rollers the common tangent needs to be determined. A procedure is presented that provides a closed form expression of the span length as function of the angular displacement of the roller.

Because of the presence of eccentricity, the governing equation for web velocity on an ideal roller cannot be used and a modified version has to be determined. First, because the center of gravity differs from the center of rotation, a torque

which takes into account the mass of the roller needs to be added in the governing equation. Second, the web tension in each of the spans adjacent to the eccentric roller generates a varying torque on the roller. To determine these torques the distance between the point where the force is applied and the center of rotation must be computed. This distance is dependant on the angular displacement of the roller because the point where the web makes contact with the eccentric roller changes.

Derivation of all the necessary equations is presented and equations for web tension and velocity in the presence of eccentric rollers are obtained. Numerical simulations of the refined model are conducted, and data from these simulations are compared with the data from experiments. Results show an improved correlation between the two.

1.4 Effect of an Out-of-Round Roll

The case of the presence of an out-of-round roll presents additional challenges compared to the case of the eccentric roller. Similar to the eccentric roller case, the presence of an out-of-round roll will induce span length variations. Hence, numerical solution of the modified governing equation for tension requires an expression for the span length as a function of the angular displacement.

As in the eccentric roller case, the main difficulty is in finding the common tangent between the out-of-round roll and the downstream idle roller. The solution to basic tangency problems can be found in [8, 9, 10]. In [11] an algorithm to find common tangents to parametric curves is described; this algorithm is based on a binary search algorithm and assumes the curves to be known in parametric form. This report will present a different approach which is easily applicable to the web

handling problem.

Finding a closed form expression for the span length is a difficult task for this situation. In fact, it will be shown that even for a simple shape, an elliptical roll, it is difficult to find a closed form expression for the length of the span, and numerical approximations have to be used instead. In the proposed procedure the problem of finding the span length is converted to the problem of finding, among the family of lines tangent to the elliptical roll, the line that is also tangent to the neighboring idle roller. The manner in which this common tangent is distinguished is by exploiting the fact that the distance between the tangent of a circle and the center of the circle is equal to the radius of the circle. A cost function is defined for every point on the surface of the material roll, which is equal to the square of the difference between the radius of the downstream roller and the distance between the line tangent to the elliptical roll at that point and the center of the downstream roller. The cost function is always positive except for the points on the elliptical roll that have a common tangent with the downstream roller where it will be zero. This problem is formulated as a minimization problem which can be solved numerically using efficient methods. This minimization problem in its simplest form has multiple solutions; a method is given to restrict the search space in such a way that the minimization problem has only the correct solution.

The computation of the span length for the case of a generally shaped roll is approached using similar ideas, but compared to the elliptical case this problem presents more challenges. First, given a generically shaped roll it is necessary to find a way to characterize its perimeter. The method to characterize the perimeter must be chosen such that it is possible to capture all the main characteristics of the roll. The method should also exhibit numerical stability and must be computationally tractable. Then, an expression for the family of tangents to the

roll must be determined. Given the expression for the family of lines tangent to the out-of-round roll, one can define the same cost function defined for the elliptically shaped roll. The solution of the minimization problem provides the common tangent between the out-of-round roll and the downstream idle roller. Again the minimization problem has multiple solutions, the approach used for the elliptically shaped roller cannot be used for this instance. A modified cost function is defined for the generally shaped material roll; this cost function penalizes certain points in the search space in such a manner that only the correct minimum is obtained.

Besides the inclusion of the span length variation induced by the presence of the out-of-round roll, there is another important aspect to consider in deriving the governing equation for tension in the web span. The derivation of the web tension governing equation is based on the the mass balance principle for a control volume that encompasses the entire web span: at any instant of time the variation of mass in the control volume must be equal to the difference between the web material flow rate entering the control volume and the material flow rate leaving the control volume. For an ideal roll it can be shown that the material flow rate is proportional to the peripheral velocity of the web on the roll and this is what is commonly used. Simple counter examples show that for an out-of-round roll the peripheral velocity can no longer be used to compute the material flow rate. A procedure to compute the material flow rate in the presence of an out-of-round material roll is presented. Similar to the problem of the computation of the span length, a closed form solution for the material flow rate is difficult to determine because of the complexity of the problem, an alternative numerical algorithm is presented instead. The procedure is based on the same characterization of the perimeter of the roll that was used for the computation of the span length.

Similar to the case of the presence of the eccentric roller, the governing equation

for the velocity of the material roll needs to be determined. Because of the out-of-round material roll, the distance between the point where the web makes contact with the roll and the center of rotation of the roll is time varying, while for the ideal case it is always equal to the radius of the roll.

Comparison between experimental data and computer simulation data will demonstrate that the modified governing equations of web tension and velocity can replicate in simulation the effects of the presence of an out-of-round roll.

1.5 Control Algorithms for the Attenuation of Tension Oscillations

Together with the investigation of the physics associated with the transport of the web in the presence of non-ideal elements, one of the objectives of this work is to identify, design and implement a suitable control algorithm for the attenuation of oscillations due to the presence of non-ideal elements. The algorithm is meant to be used in an industrial set-up for real applications. For these reasons it is necessary to consider several aspects that limit the choice of the control algorithms.

First, the control algorithm must be suitable for execution on a real-time platform. The selection of the sampling period on these platforms can vary depending on the application, ranging from a fraction of a millisecond to tens of milliseconds. In order for the algorithm to be executed in real time, the total execution time of the algorithm must be less that the sampling period. Given the computational complexity of the model of the web line when a non-ideal element is present, a model based controller may not satisfy the time constraint imposed by a real time implementation.

Another aspect to consider is the fact that the algorithm may be used by line operators who may have limited control background. Moreover, in order to reduce the idle time of the machine and avoid loss of productivity, it is desirable to have an algorithm that can be used in parallel with the existing controls for tension and speed regulation without the need to retune or redesign them.

Following an extensive literature review of available algorithms for compensation of periodic disturbances, the adaptive feed-forward (AFF) algorithm was identified as a suitable candidate for the attenuation of oscillations due to the presence of non-ideal elements. The AFF satisfies all the requirements of computational complexity and simplicity mentioned above. The idea of the controller is to estimate amplitude and phase of the periodic disturbance and generate a feed-forward signal to compensate for such disturbance. The AFF is also placed in parallel to the existing controller without the need for retuning of such controllers. Several different configurations of the AFF for different scenarios will be presented and experimental results will show the effectiveness of the control algorithm.

1.6 Contributions

The contributions of this research are summarized in the following:

- *Validation of the ideal primitive element models.* A set of significant experiments is designed to validate the model of the primitive elements. Comparison of experimental data and model simulated data shows that the ideal model can reproduce the measured data in an average sense. The fact that macroscopic response of tension is reproduced in the data from model numerical solution indicates that the first order effects are included in the

model. These models can be used in the design of control systems in situations where rejection of tension oscillations is not a priority and only the transient behavior is a concern.

- *Identification of the sources of tension oscillations.* Using the experimental data collected on the EWL with different configurations, a method to identify the sources of most of the disturbance frequencies in the tension signal is provided. The knowledge of the sources of the tension oscillations is the basic step toward the design of control systems for their attenuation.

- *Modified governing equation for web tension.* Experimental observations revealed that the presence of non-ideal elements, such as eccentric rollers or out-of-round material, roll cause the length of the spans adjacent to the non-ideal elements to be time varying. In the ideal case it is assumed that the span length is constant. In order to properly replicate in model simulations the effects of the presence of an eccentric roller and an out-of-round roll, span length variations were included in the governing equation for web tension.

- *Computation of the span length in the presence of an eccentric roller.* A procedure is developed to compute the length of the web spans adjacent to an eccentric roller. The procedure gives the expression of the span length in closed form as a function of the angular displacement of the eccentric roller. This expression is required for model simulations of a web line in the presence of an eccentric roller.

- *Computation of the span length in the presence of an out-of-round material roll.* A method to efficiently characterize the shape of the out-of-round material roll is given. A numerical algorithm to compute the length of the

span between an out-of-round material roll and the downstream idle roller is also developed.

- *Computation of the material flow rate in the presence of an out-of-round material roll.* In the presence of an out-of-round material roll, the peripheral velocity of the web on the roll is not proportional to the material flow rate. Hence, it cannot be used in the governing equation for tension in a web span. A numerical algorithm is developed for the computation of the material flow rate.

- *Implementation of a control algorithm for the attenuation of oscillations in web tension and velocity.* Adaptive feed-forward technique is selected as a feasible method to satisfy all the constraints associated with the real time execution and the ease of use by web line operator. Adaptive feed-forward algorithms are implemented for different scenarios on the EWL for compensation of tension and velocity oscillations due to eccentric rollers and out-of-round material rolls.

1.7 Organization of the Report

In Chapter 2 an overview of the primitive elements is presented and how first principles are applied to obtain the governing equations for each basic element is given. The chapter also contains a description of the validation process from a theoretical point of view. Different validation techniques are introduced, highlighting advantages and disadvantages of each approach. A description of the experimental platform and the computer simulation is given. The last part of the chapter includes the experimental validation of the ideal models and a discussion

on the identification of the source of oscillations in the tension signal.

Chapter 3 describes the modification of the governing equations of the primitive elements in the presence of an eccentric roller. The chapter concludes with a comparison of the data obtained from simulations of these modified models with the experimental data.

Chapter 4 presents the aspects related to the modeling of a web line in the presence of an out-of-round material roll. First, the problem of the computation of the span length is introduced. The case of an elliptically shaped material roll is addressed as a simple example of an out-of-round material roll. This example offers the baseline for the derivation of an algorithm for the computation of the span length in the presence of a convex shaped material roll. The second part of the chapter describes the computation of the material flow rate entering the control volume. Initially, one simple counter example is presented to show the fact that the peripheral speed of the web on the roll is not proportional to the material flow rate when the roll is out-of-round and provides a motivation for the need to compute the material flow rate using a different approach. Because of the complexity of the problem a closed form for the material flow rate is difficult and a numerical algorithm for the computation of the material flow rate is presented instead. Finally, data collected on the experimental platform with an out-of-round material roll is compared to the data generated from computer simulations using the proposed model.

Chapter 5 addresses the problem of identifying a suitable controller for the attenuation of the tension oscillations due to the presence of a non-ideal roll or roller. A literate review of the available controllers for attenuation of periodic oscillation is presented. The reasons for choosing the adaptive feed-forward are described. The implementation of the AFF is described for several configurations

and the effectiveness of the controller is shown through extensive experimental results.

Chapter 6 presents a summary of the results presented in this work and suggests possible topics for future work.

Chapter 2

Modeling and Validation of Primitive Web Handling Elements

One of the well known modeling techniques for creating a model for the entire web line is based on the concept of primitive elements. In this approach every primitive element of the web line is modeled separately using the first principles approach, and then the entire web line model is obtained by appropriately combining the primitive element models. The first part of this chapter describes the derivation of the governing equations of the fundamental elements in every web process: material rolls, idle and driven rollers and web span.

The procedure that is typically employed to corroborate the usefulness of the developed model is to compare data from model simulations with data from experiments in an open-loop setup, that is, by not using any feedback controllers. Unfortunately, it is not possible to run web machines in open-loop because maintaining web tension at some appropriate value is necessary for web transport, and without controlling web tension either the web breaks due to large tension varia-

tions or the web is slack which will hinder transport. For this reason web tension was regulated in the unwind and the rewind sections with tension control systems. The model simulations of the system also included a model of the controller for mimicking the same setup as in the experiments. In this configuration the inputs for the model are reference values of tensions and web velocity.

The model of the complete web line with control systems was formed based on the governing equations described in this chapter. The entire line is simulated for all cases but only the data from the unwind section will be shown for comparison with the experimental data.

The initial set of experiments consisted of a step change in tension reference with zero line speed. The purpose of these experiments was to verify if the model is capable of reproducing tension behavior in the absence of speed induced disturbances. Various web tension reference values were tested. For all the test cases, data from model simulations and experiments showed good correlation.

The second set of experiments considered also a step change in tension reference, but with a non-zero line speed. In this case, speed induced disturbances are observed in the tension signal. In general, the model simulations appear to be able to follow the average value of the tension but do not reproduce the speed induced oscillations. These experiments show the need for modifications to the existing models to capture the speed induced disturbances.

The chapter ends with a discussion on the frequency content of the tension signal for the experiments performed under different operating conditions: different line speeds and different unwind roll radii. Model analysis and experimentation has revealed that every non-ideal rotating element, either because of eccentricity or out-of-roundness, will introduce tension oscillations which are integer multiple of a fundamental frequency f, a frequency that can be computed by knowing the

radius of the rotating element and the line speed. This allows determination of the source of almost all the tension oscillations in the tension signal.

2.1 Primitive Elements

Web lines can differ widely, either because of their layout or because of the kind of components that are used to compose the line. In order to come up with a systematic approach to model web transport behavior and machine components that make up the web line, the concept of primitive elements is introduced. Primitive elements are a set of elementary components which form the building blocks for almost all existing web process lines. Some of the key primitive elements are material rolls, idle rollers, driven rollers, web span (the web between two consecutive rollers), dancers, accumulators, print cylinders, laminators, etc. The primitive element models are developed from the application of first principles, and a model for the entire web line is obtained by composing primitive elements models based on the specific layout of the line. The derivation of the models from the first principles the fundamental elements of every web processing machine (material roll, idle roller, driven roller, web span) are described in this section.

2.1.1 Governing Equations for Unwind and Rewind Rolls

A schematic of the unwind roll is shown in Fig. 2.1(a). The dynamic equation that describes the motion of the unwind roll is given by [5]:

$$\frac{d}{dt}\left(J_u\omega_u\right) = -b\omega_u + R_u T_1 - \tau_u \tag{2.1}$$

where J_u is the inertia of the roll, ω_u is the angular velocity, b is the viscous friction coefficient, R_u is the radius of the roll, T_1 is web tension, and τ_u is the

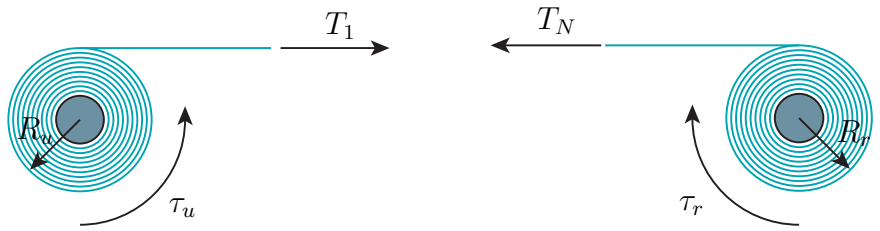

(a) Unwind Roll (b) Rewind Roll

Figure 2.1: Unwind and Rewind Rolls.

torque transmitted from the motor to the roll through a coupling. Note that all the variables refer to the roll side. Expanding (2.1):

$$J_u\dot{\omega}_u = -b\omega_u + R_uT_1 - \tau_u - \dot{J}_u\omega_u \tag{2.2}$$

The moment of inertia J_u is given by

$$J_u = J_0 + J_w \tag{2.3}$$

where J_0 is the inertia of the core shaft, core, coupling, and motor, and J_w is the inertia of the web material, which is time-varying as the web is unwound. The moment of inertia J_w can be written as a function of the radius:

$$J_w = \frac{m_w}{2}(R^2 + R_c^2) = \frac{\pi}{2}\rho_w w_w(R^2 - R_c^2)(R^2 + R_c^2) = \frac{\pi}{2}\rho_w w_w(R^4 - R_c^4) \tag{2.4}$$

where m_w is the mass of the web, R_c is the radius of the core of the roller, ρ_w is the density of the web and w_w is its width. The external radius of the roll is also a function of time, as the web leaves the roll the radius decreases. In particular, the radius decreases by $\Delta R_u = -t_w$, with t_w being the web thickness, every one revolution of the roll. The time that the roll takes to rotate 2π radians is $\Delta t = 2\pi/\omega_u$. Therefore, the dynamic equation for the roll radius can be expressed as

$$\dot{R}_u = \lim_{\Delta t \to 0} \frac{\Delta R_u}{\Delta t} = -\frac{t_w\omega_u}{2\pi} \tag{2.5}$$

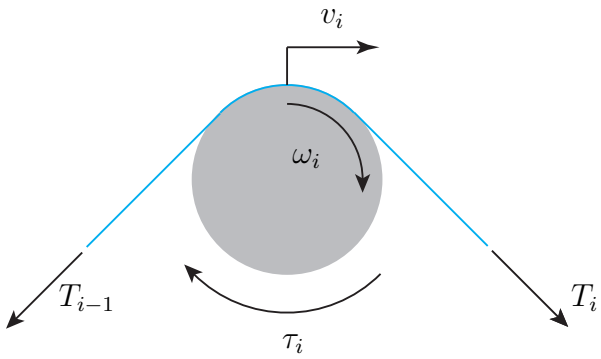

Figure 2.2: Schematic of a Driven Roller.

From (2.1) and (2.5) $\dot{J}_u$ is given by

$$\dot{J}_u = 2\pi\rho_w w_w R_u^3 \dot{R}_u = -\rho_w w_w R_u^3 t_w \omega_u \tag{2.6}$$

Hence, the governing equation for the angular velocity of the unwind roll is

$$J_u\dot{\omega}_u = -b_u\omega_u + R_u T_1 - \tau_u + \rho_w w_w R_u^3 t_w \omega_u^2 \tag{2.7}$$

For the rewind roll model an analogous discussion can be made, the only difference is that the radius will be increasing and the tension of the web will be pulling the roller in opposition to the sense of rotation of the roller (see Fig. 2.1(b)). Therefore, the dynamic equation for the rewind roll will be:

$$J_r\dot{\omega}_r = -b\omega_r - R_r T_n + \tau_r - \rho_w w_w R_r^3 t_w \omega_r^2 \tag{2.8}$$

2.1.2 Governing Equations for Idle and Driven Rollers

Figure 2.2 shows a schematic of a driven roller or for an idle roller if τ_i is set to zero. The dynamic equation is obtained by using torque balance. The equation for a driven roller is

$$J_i\dot{\omega}_i = -\tau_{fi} + R_i(T_{i+1} - T_i) + \tau_i \tag{2.9}$$

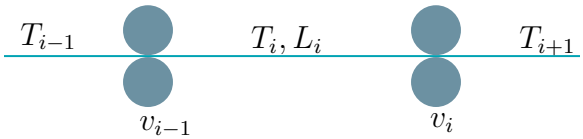

Figure 2.3: Web Span

where τ_i is the driving torque at the roller shaft, J_i is the inertia of the roller, ω_i is the angular velocity, τ_{fi} is the torque due to friction, and R_i is the radius of the roller.

2.1.3 Governing Equation for Web Tension in a Span

Modeling of tension in a web span has been addressed in several studies, examples are [1, 2]. The fundamental idea behind the derivation of the dynamic equation is the conservation of mass in the control volume encompassing a web span between two rollers, which can be stated as: at any moment, the variation of the mass of web in the span is equal to the difference between the amount of mass entering the span from the previous span and the mass leaving the span to enter the next span. For a web span between two rollers (see Fig. 2.3) mass conservation can be written as

$$\frac{d}{dt}\int_{x_{i-1}(t)}^{x_i(t)} \rho(x,t)A(x,t)dx = \rho_{i-1}A_{i-1}v_{i-1} - \rho_i A_i v_i \tag{2.10}$$

where, $x_{i-1}(t)$ and $x_i(t)$ are the entry and exit position of the i-th span, ρ is the density of the web, A is the cross sectional area of the web, and v is the velocity of the web. Note that since the i-th web span is between the $i-1$-th and i-th roller, the position $x_{i-1}(t)$ refers to the exit point of the wrapped web on the $i-1$-th roller and the position $x_i(t)$ refers to the entry point of the wrapped web on the i-th roller. Let the subscript "n" on a variable denote the normal or unstretched

state of the variable. Since the mass of an infinitesimal web in the stretched and unstretched is the same, the mass of an infinitesimal element of web in the transport direction is given by

$$dm = \rho dx w h = \rho dx A = \rho_n dx_n w_n h_n = \rho_n A_n dx_n \tag{2.11}$$

The web of length dx in the stretched state is related to its unstretched length dx_n by

$$dx = (1 + \epsilon_x) dx_n \tag{2.12}$$

where ϵ_x denotes the web strain in the transport direction. Now considering this relation, it is possible to write:

$$\frac{\rho(x,t)A(x,t)}{\rho_n(x,t)A_n(x,t)} = \frac{dx_n}{dx} = \frac{1}{1+\epsilon_x(x,t)} \tag{2.13}$$

which can be rearranged as:

$$\rho(x,t)A(x,t) = \frac{\rho_n(x,t)A_n(x,t)}{1+\epsilon_x(x,t)} \tag{2.14}$$

Substitution of (2.14) in (2.10) gives

$$\frac{d}{dt}\int_{x_{i-1}(t)}^{x_i(t)} \frac{\rho_n(x,t)A_n(x,t)}{1+\epsilon_x(x,t)} dx = \frac{\rho_{n_{i-1}}(x,t)A_{n_{i-1}}(x,t)v_{i-1}}{1+\epsilon_{x_{i-1}}(x,t)} - \frac{\rho_{n_i}(x,t)A_{n_i}(x,t)v_i}{1+\epsilon_{x_i}(x,t)} \tag{2.15}$$

Under the assumption that the cross sectional area A and the density ρ of the unstretched material is constant, (2.15) can be simplified to the following:

$$\frac{d}{dt}\int_{x_{i-1}(t)}^{x_i(t)} \frac{1}{1+\epsilon_x(x,t)} dx = \frac{v_{i-1}}{1+\epsilon_{x_{i-1}}(x,t)} - \frac{v_i}{1+\epsilon_{x_i}(x,t)} \tag{2.16}$$

Considering that $\epsilon \ll 1$, $1/1+\epsilon$ can be approximated with $1-\epsilon$, and hence (2.16) can be written as

$$\frac{d}{dt}\int_{x_{i-1}(t)}^{x_i(t)} (1-\epsilon_x(x,t)) dx = v_{i-1}(1-\epsilon_{x_{i-1}}(x,t)) - v_i(1-\epsilon_{x_i}(x,t)) \tag{2.17}$$

Using the Leibnitz rule for the differentiation of integrals:

$$\frac{d}{dt}\int_{\phi(t)}^{\psi(t)} f(x,t)dx = \int_{\phi(t)}^{\psi(t)} \frac{\partial f(x,t)}{\partial t}dx + \frac{d\psi}{dt}f(\psi(t),t) - \frac{d\phi}{dt}f(\phi(t),t) \tag{2.18}$$

and assuming uniform strain throughout the span, (2.17) can be expressed as

$$-\frac{d\epsilon_{x_i}}{dt}(x_i - x_{i-1}) + (1-\epsilon_{x_i})\frac{dx_i}{dt} - (1-\epsilon_{x_{i-1}})\frac{dx_{i-1}}{dt} = v_{i-1}(1-\epsilon_{x_{i-1}}) - v_i(1-\epsilon_{x_i}) \tag{2.19}$$

Simplifying (2.19) gives the following dynamic equation for strain in the i-th span:

$$\frac{d\epsilon_{x_i}}{dt} = \frac{v_i(1-\epsilon_{x_i}) - v_{i-1}(1-\epsilon_{x_{i-1}}) + (1-\epsilon_{x_i})\dot{x}_i - (1-\epsilon_{x_{i-1}})\dot{x}_{i-1}}{x_i - x_{i-1}} \tag{2.20}$$

Depending on the property of the web it is possible to introduce a constitutive relationship between strain and tension. Assuming the web to be elastic, Hooke's law ($T = EA\epsilon$) can be used to describe this relationship. Substituting Hooke's law in (2.20) and simplifying, the following governing equation for the tension in the i-th span is obtained:

$$\dot{T}_i = \frac{v_i(EA - T_i) - v_{i-1}(EA - T_{i-1}) + (EA - T_i)\dot{x}_i - (EA - T_{i-1})\dot{x}_{i-1}}{x_i - x_{i-1}} \tag{2.21}$$

This equation includes the hypothesis that both the end rollers are free to move, that is, the control volume boundaries are time-varying.

The basic model considers the case where both rollers are stationary; in this situation equation (2.21) is given by

$$\begin{aligned} \dot{T}_i(t) &= \frac{v_i(t)(EA - T_i(t)) - v_{i-1}(t)(EA - T_{i-1}(t))}{L} \\ &= \frac{EA}{L}(v_i(t) - v_{i-1}(t)) + \frac{1}{L}[v_{i-1}(t)T_{i-1}(t) - v_i(t)T_i(t)] \end{aligned} \tag{2.22}$$

2.2 Nonlinear Identification and Validation

Model validation aims to give a qualitative or quantitative measure of how well a simulated model matches a real system. Model validation can be considered

as the final step of the system identification process. System identification is the procedure through which a set of equations called the model is generated starting from a combination of physical insight and experimental data; the model is expected to reproduce the behavior of the real system.

In a general sense, system identification can be divided into the following phases:

- Model order: determine the number of input, output and state variables.
- Model structure: define the relations between the input, output and state variable variables.
- Parameter evaluation: find the best parameters for the chosen model.
- Model validation: test phase that guarantees the correctness of modeling and/or identification procedure.

Nonlinear system identification and validation presents a much bigger challenge over linear system identification for several reasons. First, the structure of linear systems is simpler and the use of frequency domain analysis is possible which makes the identification process easier. Second, using the superposition property of linear systems and the property of white noise, it is possible to cover the effect of all the possible inputs just using zero mean white noise as input to the system. And finally, during the validation step, it is possible to extrapolate information about the corrections that should be made to the model through a statistical analysis of the difference between the estimated model data and real data. These statements do not hold in the case of nonlinear systems. In fact, the possible structures of nonlinear systems differ widely and achievable results strongly depend on the choice of the model structure. The performance of the model can be guaranteed only for a set of inputs used during the identification

and/or validation process, in other words the ability of the model to match the output due to unseen inputs is uncertain. Also, the validation step does not in general give insights into modifications of the model when the test used to compare model and experimental data does not pass.

The rest of the section will cover a brief overview of existing nonlinear system identification techniques and some validation procedures.

2.2.1 Nonlinear System Identification

Nonlinear system identification can be achieved through several different techniques based on the problem at hand. A classification of the different techniques can be made based on the amount of a priori information available about the system. Based on this concept, the identification techniques can be classified into the following:

- Black box identification: applied when prior knowledge of the system is not available. This is used in situations where only input/output data are available to describe the system, and a model that is capable of matching this input/output data needs to be found.

- Gray box identification: applied when some prior knowledge of the system is available. This is used when most of the dynamics and parameters of the system can be determined from first principles, but still some effects are not known and system identification is left to some sort of input/output data matching.

- White box identification: it is adopted when there is total knowledge about the system and all the dynamics and the parameters can be deduced without experimental data.

Clearly, it is desirable to exploit prior information about the system as much as possible. Therefore, as a general idea it is preferable to move toward the bottom of the above classification list when possible. However undesirable, often the only choice for identification is the black box approach and, for this reason, there is a rich literature concerning strategies to perform this kind of identification, see [12] for a detailed survey. In a general sense, the problem faced during black-box identification is the following: given two sets of recorded data

$$\mathbf{u}^t = [u(1), u(2), \ldots, u(t)] \qquad \mathbf{y}^t = [y(1), y(2), \ldots, y(t)] \tag{2.23}$$

the input and the output, respectively, of a certain system, find the function:

$$\hat{y}(t) = g(\mathbf{u}^{t-1}, \mathbf{y}^{t-1}) + v(t)$$

which gives the best match between the recorded data $y(t)$ and the estimated data $\hat{y}(t)$ while keeping the additive term $v(t)$ as small as possible.

For black box system identification, validation is done by testing the performance of the model on a set of input/output data not used during the parameter estimation step. This set is, therefore, called the validation data. If the model gives satisfactory performance on the validation data, then the model is accepted. Otherwise it is necessary to go back and restart the process of testing different structures for the model.

Even though there is a well established theory about nonlinear system identification, it does not fit the purpose of model validation that is sought in the web line case. Using a black box model for web handling would mean discarding all the knowledge about the dynamic behavior of the web and other primitive elements obtained using first principles approach.

Some gray box techniques have been developed in order to exploit prior knowledge about the system in the identification process; examples are given in [13]

where the concept of semi-physical modeling is introduced, and in [14] where a priori physical knowledge is introduced in a neural network framework. The goal of these techniques is to combine strategies from black-box approaches with equations derived from physical reasoning.

As reported in [13], in order for this procedure to be applicable the model must satisfy certain requirements. Moreover, the size of the model could make the procedure computationally untractable. Unfortunately, due to the presence of non-smooth nonlinearties and because of the high complexity of web handling machines this procedure is not applicable.

Since none of the identifications techniques found in the literature can be adapted to the model that has been developed for the web machines, validation techniques that are appropriate variations of white-box modeling will be discussed next.

2.2.2 Model Validation

When a model is developed using physical laws like conservation of mass or energy, a *general model* is obtained. This general model should be able to describe all the systems belonging to the same class just by adjusting the parameters of the model. For example, it is expected that the general model developed for the web line is able to describe any web line just by adding the right amount of primitive elements with the right parameters. If the parameters in a general model are fixed, the resulting model is called the *specific model*. The model for the EWL is a specific model of a web machine. Finally, once initial conditions and both forcing and disturbance inputs are added to the model, the *particular model* is obtained. The model validation process is to infer the correctness of the general model by

means of a variety of specific models. Clearly, this process does not guarantee that the general model is exact unless every possible particular model is tested for each specific model, which is practically unrealizable [15]. Normal practice is to define a set of relevant experiments to test the model and validate the model if the performance on this set is satisfactory. The measurement of performance of the model is another key aspect of the validation process and it is difficult to define a criterion which fits all the possible scenarios. The easiest choice to judge the performance of the model is through a visual comparison of the output signals as a function of time. In this case experimental data is plotted with simulated data and it is left to the user to judge whether the model is acceptable or not. The performance can also be weighted based on selection of a norm, the most commonly used norms are L_1 (the integral of the absolute value of the error), L_2 (the integral of the squared error) or L_∞ (the maximum error); in this case the fitting error would be used as a testing parameter and the model is required to satisfy a preset bound on the chosen norm. The norm of the fitting error can also be a good parameter to judge between different models as well. Note that this does not give an absolute criterion, in fact it is possible to have a model outperforming another one based on a certain norm.

In order to have a validation test which depends less on the choices made by the user, the *model distortion* technique was introduced in [16, 17]. The concept behind the model distortion is that any set of recorded data can be followed by any model if the model is distorted using time varying parameters. Clearly, if the model matches the real system closely, less parameter variation is required in order to make the simulated data follow the recorded data. From this observation a quantitative criterion for model validation arises. In fact, since the model is derived from some physical understanding of the process, every parameter has a

physical meaning, and hence, it is reasonable to assume that for every parameter an estimation of its variance is available. Therefore, if parameter distortion necessary to have a perfect match between simulation and experimental data has variance less than the expected one, then it is possible to claim that the model is acceptable. Otherwise, the model needs to be modified. Note that the model distortion technique is just a pass or fail criterion and does not give any insights into how the model should be adjusted to better follow experimental data. This framework gives a more structured test for model validation compared to the simple visual comparison. However, reasonable bounds on the variance of the parameters are not always available. In such situations the choice of the bound and, implicitly, the acceptance or rejection of model falls on the user, and the model distortion approach does not give any real advantage over visual comparison. In certain situations model distortion can still be a useful tool to perform sensitivity analysis to parameter variations.

2.3 Experimental Validation

2.3.1 Experimental Setup

Normally, when performing validation of a model, experiments are performed in an open loop setup. Unfortunately, it is not possible to run web machines in open-loop because even a small disturbance can induce large tension variations which may cause web breakage. Another possibility is to run experiments in an hardware in the loop configuration, which is to run the experiments in closed-loop, recording the control input, and using that input as model input. Initially, the hardware in the loop configuration was tested, but this did not give satisfactory

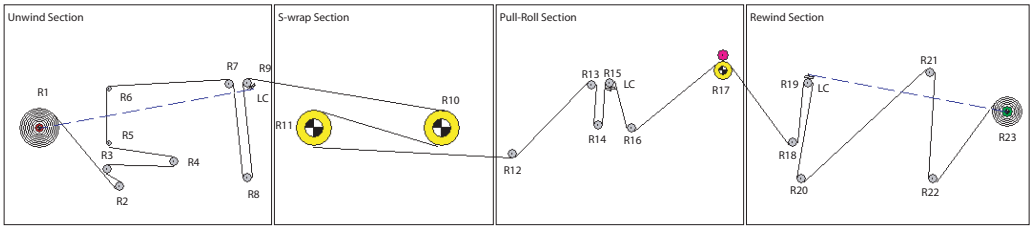

Figure 2.4: Line schematic of the EWL.

results. There are two plausible reasons for this. First, in the real control input there are adjustments for disturbances which are not modeled. Second, the control input that can be recorded is not the actual input to the motor but it is a reference for the controller that drives the AC motor. Therefore, the real input to the web machine may differ from the one recorded. For these reasons a closed-loop setup was chosen to run the experiments, meaning that the simulation of the system would also include a model of the controller. In this configuration the inputs for the model are reference values of tensions and web velocity.

All of the experimental data presented in this report has been collected on the Euclid Web Line (EWL). The web line can be divided into four sections: the unwind section, the S-wrap section, the pull-roll section, and the rewind section. The S-wrap functions as the master speed section. The S-wrap roller and the pull-roll are under pure speed control, whereas the unwind and rewind have an inner speed loop and an outer tension loop. Hence, tension is regulated in the unwind and rewind sections only.

The EWL offers the possibility of choosing different web paths with different span lengths and number of idle rollers. The configuration used to perform all the experiments is shown in Fig. 2.4. The roller number 9 is mounted on load cells which measure the tension for the unwind section and provides the feedback

	K_{ref}
Unwind	15
S-wrap leader	20
S-wrap follower	20
Pull-Roll	40
Rewind	15

Table 2.1: Values of Reference Gain for the Velocity PI Controllers.

signal for the unwind tension PI controller. The roller number 15 is also mounted on load cells and it gives the tension in the pull-roll section which is only used for monitoring purposes. Tension is measured on roller 19 in the rewind section. All the experimental data discussed in this report correspond to the unwind section of the EWL.

All the velocity controllers are in the form:

$$C_v(s) = \frac{K_p(s + \omega_{ld})}{s} \tag{2.24}$$

where $K_p = JK_{ref}$, with J being the total inertia reflected to the motor side, $\omega_{ld} = K_{ref}/4\zeta^2$, where $\zeta = 1.1$ is the damping ratio of the system. Table 2.1 shows the value of K_{ref} for each section.

The tension PI for the unwind roller is

$$C_t^{unw}(s) = \frac{2(s + 10)}{s} \tag{2.25}$$

while the PI for the rewind roller is:

$$C_t^{rew}(s) = \frac{3(s + 10)}{s} \tag{2.26}$$

A model for the entire line based on the governing equations of the primitive elements described earlier and models of the controllers has been implemented in

Simulink. The entire line is simulated for all cases but only the data from the unwind section will be compared with the experimental data.

2.3.2 Driven Rollers Parameters Identification

To simulate the governing equations of the driven rollers, the inertia and the coefficient of friction are necessary. These can be determined from experiments on the driven rollers without the web in the machine. Consider the inertia first and assume initially that the friction is negligible. Under these assumptions the dynamic equation is

$$J\dot{\omega}(t) = \tau \tag{2.27}$$

if a nominal constant torque τ_n is applied to the motor, the solution of the dynamic equation is

$$\omega(t) = \frac{\tau_n}{J}t \tag{2.28}$$

By recording the time t_n required for the motor to reach the nominal velocity ω_n the moment of inertia can be obtained using the expression:

$$J = \frac{\tau_n t_n}{\omega_n} \tag{2.29}$$

Note that this procedure only provides the value of the core inertia for unwind and rewind since the inertia will be changing as web is released or accumulated.

Once the value of the inertia is obtained, an estimation for the viscous friction coefficient b can be determined by non-linear curve fitting of the free velocity response of the driven roller. The free response is obtained by bringing the driven roller to a given velocity and then by letting the roller to freely come to a stop. Assuming the model to be given by (2.9), while having no web and imposing the control torque to be zero the free response follows the following expression:

$$\omega(t) = \omega_0 e^{-\frac{b}{J}t} \tag{2.30}$$

where ω_0 is the angular velocity of the roller at the moment the control torque τ is removed. Given a set of samples ω_k^e taken at time t_k with $k = 1, \ldots, N$ of the experimental free response, the value of the viscous friction b is determined by solving the following minimization problem:

$$\begin{aligned} &\min_b \sum_{k=1}^{N} (\omega_k^e - \omega(t_k))^2 \\ &s.t. \\ &\omega(t_k) = \omega_0 e^{-\frac{b}{J} t_k} \end{aligned} \tag{2.31}$$

An example of the result obtained from the non-linear fitting is shown in Fig. 2.5(a). The match between the experimental and the simulated data can be further improved by including a constant friction term in the model for the driven roller. With this friction model the governing equation is given by

$$J\dot{\omega} = -c - b\omega + R(T_{i+1} - T_i) + \tau \tag{2.32}$$

and the minimization problem involves now two variables:

$$\begin{aligned} &\min_{b,c} \sum_{k=1}^{N} (\omega_k^e - \omega(t_k))^2 \\ &s.t. \\ &\omega(t_k) = \max(0, -\frac{c}{b}(1 - e^{-\frac{b}{J} t_k}) + \omega_0 e^{-\frac{b}{J} t_k}) \end{aligned} \tag{2.33}$$

Using this new model the results of the non-linear curve fit are shown in Fig. 2.5(b). The plot shows a visible improvement in the curve fitting.

2.3.3 Estimation of Idle Roller Bearing Friction

Due to the absence of speed feedback signals on the idle rollers, estimation of the idle roller friction parameter must be obtained using other means. A procedure

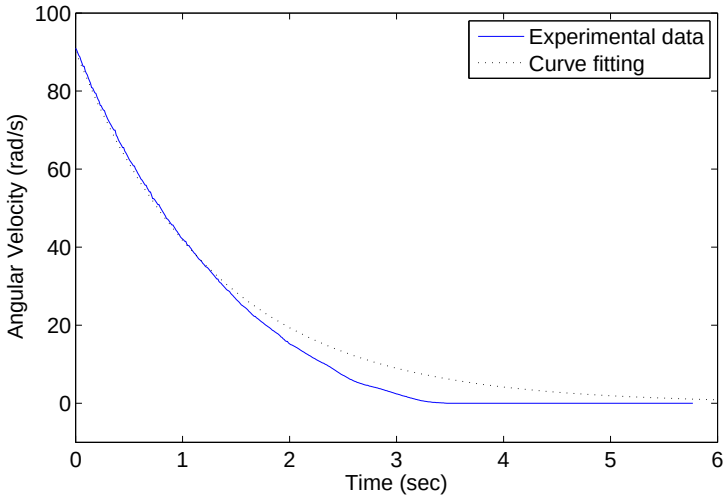

(a) Curve fitting using viscous friction model.

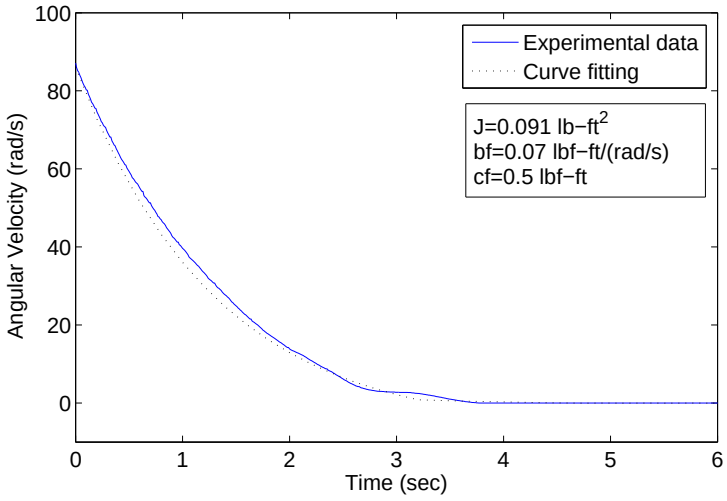

(b) Curve fitting using viscous and coulomb friction model.

Figure 2.5: Estimation of driven roller friction coefficients.

that was used to estimate torque loss due to bearing friction in the idle rollers is given in the following; this torque loss estimate was used in the model simulation. The idea is to use measurements from two pairs of load cells, each pair mounted on idle rollers which are separated by a known number of idle rollers in the unwind section of the EWL, i.e., there are a fixed number of idle rollers between the two load cell rollers within the unwind section. To illustrate the procedure consider a simple configuration like the one shown in Fig. 2.6 with load cells on two consecutive identical idle rollers.

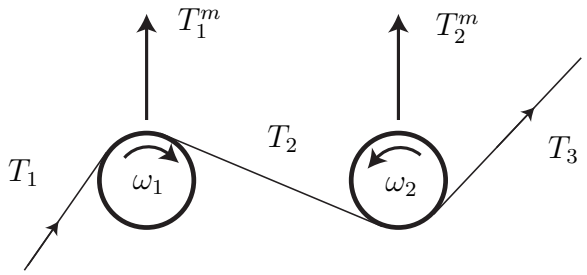

Figure 2.6: Simple Configuration for Identification of Bearing Friction Loss in Idle Rollers

The dynamic equations for the two rollers are

$$\begin{aligned} J\dot{\omega}_1 &= -\tau_f + R(T_1 - T_2), \\ J\dot{\omega}_2 &= -\tau_f + R(T_2 - T_3) \end{aligned} \tag{2.34}$$

where τ_f denotes the bearing friction torque. The tension measured by the load cells is an average of the tensions in adjacent spans, that is,

$$T_1^m = \frac{T_2 + T_1}{2}, \qquad T_2^m = \frac{T_3 + T_2}{2} \tag{2.35}$$

where T_i^m denotes the tension measured by load cells on the i^{th} roller. At the steady-state condition one can assume constant rotational speed for the idle

rollers; from equations (2.34) one can obtain the following:

$$\begin{aligned} 0 &= -\tau_f + R(T_1 - T_2) \\ 0 &= -\tau_f + R(T_2 - T_3) \end{aligned} \tag{2.36}$$

which gives

$$0 = -2\tau_f + R(T_1 - T_3). \tag{2.37}$$

Since

$$T_1^m - T_2^m = \frac{T_1 - T_3}{2}, \tag{2.38}$$

an expression for the friction torque is

$$\tau_f = R(T_1^m - T_2^m) \tag{2.39}$$

This expression for the friction torque based on the two measurements only applies for this simple configuration. The EWL is equipped with two load cell mounted rollers in the unwind section, one at R3 and the other at R9 (see Fig.2.4) and there are five additional idle rollers including the two guide rollers in between the two load cell rollers. Following the same procedure as was done for the simple configuration, the equations at steady-state are

$$\begin{aligned} 0 &= -\tau_{f1} + R(T_1 - T_2) \\ 0 &= -\tau_{f2} + R(T_2 - T_3) \\ &\vdots \\ 0 &= -\tau_{f7} + R(T_7 - T_8) \end{aligned} \tag{2.40}$$

Addition of the above equations results in

$$\sum_{i=1}^{7} \tau_{fi} = R(T_1 - T_8). \tag{2.41}$$

By assuming

$$T_1^m \simeq T_1 \qquad T_2^m \simeq T_8, \tag{2.42}$$

it is possible to define the average friction torque as

$$\bar{\tau}_f = \frac{\sum_{i=1}^{7} \tau_{fi}}{7} = \frac{R(T_1^m - T_2^m)}{7}. \tag{2.43}$$

Note that the friction torque will depend on the angular velocity of the idle roller. The following friction model which is a linear combination of a constant term and a viscous term is considered:

$$\tau_f = -c - b\omega \tag{2.44}$$

To estimate the parameters, b and c, in (2.44) the machine is run at N different line speeds. For each experiment the angular velocity of the idle rollers ω_i, the friction torque τ_{fi} are computed using (2.43). This gives N pairs of (ω_i, τ_{fi}) that can be used to estimate the friction parameters b and c by solving the following minimization problem:

$$\min_{b,c} \sum_{i=1}^{N} (-c - b\omega_i - \tau_{fi})^2 \tag{2.45}$$

For the friction model considered in (2.44), this minimization problem is a linear regression.

Table 2.2 shows the results from a set of experiments performed on the EWL following the procedure described previously. The linear regression of the data

Line speed [FPM]	100	150	200	250	300	350
ω [rad/s]	13.33	20	26.66	33.33	40	46.66
$T_1^m - T_2^m$ [lbf]	0.755	0.84	0.905	0.865	0.935	0.97

Table 2.2: Idle Roller Friction Loss Data at Various Line Speeds

reported in Table 2.2 gives the following values for the friction model coefficients:

$$c = 0.0127 \text{ [lbf-ft]}, \qquad b = 1.054\text{e-}4 \left[\frac{\text{lbf-ft}}{\text{rad/s}}\right] \tag{2.46}$$

2.3.4 Results from Web Line Simulation Using the Primitive Element Models

The initial set of experiments consisted of a step change in tension reference with zero line speed. The purpose of these experiments was to verify if the model is capable of reproducing tension behavior when speed induced disturbances are not present. Different reference values were tested with different gains for the tension PI. A sample result for a step in tension of 20 lbf is shown in Fig. 2.7. All the experiments showed that the model simulated data can follow the experimental data closely.

The second set of experiments considered also a step change in tension reference, but with a non-zero line speed. In this case, speed induced disturbances are observed in the tension signal and it is necessary to verify if the model is able to reproduce these speed induced disturbances. For this case different step changes and different PI gains were tried. Data from one of the experiments is shown in Fig. 2.8. In general, the model simulated data appears to be able to follow the average value of the tension but does not reproduce the speed induced oscillations. From these preliminary experiments the need for modifications to the existing model to capture the speed induced disturbances is clear.

2.4 Investigation of the Frequency Content in the Tension Signal

The tension disturbances that are measured experimentally show a sinusoidal behavior. The Fast Fourier Transform (FFT) of the signal can be used to analyze the frequency content in the tension signal. Under the assumption that the tension

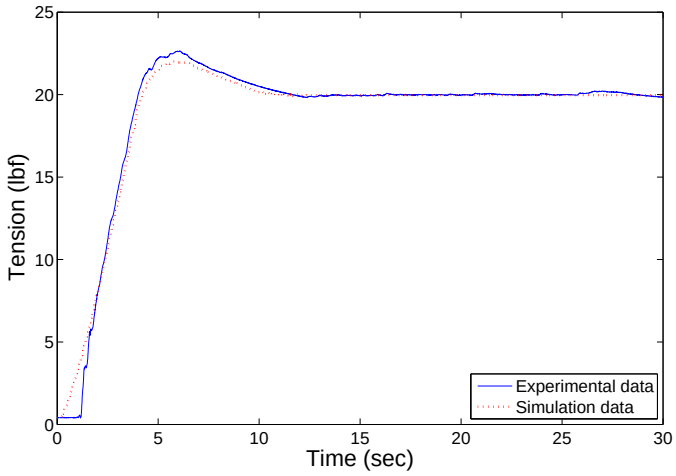

Figure 2.7: Experimental and simulated data comparison for a step reference change of 20 lbf with zero line speed.

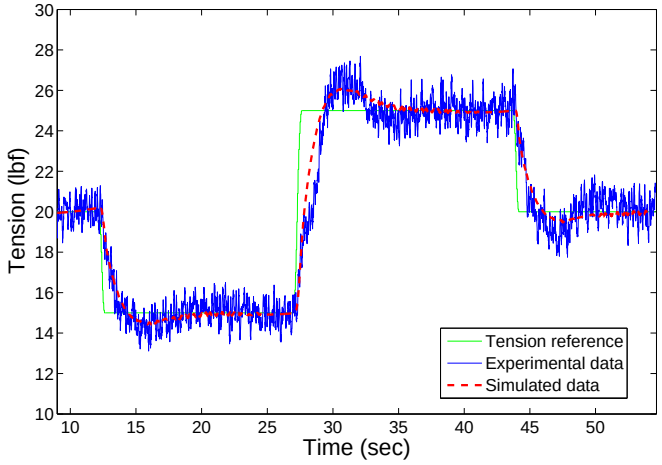

Figure 2.8: Comparison of experimental and simulated data for step reference changes with non-zero line speed.

oscillations are due to rotating machinery, there must be a correlation between the rotational frequency of the rollers and some of the frequency components in the tension signal. Consider a web line operating at line speed v [FPM], and consider a non-ideal roller of radius R [in], then the rotational frequency f [Hz] of the roller is given by

$$f = \frac{v}{10\pi R} \tag{2.47}$$

Also the integer multiples of the frequency in (2.47) in the tension signal can be generated from the same rotating element. The reasons why the higher order harmonics are generated will be discussed in the following chapters.

Note that in the case of a non-ideal roll the radius will be time varying as the material is released or accumulated on the roll, therefore the frequencies of the induced tension disturbances will be time varying.

These observations can be verified with systematic experimentation. Figure 2.9 shows the FFT of a tension signal collected on the EWL while running the machine at a web velocity of 200 FPM with unwind radius of 6.375 in; using these values in (2.47) one obtains $f = 0.97$ Hz. It is clear from Fig. 2.9 that the tension signal contains the frequency f and its higher order harmonics. To further consolidate the claim that the oscillations are due to the non-ideal material roll, other velocities have been tested. The values of the fundamental frequency computed through equation (2.47) at 100 FPM, 200 FPM and 300 FPM, respectively with the same radius of 6.375 in, are 0.485 Hz, 0.97 Hz and 1.455 Hz. Figure 2.10 shows the first peak of the FFT of the data at different velocities. Results show a match between the computed values and the experimental data, this provide a justification of how part of the disturbance frequencies can be linked to the non-ideal behavior of the unwind roll.

It is also possible to show that some of the disturbance frequencies are instead

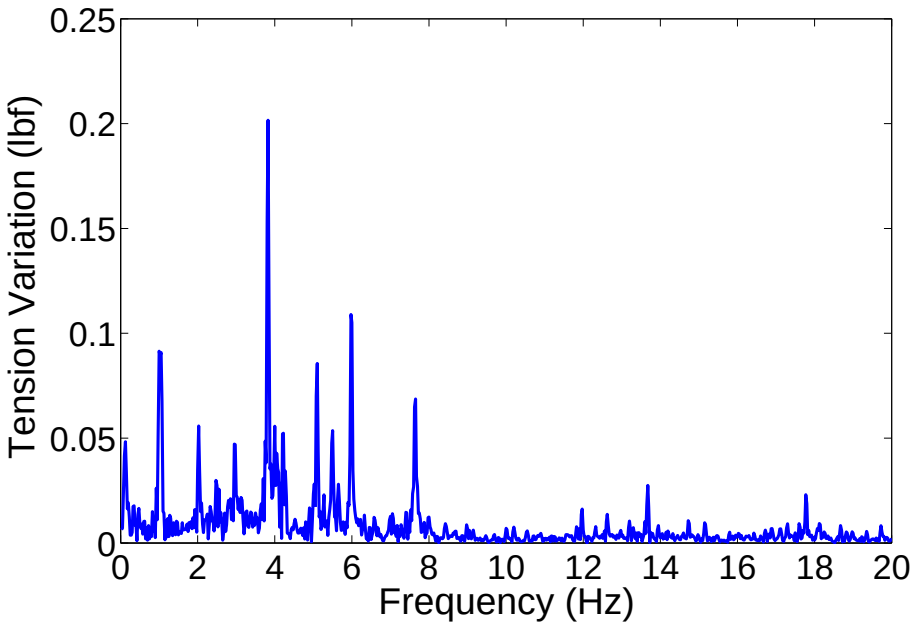

Figure 2.9: Experimental data; line speed=200 FPM, unwind radius=6.375 in

due to idle and driven rollers. A set of experiment was performed to isolate the oscillations due to eccentric rollers in the FFT of the tension signal from the one due to out-of-round material roll. Since the frequencies due to a non-ideal material roll are time dependant they will move if the FFT of the tension signal is taken at different radii and line speeds, whereas frequencies induced by rollers will maintain the same value for the same speed of the line. This strategy can be employed to identify the frequencies which are not due to the non-ideal material roll. Experiments were conducted at 200 FPM with different values for the radius of the material roll. The results are plotted in Fig. 2.11. First, it can be observed that the fundamental disturbance frequency due to the out-of-round material roll changes when the radius changes. Note that for radius values of $R_a = 6.75$ in, $R_b = 5.75$ in and $R_c = 4.75$ in, the corresponding fundamental disturbance frequencies due to the material roll are $f_a = 0.94$ Hz, $f_b = 1.11$ Hz

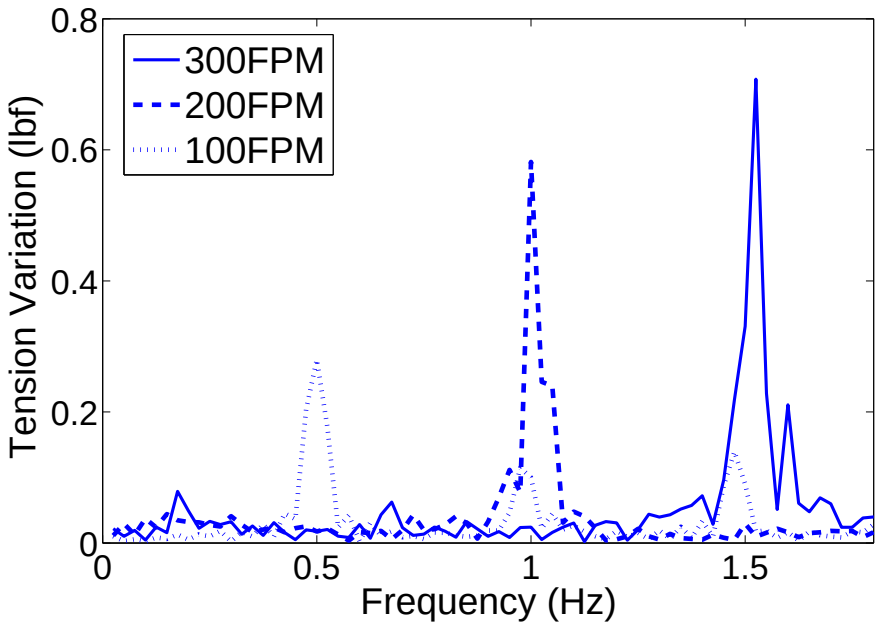

Figure 2.10: First peak of the FFT with different web velocities

and $f_c = 1.34$ Hz, which can be clearly seen in Fig. 2.12. One can also observe the presence of different disturbances that are not affected by the change in unwind roll radius, particularly evident are the values $f_1 = 1.05$ Hz (see Fig. 2.13(a)) and $f_2 = 4.23$ Hz (see Fig. 2.13(b)). The disturbance frequencies that are not affected by the radius change must be due to non-ideal rollers. It is also important to note that $f_2 = 4f_1$. Therefore, assuming that f_1 is the fundamental frequency of a disturbance due to an eccentric roller, then f_2 is its forth harmonic. Using (2.47) it is possible to determine the radius of the roller causing these disturbances. The radius corresponding to the frequency f_1 is:

$$R_1 = \frac{v}{10\pi f_1} = 6.05 \text{ in} \tag{2.48}$$

which is the radius of the S-wrap rollers.

These experiments show sufficient evidence to link the tension oscillations to the non-ideal behaviors of rotating elements such us a material roll or idle/driven

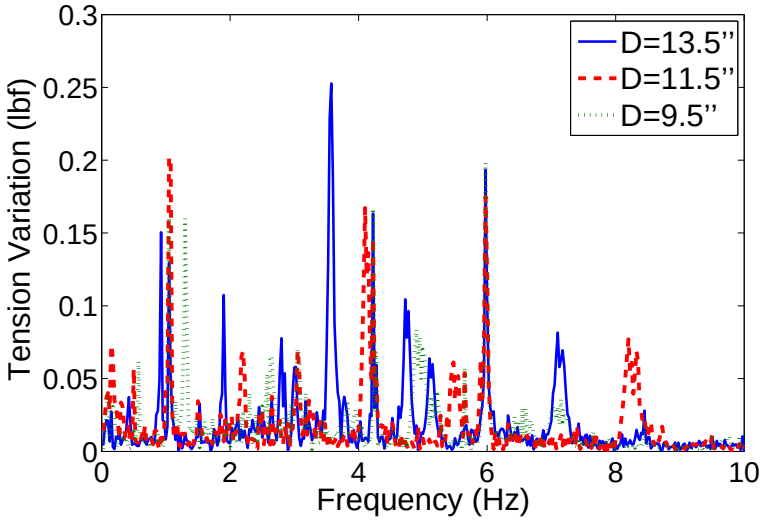

Figure 2.11: Experimental data with material roll at different radii (line speed = 200 FPM)

rollers. One way a roll or roller can show non-ideal behavior is because of eccentricity. Eccentricity occurs when the center of rotation of the roller is different from its geometrical center. Chapter 3 will focus on modeling of eccentric rollers and its effects on the governing equations of web tension and velocity. For the case of a material roll, non-ideal behavior can also be due to the roll being out-of-round. This situation with the material roll introduces additional challenges which will be discussed in chapter 4.

In this chapter experimental model validation was shown for the fundamental primitive elements. The models were able to reproduce the macroscopic behavior recorded in the experimental data, therefore these models can be used for control design in all those situations where the attenuation of the tension oscillations is not required or the tension oscillations are not significant. Also, a procedure to identify the source of the tension oscillations has been presented.

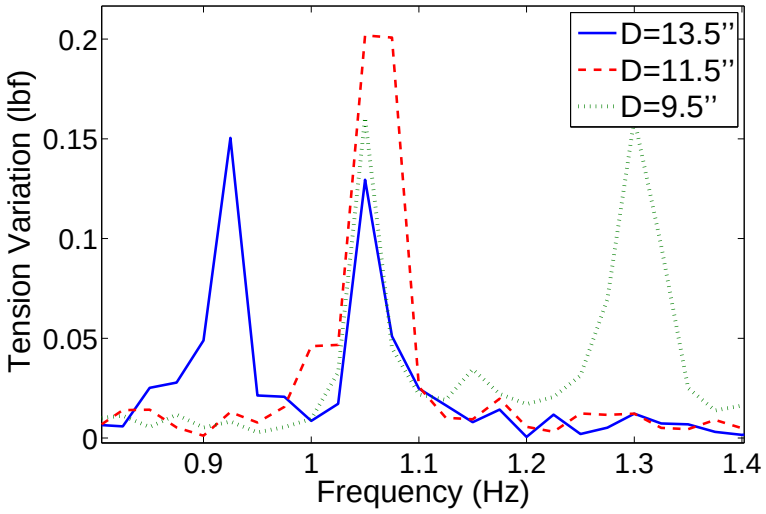

Figure 2.12: First peak due to out-of-round material roll

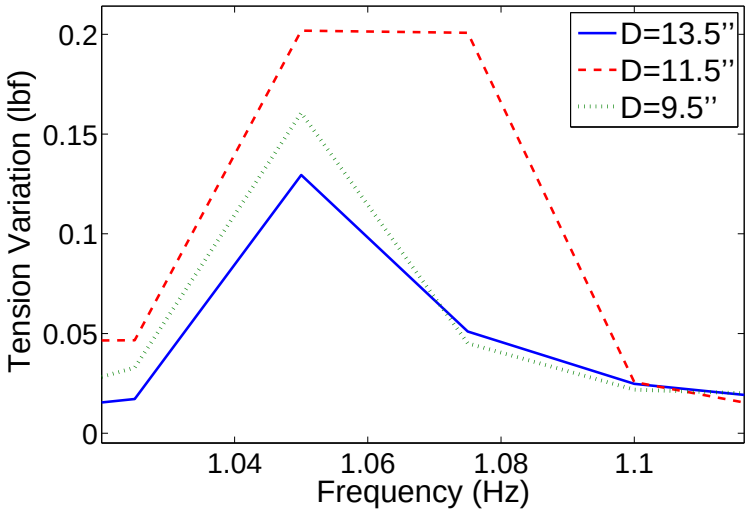

(a) Zoom around $f_1 = 1.05$ Hz

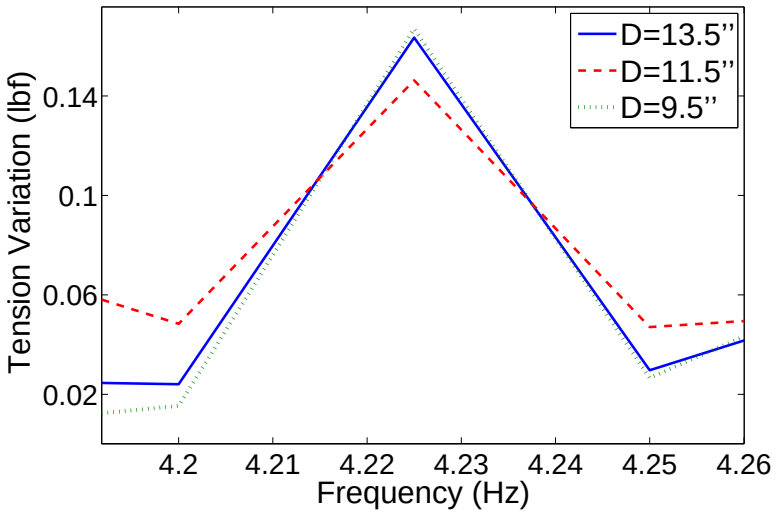

(b) Zoom around $f_2 = 4.23$ Hz

Figure 2.13: Zoom of FFT around disturbance frequencies due to S-wrap roller.

Chapter 3

Governing Equations for Web Velocity and Web Tension in the Presence of Eccentric Rollers

A roller is said to be eccentric if the center of rotation and the geometric center do not coincide, and the deviation from the geometric center to the center of rotation is called the eccentricity of the roller.

From the analysis of the frequency content of the measured tension signal, oscillations due to an eccentric roller may be readily distinguished. In particular, given the line speed and the radius of the eccentric roller, one can identify the fundamental frequency of the oscillations and its higher order harmonics. In order to reproduce in model simulations both the fundamental frequency and its harmonics, it is necessary to modify the governing equations for web velocity on the eccentric roller and web tension in span adjacent to the eccentric roller.

One key aspect that is identified is that the change in span length that is adjacent to an eccentric roller causes tension oscillations. The web span tension model is refined to include the change in span length due to non-ideal rollers.

Model simulations require computation of the change in span length. For the case of the eccentric roller, derivation of a closed form expression for the web span length as function of the angular displacement of the eccentric roller is given. By including the closed form expression for the web span length in the span tension model, one can improve the accuracy of the model simulations. In addition, the closed form expression for span length adjacent to an eccentric roller facilitates better understanding of the intrinsic connection between the rotational motion of the eccentric roller and the tension behavior in the spans, which provides insights into why higher order harmonics are found in the tension signal.

Because of the eccentricity of the roller, the governing equation for the eccentric roller angular velocity must be modified to include the additional torque acting on the roller due to the fact that the center of mass and the center of rotation are not coincident. Moreover, the torques on the eccentric roller due to the tensions in web spans adjacent to the eccentric roller are different and are functions of the angular position of the roller because the wrap angle changes with the rotation of the eccentric roller. These aspects are discussed in this chapter, and governing equations for web velocity on an eccentric roller and web tension in adjacent spans are developed.

To verify that these new models provide improved correlation between model simulations and experiments, a number of experiments are performed on the EWL. Comparison of the data from experiments and model computer simulations show that the new models are able to closely predict experimentally observed behavior.

3.1 Modeling in the Presence of an Eccentric Roller

The governing equation for web span tension in (2.22) was derived under the assumption that the web span length is constant. In the presence of a non-ideal roller or roll adjacent to the web span, this assumption does not hold anymore. In fact, as the non-ideal element rotates the point where the web leaves the surface of the roller changes with time and hence the web span length will be time varying. Because of this (2.22) cannot be used and (2.21):

$$\dot{T}_i = \frac{v_i(EA - T_i) - v_{i-1}(EA - T_{i-1}) + (EA - T_i)\dot{x}_i - (EA - T_i)\dot{x}_{i-1}}{(x_i - x_{i-1})}$$

must be used instead. The above governing equation for web tension in the i-th span can be simplified by defining the length for the free span as $L_i = x_i - x_{i-1}$:

$$\dot{T}_i = \frac{v_i(EA - T_i) - v_{i-1}(EA - T_{i-1}) + \dot{L}_i(EA - T_i)}{L_i} \tag{3.1}$$

The solution of the above governing equation requires computation of the span length. In the following the span length and its derivative will be computed as function of the angular displacement and the velocity of the eccentric roller. To reproduce all the harmonics in the measured tension signal due to the presence of the eccentric roller it is not sufficient to include only the effect of the span length but it is also necessary to modify the governing equation for web velocity on the eccentric roller. The motion of an eccentric roller will affect web tension in adjacent spans via the influence on two aspects: (1) change in length of the spans adjacent to the roller and (2) additional (gravity induced) torque acting on the eccentric roller due to imbalance which will result in a different surface velocity at each point on the eccentric roller. These two issues will be discussed

in this chapter. The length of the web in the spans adjacent to the eccentric roller as a function of its angular displacement will be derived first followed by an appropriate modification of the governing equation of the eccentric roller.

3.1.1 Derivation of Length of Web Spans Adjacent to an Eccentric Roller

Consider a span where the downstream roller is eccentric and the upstream roller is ideal. For deriving the web span length between the two rollers one has to determine the points where the web leaves the upstream ideal roller and the point where the web enters the downstream eccentric roller. For the eccentric roller the point at which the web leaves that roller changes with the rotation of the roller; therefore, one has to determine this point as a function of the angle of rotation of the roller.

Consider a span between two ideal rollers for the initial setup of the problem, and the downstream roller will be subsequently modified to an eccentric roller. Two configurations are possible for a web span between any two rollers, underwrap and overwrap. These are shown in Fig. 3.1. The under-wrap configuration is considered first. Since the line segment $\overline{ED}$ is tangent to both the rollers, the two right-angled triangles AEB and ADC are similar. Therefore, the angles $A\widehat{B}E$ and $A\widehat{C}D$ are equal, and so are the angles $B\widehat{A}E$ and $C\widehat{A}D$. This fact will be used to derive an equation for the length of the segment $\overline{DE}$.

The angles $A\widehat{B}E$ and $A\widehat{C}D$ being equal results in

$$\frac{R_1}{\overline{AB}} = \frac{R_2}{\overline{AC}} \quad \Rightarrow \quad \overline{AB} = \overline{AC}\frac{R_1}{R_2}. \tag{3.2}$$

Also, the distance between the centers of the two rollers is given by

$$d = \overline{AB} + \overline{AC}. \tag{3.3}$$

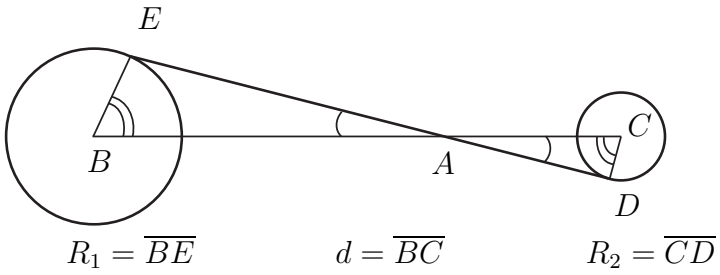

(a) Under-wrap Configuration

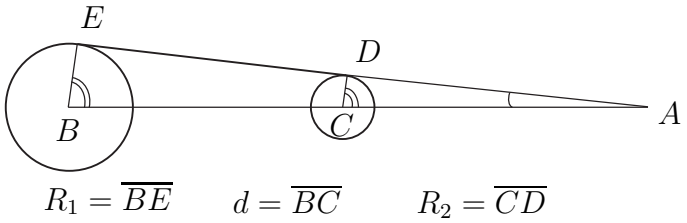

(b) Over-wrap Configuration

Figure 3.1: Roller Configurations

Solving (3.2) and (3.3) results in

$$\overline{AC}(d) = \frac{d}{1 + \frac{R_1}{R_2}}. \tag{3.4}$$

Therefore, the angle $A\widehat{C}D$ as function of $\overline{AC}$ is given by

$$A\widehat{C}D(d) = \text{acos}\frac{R_2}{\overline{AC}(d)}. \tag{3.5}$$

To define the coordinates of the contact points which will be used to determine the web span length, one must define an appropriate coordinate axis. To do this it is simpler to first consider a span between two ideal rollers. Consider a coordinate axis located at the center of the upstream roller with its abscissa (x-axis) along the line joining the two rollers.

Given the Cartesian coordinates for $B \equiv (X_B, Y_B)$ and $C \equiv (X_C, Y_C)$, the

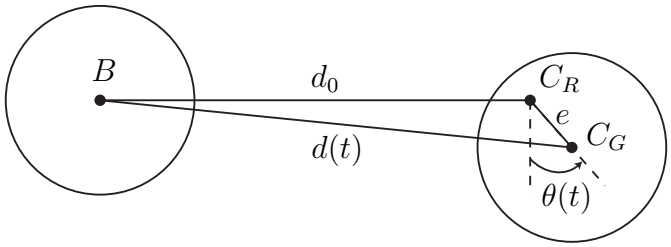

Figure 3.2: Eccentric idle roller: C_G is the geometric center, C_R is the center of rotation, e is the eccentricity, d_0 is the distance between the centers of rotation of the two rollers, and $d(t)$ is the distance between the geometric centers of the two rollers.

coordinates for $D(d)$ and $E(d)$ are

$$\begin{aligned} D(d) \equiv (X_D, Y_D) &= \begin{bmatrix} X_C - R_2 \cos(A\widehat{C}D(d)) \\ Y_C - R_2 \sin(A\widehat{C}D(d)) \end{bmatrix}, \\ E(d) \equiv (X_E, Y_E) &= \begin{bmatrix} X_B + R_1 \cos(A\widehat{C}D(d)) \\ Y_B + R_1 \sin(A\widehat{C}D(d)) \end{bmatrix}, \end{aligned} \tag{3.6}$$

and the span length is given by

$$L(d) = \sqrt{(X_D(d) - X_E(d))^2 + (Y_D(d) - Y_E(d))^2}. \tag{3.7}$$

By substituting (3.6) in (3.7) a simplified expression for the span length may be derived, which is given below:

$$L(d) = \sqrt{d^2 - R_1^2 - 2R_1R_2 - R_2^2}. \tag{3.8}$$

In the presence of an eccentric roller the distance d between the geometric centers of the idle rollers varies with the rotation of the eccentric roller because the center of the eccentric idler will be rotating. In order to use the previous procedure it is necessary to determine the value of $d(t)$. Let d_0 be the distance

between the centers of rotation and e be the eccentricity (see Fig. 3.2). The expression for $d(t)$ is given by

$$d(t) = \sqrt{(d_0 + e\sin(\theta(t)))^2 + (e\cos(\theta(t)))^2} = \sqrt{d_0^2 + 2e\,d_0\sin(\theta(t)) + e^2} \quad (3.9)$$

where $\theta(t)$ is the angle of rotation of the eccentric roller (see Fig. 3.2). The closed-form equation for the span length in the case of an eccentric roller is obtained by combining (3.8) and (3.9):

$$L(t) = \sqrt{d_0^2 + 2e\,d_0\sin(\theta(t)) + e^2 - R_1^2 - 2R_1R_2 - R_2^2}. \quad (3.10)$$

The time derivative of span length also appears in the governing equation for web tension in a span (see (3.23)); this is given by differentiating (3.10):

$$\dot{L}(t) = \frac{d_0 e\omega(t)\cos(\theta(t))}{L(t)} \quad (3.11)$$

where $\omega := \dot{\theta}$ is the angular velocity of the eccentric roller.

A similar approach can be taken to develop the span length for the over-wrap configuration. The first step is to find an expression for the length L as function of the distance between the geometric centers of the rollers (see Fig. 3.1(b)). In this case the angles $B\widehat{A}E$ and $C\widehat{A}D$ are equal. Since the triangles AED and ADC are right-angled, it is possible to find the sine of the angle $B\widehat{A}E$:

$$\sin(B\widehat{A}E) = \frac{R_2}{\overline{AC}} = \sin(C\widehat{A}D) = \frac{R_1}{\overline{AB}} = \frac{R_1}{d + \overline{AC}}. \quad (3.12)$$

Solving the above equation for $\overline{AC}$ gives

$$\overline{AC}(d) = \frac{R_2 d}{R_1 - R_2} = \frac{d}{\frac{R_1}{R_2} - 1}. \quad (3.13)$$

From $\overline{AC}(d)$ it is possible to find the angle $A\widehat{C}D$ as

$$A\widehat{C}D(d) = \operatorname{acos}\frac{R_2}{\overline{AC}(d)}. \quad (3.14)$$

The angle $A\widehat{C}D$ is also equal to $B\widehat{A}E$, which can be used to find the coordinates of the points $D(d)$ and $E(d)$:

$$\begin{aligned} D(d) \equiv (X_D, Y_D) &= \begin{bmatrix} X_C + R_2 \cos(A\widehat{C}D(d)) \\ Y_C + R_2 \sin(A\widehat{C}D(d)) \end{bmatrix} \\ E(d) \equiv (X_E, Y_E) &= \begin{bmatrix} X_B + R_1 \cos(A\widehat{C}D(d)) \\ Y_B + R_1 \sin(A\widehat{C}D(d)) \end{bmatrix} \end{aligned} \tag{3.15}$$

Note that $d(t)$ for the over-wrap configuration is also given by (3.3). Substitution of $d(t)$ obtained using (3.3) into (3.15) gives the time dependant coordinates of D and E. After simplification the closed-form expression for span length for the over-wrap configuration is given by

$$L(t) = \sqrt{d_0^2 + 2e\, d_0 \sin(\theta(t)) + e^2 - R_1^2 + 2R_1R_2 - R_2^2}. \tag{3.16}$$

3.1.2 Governing Equation for Angular Velocity of an Eccentric Roller

A sketch showing the forces acting on a web wrapped eccentric roller, the key distances, and the key angles that are required for writing the governing equations for the rotational motion of the eccentric roller is shown in Fig. 3.3. Due to the rotation of the eccentric roller the web entry point on the surface of the roller varies, and as a result d_{en} and d_{ex} also vary. These must be taken into account in the angular position and angular velocity governing equations for the eccentric roller which are given by

$$\begin{aligned} \dot{\theta} &= \omega \\ J\dot{\omega} &= -b_f\omega - T_{i-1}d_{en}\cos\theta_{en} + T_i d_{ex}\cos\theta_{ex} + mge\sin\theta. \end{aligned} \tag{3.17}$$

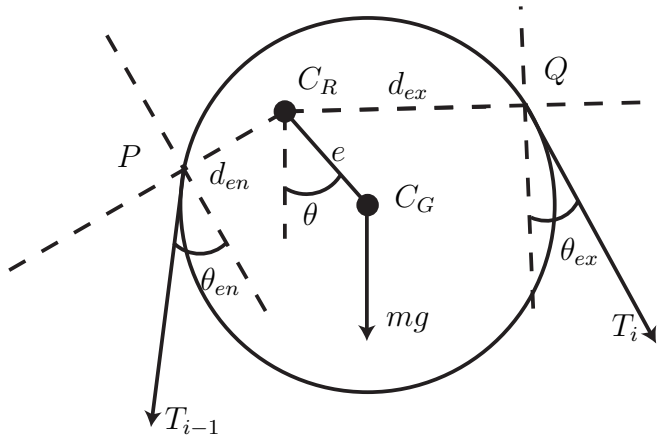

Figure 3.3: Eccentric idle roller: C_G is the geometric center, C_R is the center of rotation, e is the amount of eccentricity, P is the web entry point, Q is the web exit point, d_{en} is the distance between the center of rotation and the web entry point, and d_{ex} is the distance between the center of rotation and the web exit point.

In (3.17), d_{en}, d_{ex}, θ_{en}, θ_{ex} are all functions of θ and can be derived based on the analysis presented in the previous section.

Figure 3.4 shows the relationship between the angles at the entry contact point. Employing the cosine law, the following expression for the cosine of the angle θ_{en} can be obtained:

$$\cos(\theta_{en}) = \frac{R^2 + d_{en}^2 - e^2}{2Rd_{en}}. \tag{3.18}$$

To find d_{en}, the coordinates of the points P and C_R in the same coordinate axes must be found first. Equation (3.6) gives the coordinates of the point P in a coordinate axes having the origin at the geometric center of roller $i-1$ and the x-axis aligned with line joining the geometric centers of the two rollers (note that in the case of the eccentric roller the distance d between the geometric centers of

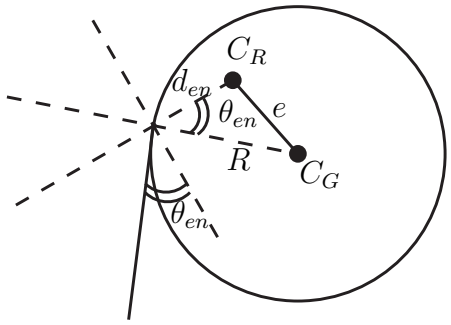

Figure 3.4: The angle θ_{en} is determined by using the the cosine law on the triangle with sides d_{en}, R and e.

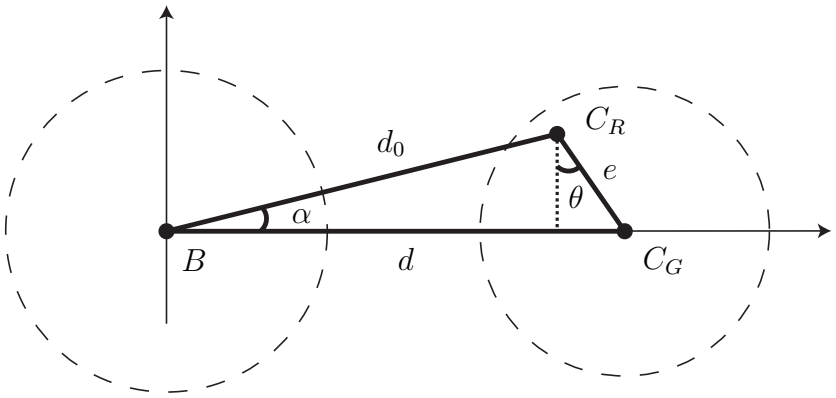

Figure 3.5: Figure to determine the coordinates of C_R in the frame having the x-axis aligned with the line joining the geometric centers of the rollers (for computation of d_{en} using (3.22)).

the rollers is function of θ; therefore, P is also function of θ). The coordinates of the center of rotation C_R in this reference frame are (see fig. 3.5)

$$C_R = \begin{pmatrix} d_0 \cos(\alpha) \\ d_0 \sin(\alpha) \end{pmatrix}. \tag{3.19}$$

Using again the cosine law for angle α as in

$$e^2 = d_0^2 + d^2(\theta) - 2d_0 d(\theta)\cos(\alpha) \tag{3.20}$$

and using the expression of $d(t)$ in (3.9), an expression for $\cos(\alpha)$ may be given

by

$$\cos(\alpha) = \frac{d_0 + e\sin(\theta)}{d(\theta)}. \tag{3.21}$$

Equipped with equations (3.6), (3.19), (3.21), the expression for the distance $d_{en}(\theta)$ may be obtained:

$$d_{en}(\theta) = ||P(\theta) - C_R(\theta)||. \tag{3.22}$$

A similar procedure may be used to determine d_{ex} and θ_{ex}.

The governing equation for web tension in a span (2.21) may be rewritten compactly by defining $L(t) = x_i(t) - x_{i-1}(t)$:

$$\dot{T}_i(t) = \frac{v_i(t)(EA - T_i(t)) - v_{i-1}(t)(EA - T_{i-1}(t)) + (EA - T_i(t))\dot{L}(t)}{L(t)} \tag{3.23}$$

Under the assumption that there is no slip between the roller surface and the web, the transport velocity of the web is given by $v_i = R_i\omega$; we have denoted the angular velocity as simply ω instead of ω_i to keep the notation simpler in the previous derivations. Therefore, the governing equation for web velocity on the eccentric roller may be obtained by substituting $v_i = R_i\omega$ in (3.17). From the analysis of the modified governing equations for web tension in a span and web velocity on an eccentric roller, it is possible to highlight the reasons for the presence of tension disturbances with higher order harmonics other than the rotation frequency of the roller. First, the appearance of the term $mge\sin\theta$ in the governing equation for the angular velocity of the eccentric roller indicates that there is a disturbance with frequency equal to the rotational frequency of the roller (the fundamental frequency of the tension disturbance). The governing equation for web tension (3.23) contains the angular velocity of the roller through two terms: $EAv_i = EAd_{en}\omega_i$ and $EA\dot{L} = EAd_0e\omega_i\cos\theta_i/L$. Because the angular velocity (ω_i) in the first term has the fundamental frequency of the disturbance, web tension will contain this frequency component also. Due to the multiplication of ω_i

and $\cos\theta_i$ in the second term, the second order harmonic will be present in the tension signal. Since the web tension appears linearly in the governing equation for web velocity on the roller, it will induce oscillation in the velocity signal with the first and second harmonic. Because the surface velocity of the roller has the first and the second harmonic, the multiplication of ω_i and $\cos\theta_i$ will also generate the third harmonic, and so on. It is evident that the coupling between roller surface velocity and web tension creates the higher order harmonics in the measured signals. Understanding this coupling and the consequences of having eccentric rollers is critical in designing control systems to regulate web tension.

3.2 Experiments and Model Simulations

To validate the proposed model for eccentric rollers, the Euclid Web Line (EWL) is used as an experimental platform; a sketch of the platform configuration is shown in Fig. 2.4. From experimental observations it was noted that the S-wrap lead in the EWL is eccentric. The eccentricity has been included in the computer simulations using the models presented in this chapter. The goal of the simulation and experimental study is to determine whether the models will be able to reproduce steady-state oscillations that are found in the measured tension signal. For this reason it was chosen to conduct experiments at constant web speeds and analyze the frequency content of the tension signal using the Fast Fourier Transform (FFT) of the signal data obtained from both the experiments and model simulations.

At a given web velocity v, the fundamental frequency of the tension disturbance induced by the eccentric S-wrap roller is given by

$$f_0 = \frac{v}{2\pi R_S}. \tag{3.24}$$

It is expected that the tension signal from both the model simulations and experiments will contain oscillations at the fundamental frequency and its harmonics at $2f_0, 3f_0, \ldots$, etc.

3.2.1 Results

Figures 3.6(a) and 3.6(b) show the FFT of the tension signals from experiments and model simulations, respectively, for the line speed of 200 FPM. At this line speed the fundamental frequency of the tension oscillations due to eccentricity in one of the S-wrap rollers is $f_0 = 1.06$ Hz. The presence of the fundamental frequency of the S-wrap and its higher-order harmonics is evident from the experimental data. The same frequencies can be easily recognized in the FFT of the tension data from model simulations, and the amplitude of these tension oscillations are also comparable. Note that the FFT of the experimental data has disturbances at other frequencies because of the presence of other non-ideal rotating elements in the web line which are not included in the model simulation. Figure 3.7 and Figure 3.8 show results for line speeds of 250 FPM and 300 FPM.

Note that achieving a good match in all the amplitude of the disturbance frequencies is a challenging task. In fact multiple factors contribute to the final amplitude of the disturbance frequencies. For example, the parameters for the friction model of the idle rollers identified with the method proposed in chapter 2 are not exact but only give a sense of the order of amplitude of the friction parameters. Moreover, the real parameters are sensible to the operative condition of the machine and can change from one run to the next. Also, the amplitude of the oscillations depends on the frequency response of the system of web spans and idle rollers. The portion of the web machine between two driven rollers

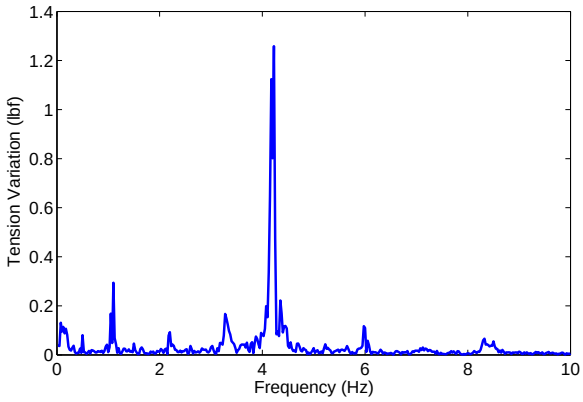

(a) FFT of the experimental data.

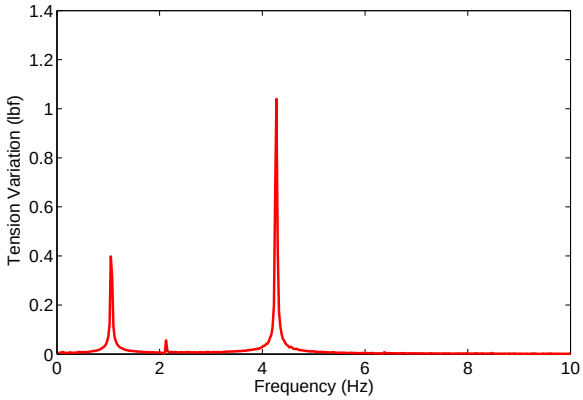

(b) FFT of the simulated data.

Figure 3.6: Comparison between experimental and simulation data at 200 FPM

can be considered as a system of masses (the idle rollers) and springs (the web span). Like a system of masses and springs the system of idle rollers and web spans will have its frequency response and it will amplify disturbances close to the resonance frequencies of the system. In order to have in simulation the same frequency response of the real system is necessary to have a good estimation of the inertias of the idle rollers, the length of the web spans and the Young modulus of the web. While computation of the inertias and measurements of the web span can be obtained with good precision, estimation of the Young modulus are not very accurate.

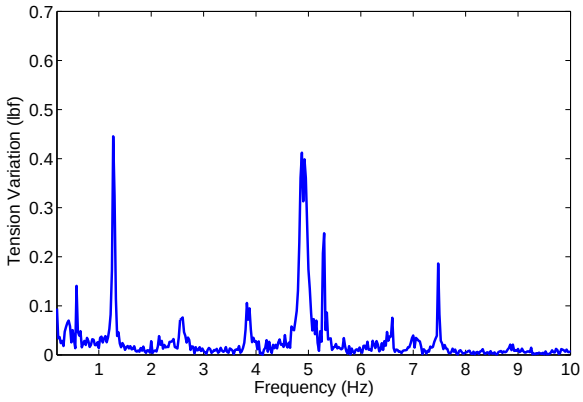

(a) FFT of the experimental data.

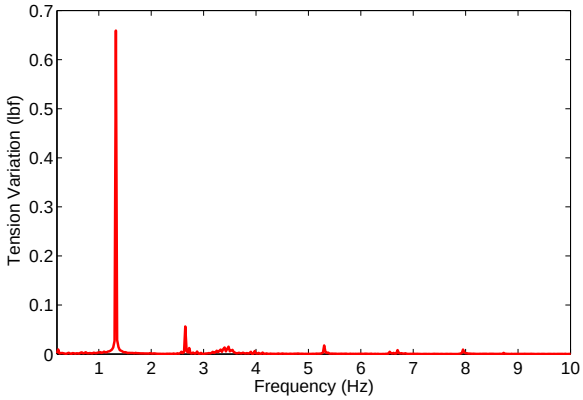

(b) FFT of the simulated data.

Figure 3.7: Comparison between experimental and simulation data at 250 FPM

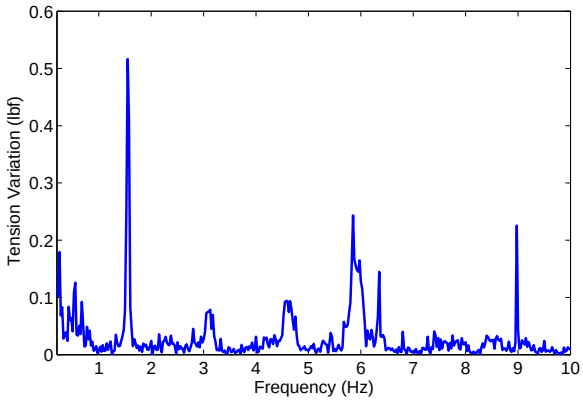

(a) FFT of the experimental data.

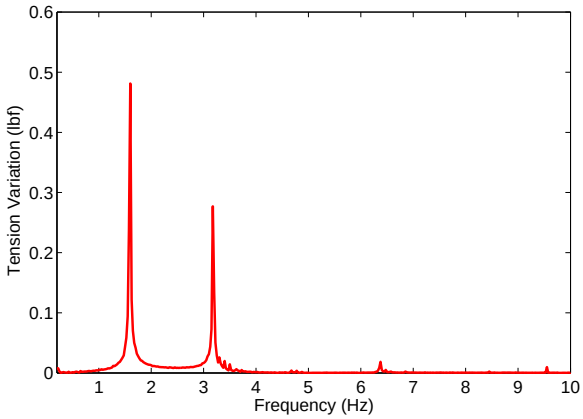

(b) FFT of the simulated data.

Figure 3.8: Comparison between experimental and simulation data at 300 FPM

Chapter 4

Governing Equations for Web Velocity and Web Tension in the Presence of an Out-of-Round Roll

The discussion in Chapter 2 demonstrated that some of the oscillations found in the tension signal can be associated to the presence of a non-ideal material roll. To a certain extent the manner in which the presence of an out-of-round roll affects web tension and velocity is similar to the case of an eccentric roller. Again both the governing equations for web tension and web velocity need to be modified to reproduce in model simulations the oscillations found in the measured signal.

Similar to the case of the eccentric roller if a material roll is out-of-round, the length of the web span between the material roll and the idle roller adjacent to it will be time varying. Variations in span length induce variations in tension as described by equation (3.1). To reproduce in simulations the oscillations due to the out-of-round material roll the first step is to find an expression for the time varying web span length. This is a considerably harder problem for the out-of-round material roll than the eccentric roller discussed in Chapter 3. Even for a

simple roll shape, a closed form expression for the web span length cannot be found and only numerical approximation can be derived. The first part of the chapter is dedicated to the development of an algorithm for the computation of the span length as function of the angular displacement of the out-of-round roll.

The problem of finding the span length can be summarized as follows. Given a generic profile for the out-of-round unwind material roll, compute the length of the adjacent span as a function of time as the material is released from the roll. It is assumed that the downstream roller is perfectly circular.

As a starting point, in Section 4.1, an elliptical material roll is taken into consideration. An analytical approach to the problem did not provide any insights into finding a closed form expression for the span length as a function of angular displacement of the material roll. To overcome this problem a convex optimization problem is formulated and an efficient numerical approach is developed to obtain the common tangent to the material roll and the downstream roller. Once the common tangent is obtained, the span length and rate of change of span length may be found numerically as well.

The case of the convex shaped material roll is considered in Section 4.2; one example that is common in practice, and falls into this category, is a roll with a flat spot. This situation presents additional challenges over that of the elliptical roll. First, it is necessary to find an efficient way to characterize the shape of the roll. Then an expression for the tangent of the roll for any point on its surface must be derived. And finally, an optimization problem may be formulated to find the common tangent to both the material roll and the downstream roller.

The modification to the velocity equations is described in Section 4.2.1. Three main adjustments are made to the ideal model. First, the center of mass of the roll might not coincide with the center of rotation. In this case an additional

torque due to gravity has to be included in the model. Second, the arm length of the torque due to the tension in the first span is not equal to the radius of the roll; it is time varying and it must be computed for solving the velocity equations. Lastly, the expression for the roll inertia needs to be obtained and it differs from the case of the ideal roll.

After including the modifications to the governing equations of web tension and web velocity, a series of experiments was performed to verify the proposed model. Section 4.3 gives a discussion of the results obtained from the comparison of the experimental data with data from model simulations. Since the results of the comparison showed poor correlation between the two sets of data, it was evident that the model needed further improvements and this was the motivation for the modification of the governing equation of web tension described in Section 4.4. To understand the reasoning for this last modification one has to revert back to the first principles derivation of governing equations. In particular the governing equation for web tension is obtained applying the law of conservation of mass for the control volume containing the web span, i.e., at any instant in time the variation of mass in the control volume is equal to the difference of entering and exiting material flow rate. In the case of an ideal roll it can be shown that the peripheral velocity of the web on the neighboring rolls is proportional to the material flow rate. Section 4.4 provides a discussion about how in the presence of a non-ideal roll the the peripheral velocity and the material flow rate are not proportional. An explicit expression for the material flow rate has to be computed instead, without relying on it being proportional to the peripheral velocity. The chapter is concluded with the discussion of the comparison of the data from model simulations and experiments after an explicit expression for material flow rate is included in the model.

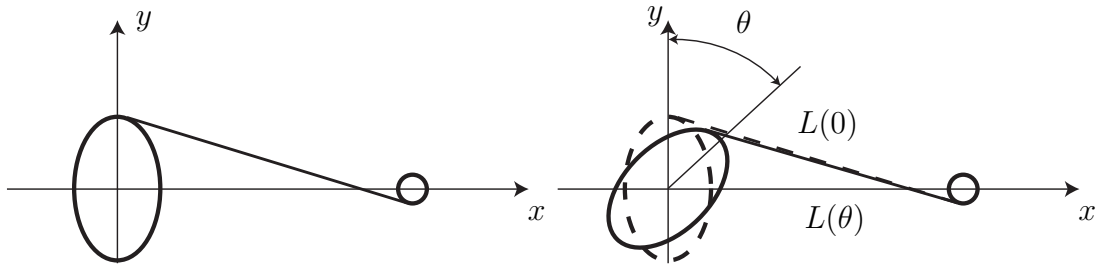

(a) Elliptical unwind roll in the initial position. (b) Elliptical unwind roll rotated by θ.

Figure 4.1: Example of an out-of-round material roll.

4.1 Elliptically Shaped Material Roll

Consider the case of an elliptical unwind roll, and suppose that the major axis of the ellipse coincides with the y axis of the Cartesian coordinate axis as shown in Fig. 4.1(a). In order to compute the length of the span, the line tangent to both the ellipse and the downstream roller must be found. When the material roll rotates by an angle θ (see Fig. 4.1(b)), the point of release of the material changes and so does the span length, which is a function of the angular displacement θ. Finding an analytical expression for $L(\theta)$ is not a trivial problem since the system of equations that must be solved is nonlinear. In fact, it is difficult to find a solution in closed form even for this simple shape. One way the problem can be approached is as follows: given a point P_0 on the ellipse, find the line $\mathbf{t}$ tangent to the ellipse at that point. If the distance between the line $\mathbf{t}$ and the center of the idle roller is equal to the radius of the idle roller, then the line $\mathbf{t}$ is tangent to both the ellipse and the roller and hence it is the desired line. Once the tangent $\mathbf{t}$ is found, finding the length L is straightforward. An illustration of how this construction works is shown in Fig. 4.2. The same figure shows that there are two tangents $\mathbf{t_2}$ and $\mathbf{t_3}$ which satisfy the previous condition; this will also cause additional difficulties when the problem is solved numerically. The procedure is

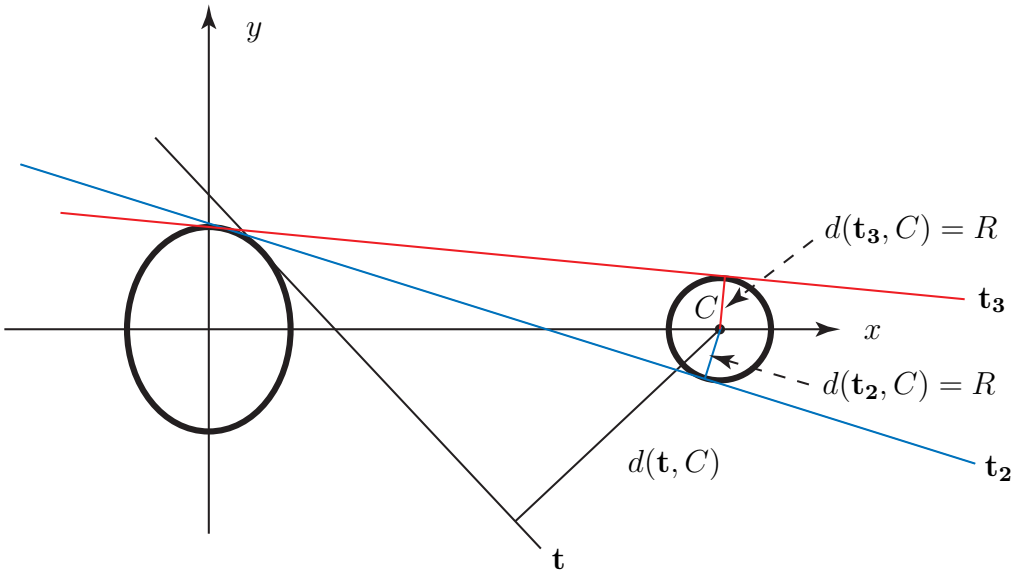

Figure 4.2: Procedure to find the length of the span.

explained in more detail in the following.

Consider an ellipse $\mathbf{e}$, representing the material roll, centered at the origin of the Cartesian reference frame with the equation:

$$\mathbf{e} : \frac{x^2}{a^2} + \frac{y^2}{b^2} - 1 = 0. \tag{4.1}$$

Note that this equation only describes an ellipse centered at the origin with major and minor axes along the axes of the Cartesian coordinate system. Also consider a circle centered at $C \equiv (x_c, y_c)$ of radius R, representing the first idle roller. The problem is to find the equation of the line tangent to both the ellipse and the circle, which will represent the first web span. For any given point $P_e \equiv (x_e, y_e)$ on the ellipse, satisfying the equation in (4.1), the equation for the tangent to the ellipse at the point P_e is

$$\mathbf{t}(x_e, y_e) : \frac{x_e x}{a^2} + \frac{y_e y}{b^2} - 1 = 0. \tag{4.2}$$

Now consider a generic line $\ell : \alpha x + \beta y + \gamma = 0$ and a point $P_0 \equiv (x_0, y_0)$; the

equation that gives the distance between the line and the point is given by

$$d(\ell, P_0) = \sqrt{\frac{\alpha x_0 + \beta y_0 + \gamma}{\alpha^2 + \beta^2}}. \tag{4.3}$$

For this line to be a tangent $\mathbf{t}$ to the ellipse, the following must be true:

$$\alpha = \frac{x_e}{a^2},\ \beta = \frac{y_e}{b^2},\ \text{and } \gamma = -1. \tag{4.4}$$

Therefore, the distance between the tangent $\mathbf{t}$ and the center of the roller C is

$$d(\mathbf{t}(x_e, y_e), C) = \sqrt{\frac{|\alpha x_c + \beta y_c + \gamma|}{\alpha^2 + \beta^2}} \tag{4.5}$$

Note that since x_e and y_e are on the ellipse, they are not independent. In fact, they can be parameterized in the following way:

$$x_e = a\cos(\phi),\ y_e = b\sin(\phi) \tag{4.6}$$

with $\phi \in [0, \pi/2]$, a and b being the length of the minor and major axes of the ellipse, respectively. Hence the distance $d(\mathbf{t}(x_e(\phi), y_e(\phi)), C) = d(\phi)$ is a function of the parameter ϕ only. This distance will equal R only for the two tangents $\mathbf{t}_2$ and $\mathbf{t}_3$ in Fig. 4.2. Therefore the cost function

$$J = (d(\phi) - R)^2 \tag{4.7}$$

will be positive everywhere except for the two values of ϕ corresponding to the tangents $\mathbf{t_2}$ and $\mathbf{t_3}$ in Fig. 4.2, for which it will be zero. Hence, by solving the optimization problem

$$\min_{\phi} J(\phi), \tag{4.8}$$

the desired ϕ can be found, which when substituted into (4.6) and (4.2) will give the equation of the common tangent. In order to avoid the possibility that the numerical algorithm gives the solution corresponding to the tangent $\mathbf{t}_3$ it

is possible to constrain the numerical algorithm to search in the interval $[0, \phi_0]$ instead of $[0, \pi/2]$, where ϕ_0 is the value of ϕ for which the tangent to the ellipse passes through the center C of the idle roller. More specifically, ϕ_0 solves the equation:

$$d(\phi_0, C) = 0.$$

This equation can be easily solved analytically and its solution is

$$\phi_0 = \arcsin \frac{-\frac{y_c}{b} + \sqrt{\frac{x_c^2}{a^2}\left(\frac{x_c^2}{a^2} + \frac{y_c^2}{b^2} - 1\right)}}{\frac{x_c^2}{a^2} + \frac{y_c^2}{b^2}}. \tag{4.9}$$

Note that restricting the search between $[0, \phi_0]$ not only avoids the problem of getting the undesired solution but it also results in achieving a faster convergence time for the numerical algorithm. In fact, the objective function $J(\phi)$ is a strictly convex function in the interval $[0, \phi_0]$ and numerical algorithms for minimum search are extremely efficient when applied to convex functions. Once the equation of the tangent $\mathbf{t}_2$ is obtained, finding the length of the span is straightforward.

Note that the equation for the tangent to the ellipse in (4.2) is valid only if the major and minor axes of the ellipse are aligned with the fixed coordinate system $\mathfrak{F}$. If the major and minor axes of the ellipse are not aligned with the fixed coordinate axes, as is the case with a rotating ellipse, one can perform appropriate transformations to resolve the issue in the following manner. Let the major axes be rotated by an angle ωt with respect to the fixed coordinate system $\mathfrak{F}$, where ω is the angular velocity of the elliptical material roll. Given a point $P_0 \equiv (x_0, y_0)$ on the surface of the rotated material roll, the problem of finding the tangent $\mathbf{t}$ to the material roll at the point P_0 needs to be solved. Now consider a second coordinate system $\mathfrak{F}'$ having its axes along the major and minor axes of the elliptical material

roll. The coordinates of point P_0 in $\mathfrak{F}'$ are

$$\begin{pmatrix} x_0' \\ y_0' \end{pmatrix} = \begin{pmatrix} \cos\omega t & \sin\omega t \\ -\sin\omega t & \cos\omega t \end{pmatrix} \begin{pmatrix} x_0 \\ y_0 \end{pmatrix}. \tag{4.10}$$

In $\mathfrak{F}'$ since the major and minor axes of the ellipse are aligned with the coordinate axes, (4.2) can be used to find the equation of the tangent $\mathbf{t}$. So (4.2) in $\mathfrak{F}'$ can be written as

$$\mathbf{t}(x_0', y_0') : \frac{x_0' x'}{a^2} + \frac{y_0' y'}{b^2} - 1 = 0. \tag{4.11}$$

To transform $\mathbf{t}$ back to the coordinate system $\mathfrak{F}$, the following change of coordinates must be performed:

$$\begin{pmatrix} x' \\ y' \end{pmatrix} = \begin{pmatrix} \cos\omega t & \sin\omega t \\ -\sin\omega t & \cos\omega t \end{pmatrix} \begin{pmatrix} x \\ y \end{pmatrix}. \tag{4.12}$$

By substituting (4.12) into (4.11) the equation for $\mathbf{t}$ in $\mathfrak{F}$ is obtained. This equation can be used instead of (4.2) to set up the optimization problem when the major and minor axes of the ellipse are not aligned with the axes of the fixed coordinate system $\mathfrak{F}$. It should be noted that as a consequence of (4.10), (4.11) and (4.12), $\mathbf{d}$ is also a function of ωt. Therefore, the new optimization problem is given by

$$\min_{\phi \in [\phi_{min}, \phi_{max}]} J(\phi, \omega t). \tag{4.13}$$

The algorithm for computing the length $L(t)$ is given in Algorithm 1. Algorithm 2 gives a basic implementation for the cost function $J(\phi, \omega t)$ that defines the optimization problem.

4.2 Convex Shaped Material Roll

The problem of computing the length of the web span between a convex shaped material roll and a perfect idle roller is considered in this section. This problem can

Algorithm 1: Computation of the web span length in the presence of an elliptical material roll

input : Roller coordinates (X_i, Y_i), length of major and minor axes a and b, roller radius R, angular velocity of the material roll ω, configuration (over-wrap, under-wrap)

output: Length of the web span $L(t)$

begin

compute ϕ_0 as in (4.9);

if *Under-wrap* **then**

$\phi_{min} \leftarrow 0, \qquad \phi_{max} \leftarrow \phi_0;$

else

$\phi_{min} \leftarrow \phi_0, \qquad \phi_{max} \leftarrow \pi/2;$

for $t \leftarrow 0$ **to** t_{fin} **do**

$\delta \leftarrow \omega t;$

solve $\min_{[\phi_{min}, \phi_{max}]} J(\phi, \delta)$;

begin Compute the contact point $P_{cont} \equiv (X_{cont}, Y_{cont})$ on roller

AngleOfTangent $\leftarrow \text{atan2}(\beta, -\alpha)$;

if *Under-wrap* **then**

$X_{cont} \leftarrow x_c + R\cos(\text{AngleOfTangent} - \pi/2);$

$Y_{cont} \leftarrow y_c + R\sin(\text{AngleOfTangent} - \pi/2);$

else

$X_{cont} \leftarrow x_c + R\cos(\text{AngleOfTangent} + \pi/2);$

$Y_{cont} \leftarrow y_c + R\sin(\text{AngleOfTangent} + \pi/2);$

$L(t) \leftarrow \text{norm}(P - P_{cont});$

Algorithm 2: J(ϕ, δ)

input : A point $P_0(\phi)$ on the surface of the ellipse, the angle of rotation $\delta = \omega t$ of the ellipse respect to the fixed frame $\mathfrak{F}$, the data describing the rollers (radii, coordinates etc.)

output: Distance between the tangent at the point $P_0(\phi)$ and the center C of the roller

begin

compute the point P_0' as in (4.10);

compute the tangent to P_0' as in (4.11);

compute the equation of the tangent in the frame $\mathfrak{F}$ using (4.12);

compute the distance as in (4.3) using the coefficient obtained in the previous step;

be divided in three sub-problems. First, given a convex shaped roll it is necessary to find a way to characterize the roller, which is to find a way to associate a parametric equation that is, at the same time, accurate enough to describe the surface of the roller but simple enough to allow the computations necessary for the subsequent steps. Second, once the equation describing the shape of the roller is obtained, it is necessary to obtain an equation for the tangent of the roller as a function of the angular displacement. Finally, an adjusted optimization problem must be formulated to find the equation for the line tangent to the generally shaped roller and the idle roller.

To describe the shape of the roller it is assumed that a list of all the maximum and minimum radii of the roll and their angular position with respect to a fixed coordinate axis is known; an illustration of this characterization is shown in Fig. 4.3. Note that the positions of the radius maximum and minimum are func-

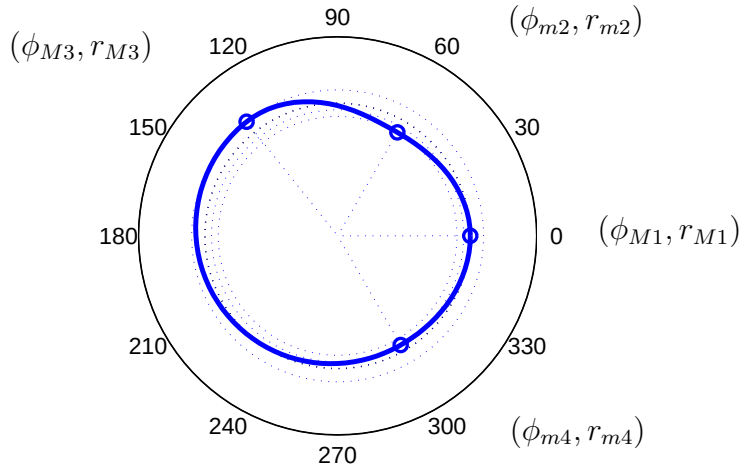

Figure 4.3: Characterization of a generic shaped material roll.

tions of the angular displacement of the roll θ. The algorithm for the computation of the span length is derived assuming that the roll is fixed. The modifications to the algorithm to account for the movement of the roll are discussed later in the section.

One possible approach to characterize the convex shape is to find a single function that can describe the entire profile of the roll; this approach leads to undue complexity. In fact, finding such a function is non-trivial and, moreover, the resulting function will be either a highly nonlinear function or a function with many parameters; this would also result in numerical implementation of subsequent steps to be more computationally intensive. To avoid this problem the characterization of the shape is done in intervals, that means a different function is used to describe the shape of the roller between each minimum and maximum. In other words, given the list of the locations $(\phi_{m1}, \phi_{M1}, \phi_{m2}, \phi_{M2}, \ldots, \phi_{mn}, \phi_{Mn})$ and the values of minima and maxima of the radius $(r_{m1}, r_{M1}, r_{m2}, r_{M2}, \ldots, r_{mn}, r_{Mn},)$,

the function takes the form:

$$r(\phi) = \begin{cases} r_1(\phi_{m1}, \phi_{M1}, r_{m1}, r_{M1}, \phi) & \text{if } \phi_{m1} \leq \phi \leq \phi_{M1}; \\ r_1(\phi_{M1}, \phi_{m2}, r_{M1}, r_{m2}, \phi) & \text{if } \phi_{M1} \leq \phi \leq \phi_{m2}; \\ & \vdots \\ r_{2n}(\phi_{Mn}, \phi_{m1}, r_{Mn}, r_{m1}, \phi) & \text{if } \phi_{Mn} \leq \phi \leq \phi_{m1}. \end{cases} \tag{4.14}$$

To guarantee that each junction point is an extreme point and in order to avoid any kind of discontinuity, each function r_i must be such that

$$\begin{aligned} r_i(\phi_{mj}) &= r_{i+1}(\phi_{mj}) = r(\phi_{mj}), \\ r_i'(\phi_{mj}) &= r_{i+1}'(\phi_{mj}) = 0. \end{aligned} \tag{4.15}$$

Let us now consider a specific interval (ϕ_m, ϕ_M), the problem is to find a function $r(\phi)$ such that $r(\phi_m) = r_m$, $r(\phi_M) = r_M$ and $r'(\phi_m) = r'(\phi_M) = 0$. We start with the simplest scenario, which is $\phi_m = 0$, $\phi_M = 1$, $r_m = 0$ and $r_M = 1$, and consider the function:

$$\begin{aligned} r_0(\phi) &= a_3\phi^3 + a_2\phi^2 + a_1\phi + a_0, \\ r_0'(\phi) &= 3a_3\phi^2 + 2a_2\phi + a_1. \end{aligned} \tag{4.16}$$

Note that a third order polynomial is the simplest function that can satisfy all the constraints. Now considering the constraints on the extreme points zero and one. It is possible to solve for (a_0, a_1, a_2, a_4) as follows:

$$\begin{aligned} r_0(0) = 0 \quad &\Rightarrow \quad a_0 = 0, \\ r_0(1) = 1 \quad &\Rightarrow \quad a_1 + a_2 + a_3 = 1, \\ r_0'(0) = 0 \quad &\Rightarrow \quad a_1 = 0, \\ r_0'(1) = 0 \quad &\Rightarrow \quad 2a_2 + 3a_3 = 1. \end{aligned} \tag{4.17}$$

Solving the system of equations gives $r_0(\phi) = -2\phi^3 + 3\phi^2$. The function r_0 solves the problem for the simplest case, but this solution can be used to find the solution

to the general case just by scaling and translating r_0. First, consider the function r_0 in the new variable $\tilde{\phi} = \Delta\phi\,\phi$ with $\Delta\phi = \phi_M - \phi_m$:

$$\tilde{r}(\tilde{\phi}) = -2\frac{\tilde{\phi}^3}{\Delta\phi^3} + 3\frac{\tilde{\phi}^2}{\Delta\phi^2}. \tag{4.18}$$

It is simple to verify that the function $\tilde{r}$ still holds all the properties of r_0 except for $\tilde{r}(\Delta\phi) = 1$. Now consider the new variable $\widehat{\phi} = \tilde{\phi} + \phi_m$ and a new function $\widehat{r}$ given by

$$\widehat{r}(\widehat{\phi}) = -2\frac{(\widehat{\phi} - \phi_m)^3}{\Delta\phi^3} + 3\frac{(\widehat{\phi} - \phi_m)^2}{\Delta\phi^2}. \tag{4.19}$$

The function $\widehat{r}(\widehat{\phi})$ has the property that $\widehat{r}(\phi_m) = 0$ and $\widehat{r}(\phi_M) = 1$. With a scaling and translation along the y axis one can find the function for the general case which is

$$r(\phi) = (r(\phi_M) - r(\phi_m))\left[-2\frac{(\phi - \phi_m)^3}{\Delta\phi^3} + 3\frac{(\phi - \phi_m)^2}{\Delta\phi^2}\right] + r(\phi_m). \tag{4.20}$$

Note that the same function can be used for intervals starting in a maximum and ending in a minimum by simply switching ϕ_m with ϕ_M.

The next step is to find an expression for the line tangent to the perimeter of the roller for a given point on the perimeter identified in polar coordinates by the pair $(\phi, r(\phi))$. Consider two points on the perimeter $(\phi, r(\phi))$ and $(\phi + d\phi, r(\phi + d\phi))$ such that ϕ and $\phi + d\phi$ belong to the same interval (ϕ_m, ϕ_M). The line crossing the two points is given by the equation

$$\begin{aligned} y &= y_1 + \frac{y_1 - y_2}{x_1 - x_2}(x - x_1) \\ &= r(\phi)\sin(\phi) + m(\phi, \phi + d\phi)(x - r(\phi)\cos(\phi)) \end{aligned} \tag{4.21}$$

where

$$m(\phi, \phi + d\phi) = \frac{r(\phi + d\phi)\sin(\phi + d\phi) - r(\phi)\sin(\phi)}{r(\phi + d\phi)\cos(\phi + d\phi) - r(\phi)\cos(\phi)}. \tag{4.22}$$

The angular coefficient m of the tangent at the point $(\phi, r(\phi))$ may be obtained by

$$m = \lim_{d\phi \to 0} \frac{r(\phi + d\phi)\sin(\phi + d\phi) - r(\phi)\sin(\phi)}{r(\phi + d\phi)\cos(\phi + d\phi) - r(\phi)\cos(\phi)}. \tag{4.23}$$

The function $r(\phi)$ in (4.20) can be rearranged in the form:

$$r(\phi) = \delta\phi^3 + \gamma\phi^2 + \beta\phi + \alpha. \tag{4.24}$$

Therefore the expression for the angular coefficient is given by

$$\begin{aligned}
m &= \frac{n_3\phi^3 + n_2\phi^2 + n_1\phi + n_0}{d_3\phi^3 + d_2\phi^2 + d_1\phi + d_0}, \\
n_0 &= \alpha\sin\phi - \beta\cos\phi, \quad n_1 = \beta\sin\phi - 2\gamma\cos\phi \\
n_2 &= \gamma\sin\phi - 3\delta\cos\phi, \quad n_3 = \delta\sin\phi \\
d_0 &= \alpha\cos\phi - \beta\sin\phi, \quad d_1 = \beta\cos\phi + 2\gamma\sin\phi \\
d_2 &= \gamma\cos\phi + 3\delta\sin\phi, \quad d_3 = \delta\cos\phi.
\end{aligned} \tag{4.25}$$

This expression will be used in the next step to setup the optimization problem that will be used to find the equation for the common line tangent to the material roll and the idle roller.

The basic idea to find the line tangent for this case is the same as the one used for the elliptically shaped roll. In fact, among all the tangents to the convex shaped roller, the one which is tangent to the idle roller is the one having the distance to the center of the idle roller equal to the radius. Therefore the same minimization problem can be used. Given a generic point on the surface of the material roll described in polar coordinates by $(\phi, r(\phi))$, the line tangent to the surface at that point is given by

$$\begin{aligned}
y &= r(\phi)\sin\phi + m(x - r(\phi)\cos\phi), \\
\mathbf{t}(\phi) &: y - m(\phi)x + m(\phi)r(\phi)\cos\phi - r(\phi)\sin\phi = 0
\end{aligned} \tag{4.26}$$

with m as given in (4.25).

The distance between the tangent $\mathbf{t}$ and the center of the roller C is

$$\mathbf{d}(\mathbf{t}(\phi), C) = \sqrt{\frac{|\alpha x_c + \beta y_c + \gamma|}{\alpha^2 + \beta^2}} \tag{4.27}$$

where $\alpha = -m(\phi)$, $\beta = 1$ and $\gamma = m(\phi)r(\phi)\cos\phi - r(\phi)\sin\phi$.

By solving the optimization problem

$$\phi_{ex} = \min_{\phi} J(\phi) = \min_{\phi}(\mathbf{d}(\phi) - R)^2, \tag{4.28}$$

a point $(\phi_{ex}, r(\phi_{ex}))$ is found on the generally shaped roller perimeter whose tangent distance from the center of the idle roller is equal to R. Notice that, similar to the case of elliptical material roll, the optimization problem has two solutions one corresponding to the over-wrap on the idle roller and the other to the under-wrap (which is shown in Fig 4.2). For the elliptical roll the ambiguity was solved by finding an expression for ϕ_0 and limiting the search space to a domain containing only one of the solutions. The same procedure is not applicable in this case because it is not possible to find a closed form for ϕ_0; a slightly different approach is taken for this case. In fact, instead of limiting the search space for ϕ to a region with one solution, a modified cost function $J_p(\phi)$ which has only one solution is suggested. First, consider the cost function $J(\phi)$ as in (4.28), in general it will have a behavior similar to the graph shown in Fig. 4.4 with the two minima corresponding to the under-wrap and over-wrap configurations, and the maximum corresponding to the angle ϕ_0 for which the tangent passes through the center of the idle roller.

First consider the under-wrap configuration. The objective is to add in the cost function a term that penalizes all the angles (ϕ) that are greater than ϕ_0. Even though ϕ_0 is unknown, it is possible to find a way to determine whether ϕ

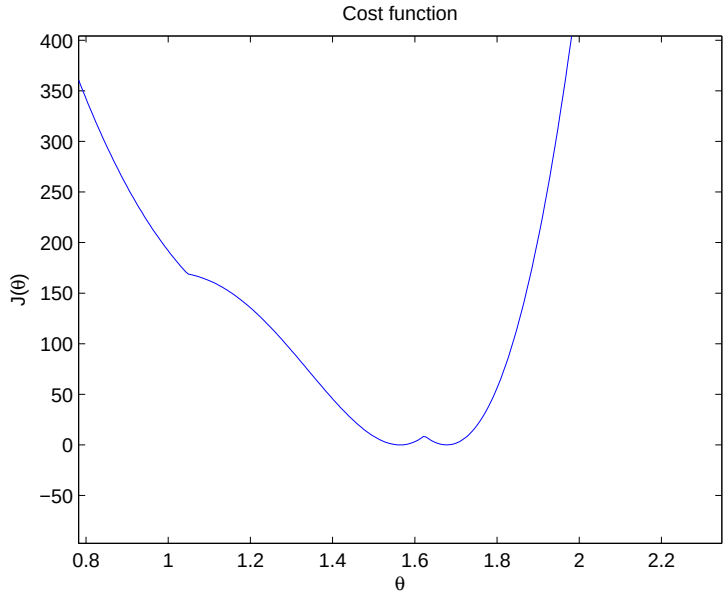

Figure 4.4: Cost function $J(\phi)$ for the roller in Fig. 4.3.

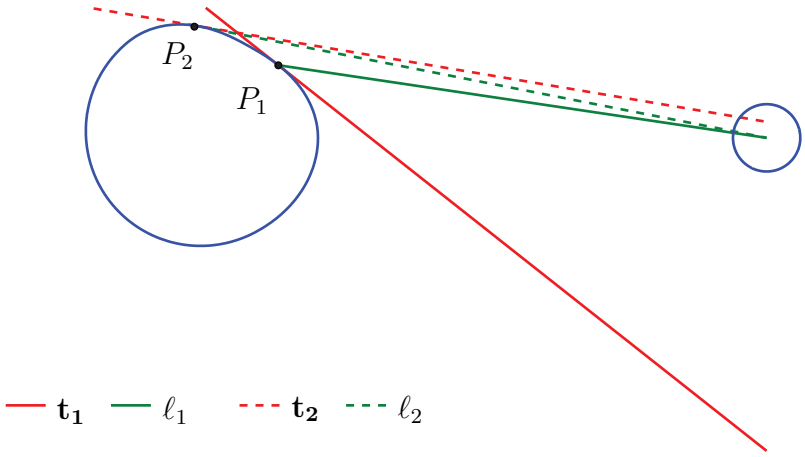

Figure 4.5: Penalization example: P_1 is not penalized since $m_{\ell_1} > m_{\mathbf{t_1}}$, while P_2 is penalized since $m_{\ell_2} > m_{\mathbf{t_2}}$.

is greater or smaller than ϕ_0. Consider a point $P \equiv (\phi, r(\phi))$ on the perimeter, its tangent $\mathbf{t}$, and the line ℓ connecting P with the center of the idle roller C. If the angular coefficient m_t of $\mathbf{t}$ is smaller than the angular coefficient m_ℓ of ℓ then $\phi < \phi_0$, otherwise, $\phi \geq \phi_0$. This is graphically shown in Fig. 4.5. Define the penalty variable

$$\text{penalty}_u = \begin{cases} 1, & \text{if } m_t \geq m_\ell; \\ 0, & \text{otherwise.} \end{cases} \tag{4.29}$$

A new cost function that uses the variable penalty_u can now be defined:

$$J_p(\phi) = (1 - \text{penalty}_u)(\mathbf{d}(\phi) - R)^2 + \text{penalty}_u(P + Q\phi) \tag{4.30}$$

with P and Q being two large positive numbers, $P > Q$. For this new cost function, whenever $\phi < \phi_0$, J_p will be the same as in (4.28), whereas when $\phi \geq \phi_0$ $J_p = (P + Q\phi)$ which makes the overall cost function look like the one shown in Fig. 4.6. The cost function J_p now has only one minimum corresponding to the under-wrap solution. Moreover, since the cost function J_p is quasi-convex, the optimization algorithm is expected to have better numerical properties compared to the non-convex function J.

A dual situation arises for the over-wrap case. The algorithm will search for solutions with $\phi > \phi_0$; the penalty variable will be 1 when $\phi \leq \phi_0$ which is true when $m_t \leq m_\ell$. Also in order to make the cost function quasi-convex, the expression of J_p must be adjusted as follows:

$$J_p(\phi) = (1 - \text{penalty}_o)(\mathbf{d}(\phi) - R)^2 + \text{penalty}_o(P - Q\phi) \tag{4.31}$$

where penalty_o is the new penalty variable and the penalty term $(P - Q\phi)$ now has a negative slope.

An expression for the penalty variable and the cost function J_p that covers both scenarios may be found in the following manner. We first define the wrap

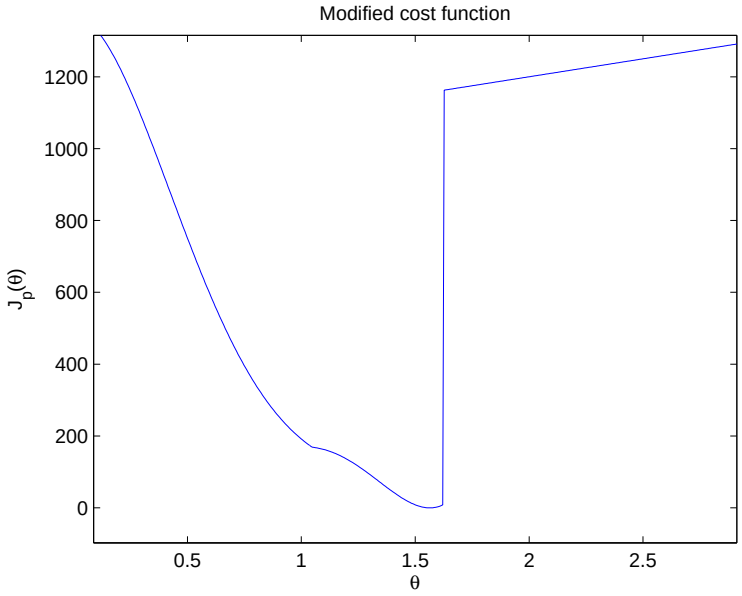

Figure 4.6: Modified cost function $J_p(\phi)$ for the roller in Fig. 4.3.

configuration as

$$\text{wrap} = \begin{cases} 1, & \text{for over-wrap configurations;} \\ -1, & \text{for under-wrap configurations.} \end{cases} \tag{4.32}$$

Using the new wrap configuration variable a general expression for the penalty variable and the cost function may be given by

$$\begin{aligned} \text{penalty} &= ((\text{wrap} < 0)(m_t \geq m_\ell)) \\ &\quad + ((\text{wrap} > 0)(m_t \leq m_\ell)) + (m_t > 0) \\ J_p(\phi) &= (1 - \text{penalty})(\mathbf{d}(\phi) - R)^2 + \text{penalty}(P - (\text{wrap})Q\phi) \end{aligned} \tag{4.33}$$

In the expression for the for the penalty variable, note that the term $(m_t > 0)$ has been added. This will force the the penalty to be 1 when the angular coefficient is positive. In fact, assuming the center of the generally shaped idle roller and the center of the idle roller to be aligned on the x axis and the material roll having radius greater then the radius of the idle roller, the line tangent to both

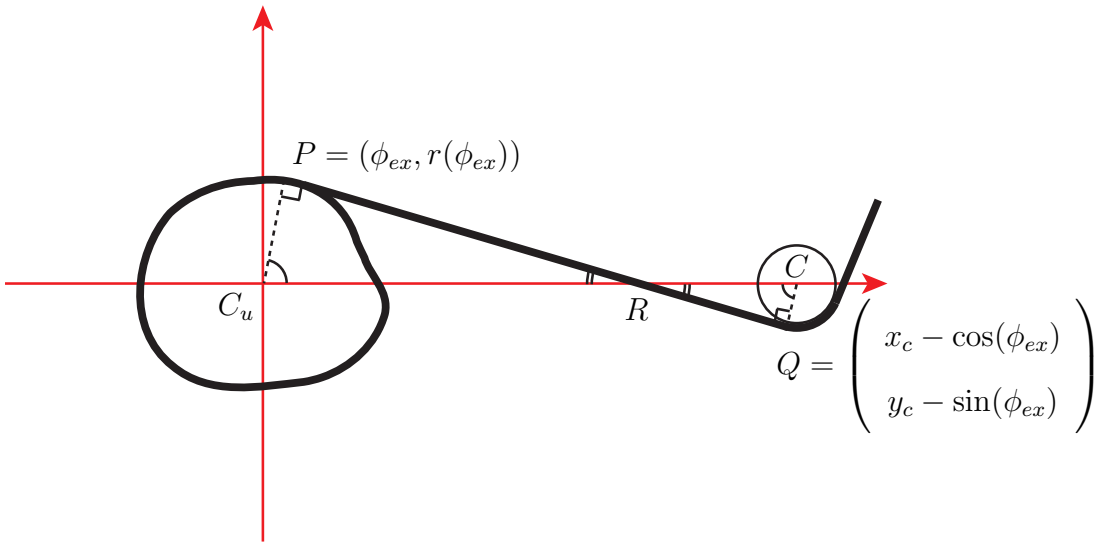

Figure 4.7: Computation of the web span extreme points. Because of the similarity of the triangles C_uRP and CRQ, the angles in C_u and C are equal.

rollers has to have a negative slope, therefore points corresponding to tangents with positive slopes can be penalized since they cannot be a solution to the minimization problem. Observe also that both assumptions are reasonable: material rolls are commonly bigger than idle rollers, and, it is always possible to set up the optimization problem in a cartesian frame in which the center of the rollers are aligned since the length of the span and its derivative are invariant to isometric frame transformations.

Once the optimization problem is solved, the coordinates of the exit point of the web on the roll $P = (\phi_{ex}, r(\phi_{ex}))$ are determined. The polar coordinates for P can easily be converted into Cartesian coordinates. Also, the coordinates of the contact point of the web on the downstream roller can be obtained as shown in Fig. 4.7. With the expressions for the extreme points P and Q of the web span the computation of the length of the span is straight forward:

$$L = ||P - Q||. \tag{4.34}$$

As explained earlier in the section, the algorithm has been derived without considering the movement of the roll. When the roll moves the positions of the minimum and maximum radius on the roll change. Specifically, assuming that the original list of radius minima and maxima $\{(\phi_{m1}, r_{m1}), (\phi_{M1}, r_{M1}), \ldots, (\phi_{mn}, r_{mn},), (\phi_{Mn}, r_{Mn})\}$ is given for the initial displacement of the roll $\theta(0) = 0$. Once the roll moves to a new position $\theta(t)$ the position of the radius minima and maxima will shift by an angle equal to $\theta(t)$. Therefore, the list of radius minima and maxima changes to $\{(\phi_{m1} + \theta(t), r_{m1},), (\phi_{M1} + \theta(t), r_{M1}), \ldots, (\phi_{mn} + \theta(t), r_{mn},), (\phi_{Mn} + \theta(t), r_{Mn})\}$ and the algorithm for the span length can be applied to the new list. Therefore, for any given angular displacement of the roll $\theta(t)$ the corresponding span length $L(\theta(t))$ can be computed.

Because it is not possible to obtain a closed form expression for the web span length, the inclusion of the effects of an out-of-round roll in the computer simulation is more complex compared to the case of the eccentric roller. The optimization problem can only be solved off-line before the computer simulation starts, but the optimization problem is completely defined only when the angular displacement is known. The angular displacement of the roll is obtained from the integration of the dynamic equation of the roll once the simulation starts. Moreover, the span length derivative $\dot{L}(t)$ that is required to solve the governing equation of tension cannot be obtained analytically, therefore, a numerical approximation for $\dot{L}(t)$ is required.

From these observations it is clear that in order to implement in model simulations the effects of the presence of the out-of-round roll, it is necessary to have a discretization of the angular displacement of the roll. By doing so, the optimization problem can be solved off-line before the simulation starts, and a look-up table can be used on-line to approximate the web span length when the

simulation is running. Suppose the roll displacement is discretized with N equally distributed points, then the finite set of angular displacements is given by:

$$\Theta = \{\theta_1, \ldots, \theta_N\}, \qquad \theta_i = (i-1)\delta\theta, \qquad \delta\theta = \frac{2\pi}{N}. \tag{4.35}$$

The web span length for each angular position in Θ can be computed using the algorithm described in this section. The couples $(\theta_i, L(\theta_i))$ will constitute a look-up table that can be used during the execution of the simulation to compute an approximation of the web span length and its derivative. In particular, suppose that at simulation time t_k the angular displacement $\theta(t_k)$ is obtained from the integration of the governing equations of velocity with $\theta_i \leq \theta(t_k) < \theta_{i+1}$, $\theta_i, \theta_{i+1} \in \Theta$, then the span length and span length derivative can be approximated with:

$$\begin{aligned} L(\theta(t_k)) &= L(\theta_i) + \frac{\theta_{i+1} - \theta(t_k)}{\theta_{i+1} - \theta_i}(L(\theta_{i+1}) - L(\theta_i)), \\ \dot{L}(\theta(t_k)) &= \frac{L(\theta(t_k)) - L(\theta(t_{k-1}))}{t_k - t_{k-1}}. \end{aligned} \tag{4.36}$$

In summary, because of the presence of the out-of-round material roll, the governing equation for web tension need to include the effect of the time varying web span length. Therefore, equation (3.23) must be used to simulate the effect of the presence of the non-ideal roll. The span length and its derivative cannot be computed in closed form, a numerical approximation is used instead and a procedure to obtain this numerical approximation was described in this section.

4.2.1 Governing Equation for Angular Velocity in the Presence of an Out-of-round Roll

The governing equation for the angular velocity in (2.1) is not valid for an out-of-round material roll. This is mainly due to three reasons: the location of the center of rotation may not coincide with the center of mass of the roll, the expression for

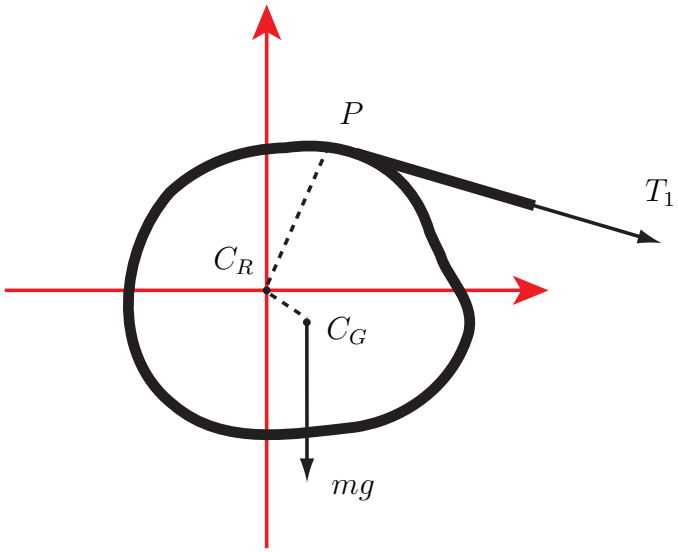

Figure 4.8: Sketch of the out-of-round roll and torques acting on it. Note: C_R is the center of rotation of the roll and C_G is its center of gravity.

the time varying inertia is different and the torque due to the tension of the web is not equal to $R_u T_1$. The necessary corrections to equation (2.1) to account for these aspects will be discussed in this section. A sketch of the out-of-round roll and all the torques acting on it is shown in Fig. 4.8. The new governing equations for the roll are

$$\begin{aligned} \dot{\theta} &= \omega, \\ J_u \dot{\omega} &= -\tau_f - d_{C_G C_R} mg \sin\theta - d_{ex} T_1 - \dot{J}_u \omega + \tau_u \end{aligned} \tag{4.37}$$

where τ_f is the friction torque, $d_{C_G C_R}$ is the distance between the center of gravity and the center of rotation, m is the mass of the roll, g is the acceleration due to gravity, d_{ex} is the distance between the exit point of the web P and the center of rotation of the roll C_R, J_u is the total roll inertia and τ_u is the input torque. The remainder of the section explains how each term in (4.37) is derived.

First, because of the out-of-roundness of the roll, it is possible that the center of mass of the roll is different from its center of rotation. In this case an extra

torque term due to gravity needs to be added to the governing equation of the angular velocity. The equations to compute the center of gravity C_R of the roll are

$$\begin{aligned} \bar{x} &= \frac{\iint x\rho dA}{m} = \frac{\iint r^2(\phi)\cos(\phi)\rho(\theta)drd\phi}{m}, \\ \bar{y} &= \frac{\iint y\rho dA}{m} = \frac{\iint r^2(\phi)\sin(\phi)\rho(\theta)drd\phi}{m} \end{aligned} \tag{4.38}$$

where $dA = r(\phi)d\phi dr$, ρ is the roll density, and $r(\phi)$ describe the roll in polar coordinates as described in the previous section. The lever arm of the torque due to gravity is given by the distance between the center of rotation C_R and the center of gravity $C_G = (\bar{x}, \bar{y})$.

The computation of the roll inertia is also more complex compared to the case of an ideal roll. The total moment of inertia is given by the sum of the core inertia, shaft inertia and the inertia due to the web. To obtain the component of the inertia due to the web J_w, it is necessary to start from the general expression for the computation of the moment of inertia:

$$J_w = \iiint_V \rho d^2(\phi)\mathbf{d}V = \rho \int_0^{w_w} \mathbf{d}\ell \iint_S d^2(\phi)\mathbf{d}S$$

where the infinitesimal volume $\mathbf{d}V = \mathbf{d}S\mathbf{d}\ell$ and since the function $d(\phi)$ equal along the width of the web, the integral along the width can be separated resulting in

$$J_w = \rho w_w \iint_S d^2(\phi)\mathbf{d}S = \rho w_w \int_0^{2\pi} \int_{R_c}^{r(\phi)} d^2(\phi)d(\phi)\,\mathbf{d}\phi\,\mathbf{d}d$$

where the infinitesimal area $\mathbf{d}S = d(\phi)\,\mathbf{d}\phi\,\mathbf{d}d(\phi)$ giving

$$\begin{aligned} J_w =& \rho w_w \int_0^{2\pi} \int_{R_c}^{r(\phi)} d^3(\phi)\,\mathbf{d}d\,\mathbf{d}\phi = \rho w_w \int_0^{2\pi} \frac{r^4(\phi) - R_c^4}{4}\,\mathbf{d}\phi \\ =& \rho w_w \left[\sum_{j=1}^{n-1} \int_{\phi_{m_j}}^{\phi_{M_j}} \frac{r_{2j-1}^4(\phi) - R_c^4}{4}\mathbf{d}\phi + \int_{\phi_{M_j}}^{\phi_{m_{j+1}}} \frac{r_{2j}^4(\phi) - R_c^4}{4}\mathbf{d}\phi \right] \\ &+ \rho w_w \left[\int_{\phi_{m_n}}^{\phi_{M_n}} \frac{r_{2n-1}^4(\phi) - R_c^4}{4}\mathbf{d}\phi + \int_{\phi_{M_n}}^{\phi_{m_1}} \frac{r_{2n}^4(\phi) - R_c^4}{4}\mathbf{d}\phi \right] \end{aligned} \tag{4.39}$$

the last expression for J_w in (4.39) is obtained from the previous integral by using the definition of $r(\phi)$ given in (4.14). Note that equation (4.39) is obtained considering J_w constant in time. The shape of the roll is defined using the location of the minimum and maximum radius $\{(\phi_{m1}, r_{m1}), (\phi_{M1}, r_{M1}), \ldots, (\phi_{mn}, r_{mn},), (\phi_{Mn}, r_{Mn})\}$, as the web is released the value of the radii decreases making J_w in (4.39) time dependant. To obtain $J_w(t)$ it is necessary to obtain the interpolation functions $r_i(\phi)$ as in (4.20) where now $r(\phi_m)$ and $r(\phi_M)$ are functions of time, and then explicitly solve the integral in (4.39). However, since obtaining the time dependance of $r(\phi_m)$ and $r(\phi_M)$ is not practical, it is assumed that the web line is simulated for a short period of time such that the inertia can be considered constant and the term $\dot{J}_u$ in (4.37) can be neglected.

The last modification to the governing equation of the angular velocity of the roll is to consider the fact that the arm length of the torque due to the tension in the web is not constantly equal to the radius of the roll as in equation (2.7) but it changes with time and depends on the point where the web leaves the roll. Clearly the arm length depends on the angular displacement of the roll and, similar to the web span length, a closed form expression cannot be determined. The optimization problem described in the previous section to compute the span length can also be used to determine the arm length of the torque due to the web tension. In fact, once the solution of the optimization problem ϕ_{ex} is obtained the arm length is simply given by $d_{ex}(\theta) = r(\phi_{ex}(\theta))$. From the implementation point of view, a look-up table can be used for the arm length in a similar fashion to what was done for the web span length. The same discretization of the angular displacement in (4.35) is used to obtain the look up table for $d_{ex}(\theta)$.

The equations presented in this section are used to conduct model simulations in the presence of an out-of-round material roll. Next section describes the

experiments that were performed on the EWL to validate the proposed model.

4.3 Experiments and Model Simulations

Roll imperfections are commonly seen in the web handling industry, these include, for example, a flat spot due to the roll being laid on the floor for an extended period of time, and elliptically shaped roll as a consequence of holding a heavy roll on mandrels causing the bottom portion of the material to bulge due to gravity or improper winding in a process line. The rolls available for this research are fairly round, therefore in order to verify the proposed model one of the rolls was made purposely out-of-round by winding material on top of a wooden insert. The wooden insert was designed so that the resulting out-of-round roll would mimic a roll with a flat spot. The profile of the wooden insert is shown in Fig. 4.9(a). The equations that describe the profile of the wooden insert in Cartesian coordinates are

$$\begin{cases} y = (r+t_f)\sqrt{1-\left(\frac{x-\ell_f/2}{r-\ell_f/2}\right)^2}, & -r \le x \le -\ell_f/2, \\ y = r + t_f & -\ell_f/2 \le x \le \ell_f/2, \\ y = (r+t_f)\sqrt{1-\left(\frac{x+\ell_f/2}{r-\ell_f/2}\right)^2}, & \ell_f/2 \le x \le r, \\ y = -\sqrt{r^2-x^2}, & -r \le x \le r \end{cases} \tag{4.40}$$

where r is the inner radius of the wooden insert, ℓ_f is the length of the flat spot and t_f the thickness of the wooden insert. The resulting out-of-round roll is shown in Fig. 4.9(b). In order to use the procedure described in the previous section for the computation of the span length and its derivative, it is required to obtain the list of maximum and minimum radii in order to divide the profile in segments. Normally one would measure the roll radius to identify the maxima and minima, in this case since the roll is made artificially out-of-round this information can

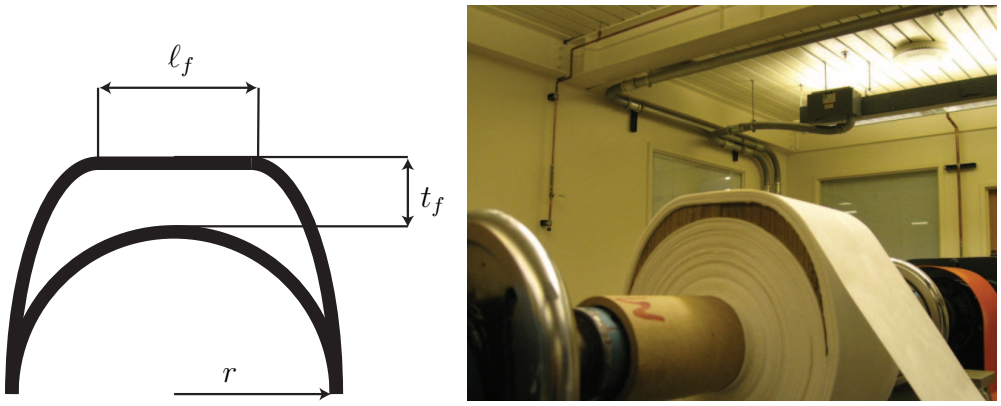

(a) Wooden insert profile. (b) Resulting out-of-round roll.

Figure 4.9: Design of the wooden insert to mimic a flat spot. The values chosen for the design are r =5.5in , ℓ_f =3in and t_f =0.5in

be obtained analytically by transforming the Cartesian coordinates of the roll profile in equation (4.40) into polar coordinates. A plot of the profile in polar coordinates is shown in Fig. 4.10(a), from the plot the list of the radius minima and maxima can be easily established. Figure 4.10(b) shows a comparison between the real profile of the flat spot and the interpolation obtained using the suggested procedure, the interpolation closely approximates the real profile. Using the model proposed in this chapter a computer model simulation is set up to simulate the EWL running with the unwind roll shown in Fig. 4.9(b). The results from the experiment are shown in Fig. 4.11; it is evident there is very little correlation between the two data. This clearly shows that some effects are neglected in the simulation and was the motivation for the need for additional analysis of the model for the web tension in the presence of an out-of-round roll. One key issue that may be responsible for this discrepancy in the data is discussed in the next section.

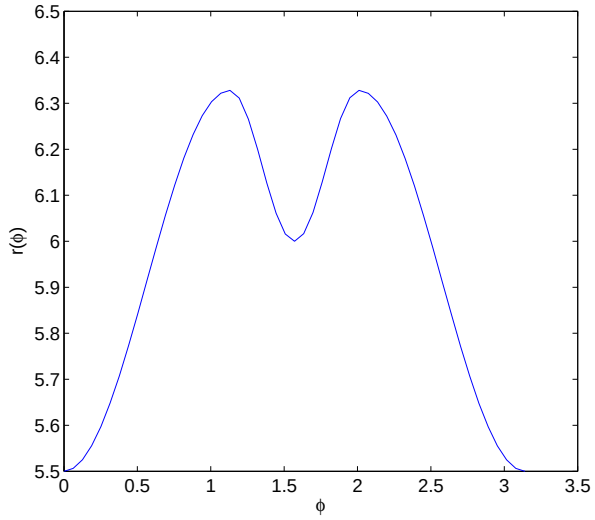

(a) Plot of the radius as function of the angular displacement for the flat spot profile.

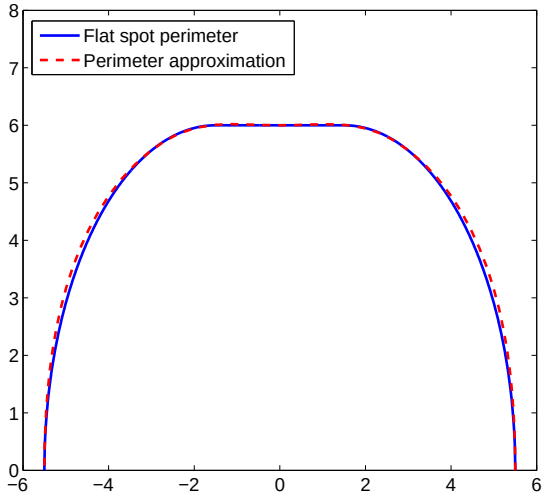

(b) Comparison of the flat spot profile with the interpolation obtained from the suggested procedure

Figure 4.10: Flat spot profile and its approximation.

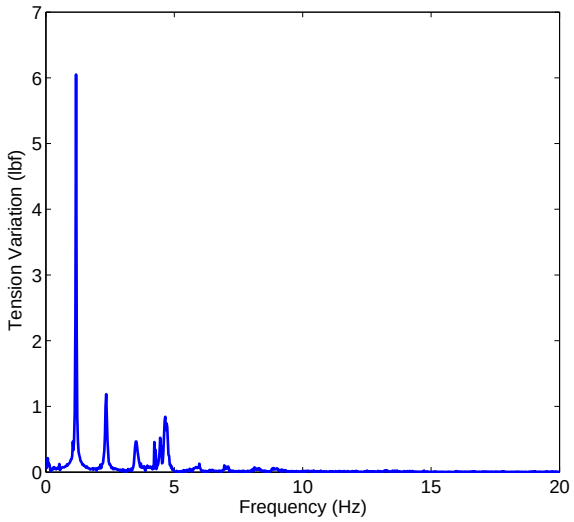

(a) FFT of the experimental data.

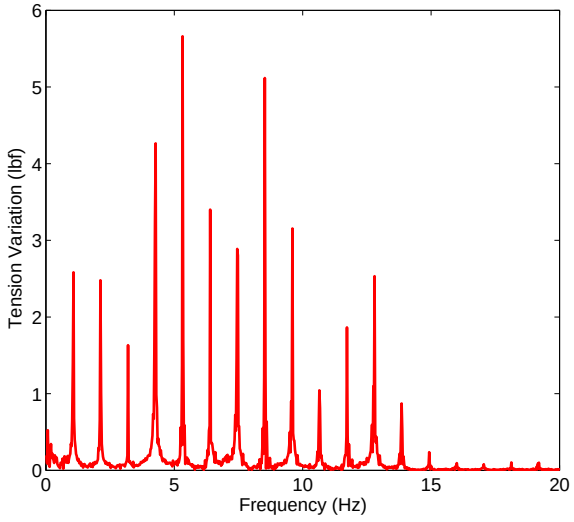

(b) FFT of the simulated data.

Figure 4.11: Comparison between experimental and simulation data at 200 FPM with wooden insert simulating a flat spot.

4.4 Material Flow Rate Equation in the Presence of a Non-ideal Roll

The derivation of the web tension governing equation described in Chapter 2 is based on the conservation of mass in the control volume defined by the web span. In the resulting governing equation for web tension (3.1):

$$\dot{T}_i = \frac{v_i(EA - T_i) - v_{i-1}(EA - T_{i-1}) + \dot{L}_i(EA - T_i)}{L_i},$$

it is assumed that v_{i-1} and v_i, the peripheral velocities of the web on the entry and exit rollers of the span, are proportional to the material flow rate entering and leaving the control volume. It can be shown that this assumption may not hold in the presence of a non-ideal roll.

Consider the extreme situation of a square roller as shown in Fig. 4.12. When the roller moves from the position in Fig. 4.12(a) to the position in Fig. 4.12(b) there is clearly no material transfer into the control volume of the web span, however, the peripheral velocity of the web on the roller is not zero. It is clear that in this situation the peripheral velocity of the web on the roller cannot be used to describe the material flow from the roller to the control volume of the web. The mass balance equation for the control volume can be expressed in a more general fashion compared to the one in (2.10):

$$\frac{d}{dt}\int_{x_{i-1}(t)}^{x_i(t)} \rho(x,t)A(x,t)dx = \frac{dm_{in}}{dt} - \frac{dm_{out}}{dt} \tag{4.41}$$

where now the material flow rate in the right hand side appears explicitly instead of the peripheral velocity. For an ideal roller, the relationship between the material flow rate and the peripheral velocity can be obtained in a straight forward manner

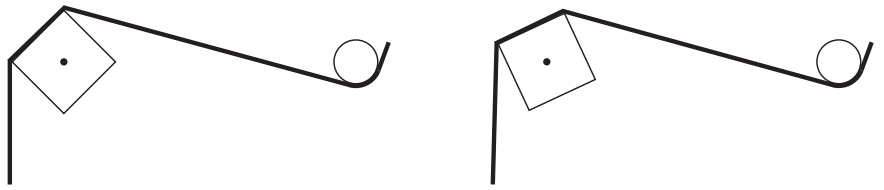

(a) Span with square roller at time t.

(b) Span with square roller at $t+dt$.

Figure 4.12: Example of a span with a square roller. In this situation the square roller rotates from the position at time t to the position at time $t + dt$ but there is no material flow into the span from the square roller.

as:

$$\frac{dm}{dt} = \frac{d}{dt}\left(\rho V(t)\right) = \rho\frac{dV}{dt} = \rho\frac{d}{dt}\left(A\ell(t)\right) = \rho A\frac{d\ell}{dt} = \rho A\frac{d}{dt}\left(R\theta(t)\right) = \rho AR\dot{\theta} = \rho Av(t) \tag{4.42}$$

where $d\ell$ is the length of the infinitesimal segment of material dm that moved from the surface of the roller into the control volume in the infinitesimal time interval dt. The reason for using the peripheral velocity for ideal rollers to describe the material flow rate is the relationship between $d\ell$ and the angular displacement $d\theta$. For a non-ideal roller or roll the relationship between ℓ and θ is not as simple as in the case of the ideal roller/roll.

Assuming the shape of a roller is given in polar coordinates $(r(\phi), \phi)$, then a procedure to find an expression for the material flow rate can be obtained. Two coordinate frames must be defined first. The first coordinate frame $\mathcal{F}_a$ is absolute and time invariant, this is the coordinate frame with respect to the angular displacement of the roller is measured. The second coordinate frame $\mathcal{F}_r$ is a relative coordinate frame that moves together with the roller; this is the coordinate frame in which the polar coordinates of the roller are defined. An example of these two coordinate frames for a non-ideal roller is given in Fig. 4.13.

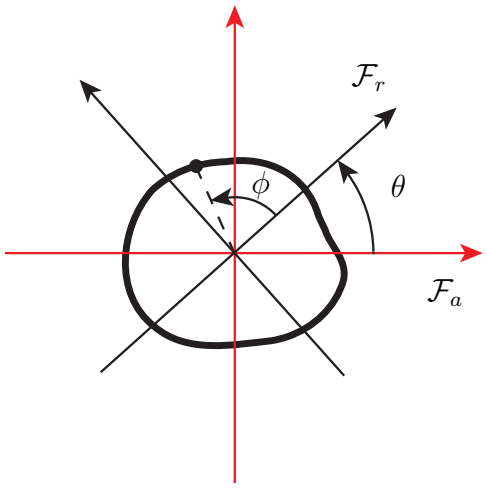

Figure 4.13: Definition of the absolute frame $\mathcal{F}_a$ and the relative frame $\mathcal{F}_r$.

The reason for requiring two coordinates frame will be clarified later. Note that the angular displacement of the roller is indicated by θ whereas ϕ is used to denote the angular position of a point on the perimeter of the roller in its polar coordinates in the frame $\mathcal{F}_r$.

Consider a non-ideal roller and a span adjacent to it as shown in Fig. 4.14. Let A be the point at which the web makes contact with the roller at time t and the corresponding angle be $\phi_{en}(t)$ with respect to $\mathcal{F}_r$ as shown in Fig. 4.14(a). At time $t+dt$, let B be the web entry point on the roller and $\phi_{en}(t+dt)$ be the angle of B with respect to $\mathcal{F}_r$. When the roller rotates from the position in Fig. 4.14(a) at time t to the position in Fig. 4.14(b) at time $t+dt$, the infinitesimal segment of material dm that leaves the control volume of the web span is given by

$$dm = \rho dV = \rho A d\ell \tag{4.43}$$

where $d\ell$ is the web length between the points B and A as shown. The length $d\ell$ can be computed by using the formula for the perimeter of a curve in polar coordinates. Given the curve $\mathcal{C} \equiv (r(\phi), \phi)$ in polar coordinates, the arc length ℓ_c

between two points $(r(\phi_1), \phi_1)$ and $(r(\phi_2), \phi_2)$ is given by

$$\ell_c = \int_{\phi_1}^{\phi_2} \sqrt{r^2(\phi) + \left(\frac{dr}{d\phi}\right)^2} d\phi. \tag{4.44}$$

Note that to use the expression in (4.44) the curve is required to be time invariant. This is the reason why the relative reference frame needs to be introduced, otherwise the curve would be varying with time in the absolute reference frame and it is not possible to compute $d\ell$. Using (4.44) to compute the length $d\ell$ gives

$$d\ell = \int_{\phi_{en}(t)}^{\phi_{en}(t+dt)} \sqrt{r^2(\phi) + \left(\frac{dr}{d\phi}\right)^2} d\phi \tag{4.45}$$

The equation in (4.45) is the most general expression to compute length change which can be used to compute the rate of web material entering and exiting the web span.

One can verify whether the expression in (4.45) for $d\ell$ works for the ideal roller case. An ideal roller in polar coordinates is described by $r(\phi) = R$. Moreover, since the point where the web makes contact with the roller does not change in the absolute reference frame, $\phi_{en}(t + dt)$ can be easily obtained as

$$\phi_{en}(t + dt) = \phi_{en}(t) + d\theta.$$

Substituting this expression in (4.45) gives

$$d\ell = \int_{\phi_{en}(t)}^{\phi_{en}(t+dt)} \sqrt{r^2(\phi) + \left(\frac{dr}{d\phi}\right)^2} d\phi = \int_{\phi_{en}(t)}^{\phi_{en}(t)+d\theta} R d\phi = R d\theta$$

which leads to the same expression for $d\ell$ that was obtained in (4.42), therefore indicating (4.45) is a more general form for the computation of the infinitesimal length of span entering and exiting the control volume.

From the discussion on the previous paragraph it is clear that in the governing equation of web tension (3.1), the peripheral velocity of the web on the roll v_i

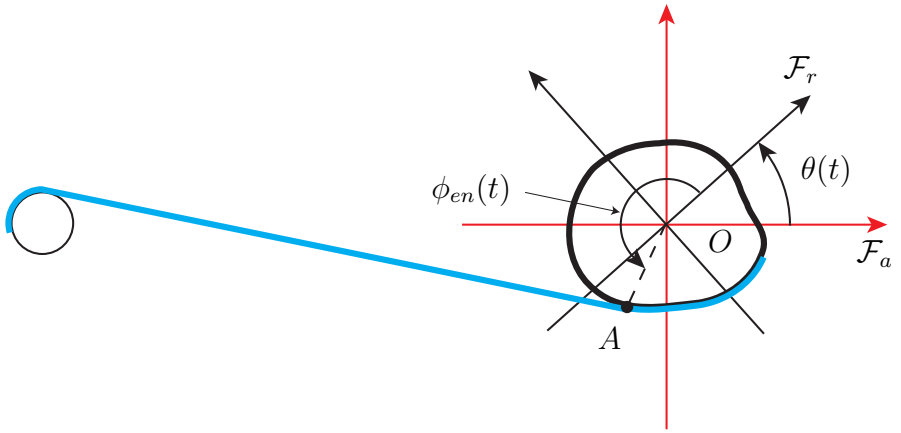

(a) Non-ideal roller at time t.

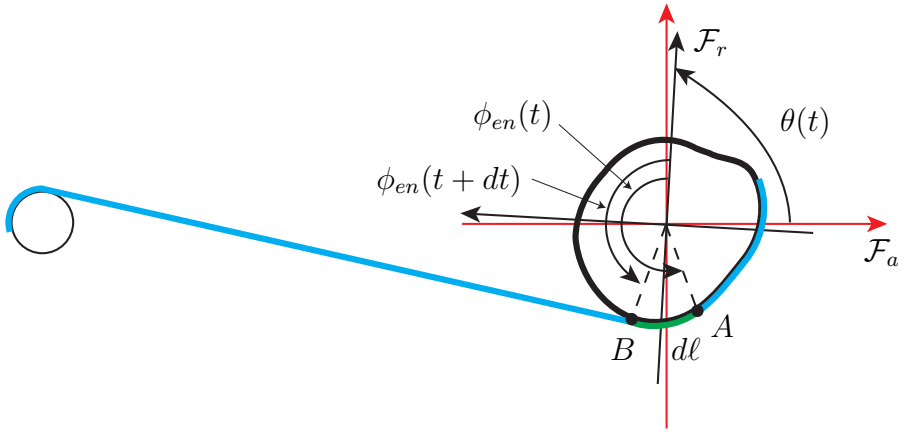

(b) Non-ideal roller at time $t + dt$.

Figure 4.14: Example of an out-of-round roller showing the length ($d\ell$) of web leaving the span in time dt.

must be replaced by $d\ell_i/dt$ with $d\ell$ as in (4.45) whenever the roll i is a non-ideal roll. The generalization of equation (3.1) is:

$$\dot{T}_i = \frac{d\ell_i/dt(EA - T_i) - d\ell_{i-1}/dt(EA - T_{i-1}) + \dot{L}_i(EA - T_i)}{L_i} \tag{4.46}$$

In order to simulate the equation (4.46) the expression for $d\ell/dt$ is required. Both $\phi_{en}(t)$ and $\phi_{en}(t + dt)$ in equation (4.45) depend on the angular displacement $\theta(t)$ and they are computed numerically solving the optimization problem introduced in this chapter. Hence, the integral in (4.45) cannot be solved off-line. For this reason it is necessary to develop an approximation of equation (4.45) that uses a discretization of the angular displacement θ in a similar manner to what was done for the computation of the span length L. In particular, the same discretization for θ in (4.35) used for the computation of L is used for the computation of the approximation for $d\ell$. For every point θ_i in the set Θ the corresponding value of ϕ_i can be obtained from the solution of the optimization problem. For every pair $(\theta_i, \theta_j) \in \Theta$ with $j > i$ the length of the span $\Delta\ell$ entering the control volume when the roll moves from θ_i to θ_j can be computed by

$$\Delta\ell(\theta_i, \theta_j) = \int_{\phi_i}^{\phi_j} \sqrt{r^2(\phi) + \left(\frac{dr}{d\phi}\right)^2} d\phi. \tag{4.47}$$

Note that for all pairs (θ_i, θ_j) with $j < i$, $\Delta\ell(\theta_i, \theta_j) = -\Delta\ell(\theta_j, \theta_i)$. The value obtained from equation (4.47) can be arranged in a table where the element $\Delta\ell(i, j) = \Delta\ell(\theta_i, \theta_j)$. This table can be used during the simulation to compute an approximate value for $d\ell/dt$.

Assuming that at simulation time t_{k-1} the value of the angular displacement is θ_{k-1} with $\theta_i < \theta_{k-1} < \theta_{i+1}$ and that at time t_k the angular displacement is θ_k with $\theta_j < \theta_k < \theta_{j+1}$, since no value for the movement from θ_{k-1} to θ_k is defined in the table for $\Delta\ell$, it is necessary to define an interpolation function to define

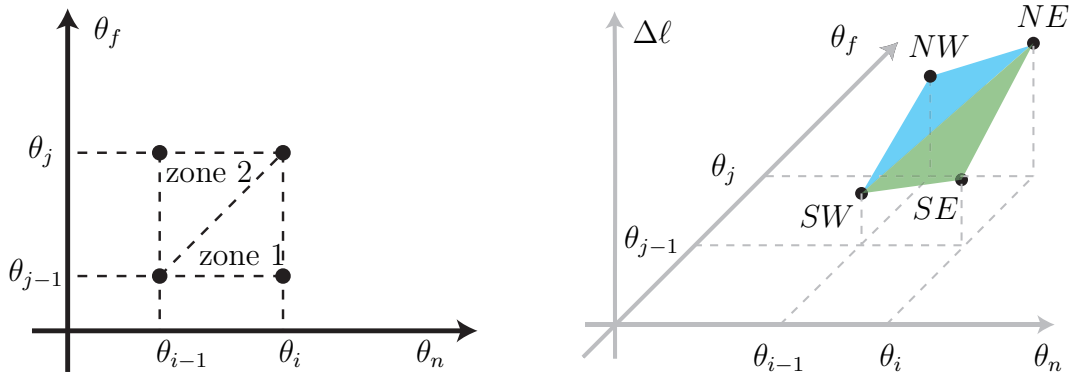

(a) Division of the area defined by the square $\{\theta_{i-1}, \theta_i\} \times \{\theta_{j-1}, \theta_j\}$ in the two zones.

(b) Construction of the two interpolation planes.

Figure 4.15: Construction of the interpolation function for $\Delta\ell$.

the value of $\Delta(\theta_{k-1}, \theta_k)$ given the discretized values $\Delta\ell(i-1, j-1)$, $\Delta\ell(i-1, j)$, $\Delta\ell(i, j-1)$ and $\Delta\ell(i, j)$ in the $\Delta\ell$ table.

First, the space for the interpolation in $\mathbb{R}^3$ is defined by the coordinates $\mathbb{L} \equiv (\theta_n, \theta_f, \Delta\ell)$ where θ_n is the initial angular displacement, θ_f is the final angular displacement and $\Delta\ell$ is the length of the span entering the control volume when the roll moves from θ_n to θ_f. Given the pair (θ_{k-1}, θ_k), using the table $\Delta\ell$ four points in $\mathbb{L}$ are defined: $SW \equiv (\theta_{i-1}, \theta_{j-1}, \Delta\ell(i-1, j-1))$, $NW \equiv (\theta_{i-1}, \theta_j, \Delta\ell(i-1, j))$, $SE \equiv (\theta_i, \theta_{j-1}, \Delta\ell(i, j-1))$ and $NE \equiv (\theta_i, \theta_j, \Delta\ell(i, j))$, see Fig. 4.15(b). For simplicity and to ensure continuity of the interpolation function, a linear interpolation is chosen. However, given four independent points in a three dimensional space it is not possible to find a single plane that contains all the points. For this reason the square defined by $(\theta_{i-1}, \theta_{j-1}), (\theta_{i-1}, \theta_j), (\theta_i, \theta_{j-1}), (\theta_i, \theta_j)$ is split into two zones (see Fig. 4.15(a)). If the combination (θ_{k-1}, θ_k) belongs to zone 1 then the interpolation is from the plane defined by the points $\{SW, SE, NE\}$, otherwise the interpolation is from the plane defined by the points $\{SW, NW, NE\}$,

see Fig. 4.15(b). Once the three points $\{P_1, P_2, P_3\}$ that define the plane are determined, the vector orthogonal to the plane is given by

$$n \equiv \begin{pmatrix} n_x \\ n_y \\ n_z \end{pmatrix} = (P_2 - P_1) \times (P_3 - P_1). \tag{4.48}$$

All the points on the plane defined by $\{P_1, P_2, P_3\}$ satisfy the equation

$$x(n_x - P_{1_x}) + y(n_y - P_{1_y}) + z(n_z - P_{1_z}) = 0. \tag{4.49}$$

therefore the value of the interpolation function for (θ_{k-1}, θ_k) is

$$\Delta\ell(\theta_{k-1}, \theta_k) = -\frac{1}{n_z - P_{1_z}} \left[\theta_{k-1}(n_x - P_{1_x}) + \theta_k(n_y - P_{1_y})\right]. \tag{4.50}$$

This procedure can be used to compute an on-line approximation of $d\ell/dt$ in (4.46) during the execution of the simulation.

A new computer simulation was implemented for the EWL with the initial governing equation for tension (3.1) replaced by the new governing equation in (4.46). The objective of this new simulation is to verify if the modified governing equation leads to better correlation between the experimental and the model simulation data. The results of the new simulation are shown in Fig. 4.17. With the modified governing equation for web tension there is a better correlation between the two data. Moreover, it can now be explained why the results from the simulation in Fig. 4.11(b) show larger oscillations compared to the experimental data. In the first simulation the governing equation for tension uses the peripheral velocity, see Fig. 4.16(a) and the span length variations, see Fig. 4.16(b), while the second simulation uses the equivalent material flow rate, see Fig. 4.16(a), and the span length variations. Figure 4.16(a) and Fig. 4.16(b) indicates how some of the span length variations are compensated by an increase in the equivalent material

flow rate. When using the the peripheral velocity this compensation does not take place which explains the higher amplitude in the oscillations. This further demonstrates why one must use the equivalent material flow rate instead of the peripheral velocity in the governing equation of tension in order to appropriately simulate the system.

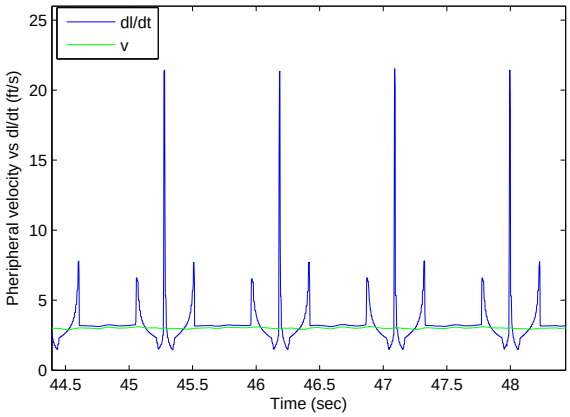

(a) Peripheral velocity vs $d\ell/dt$.

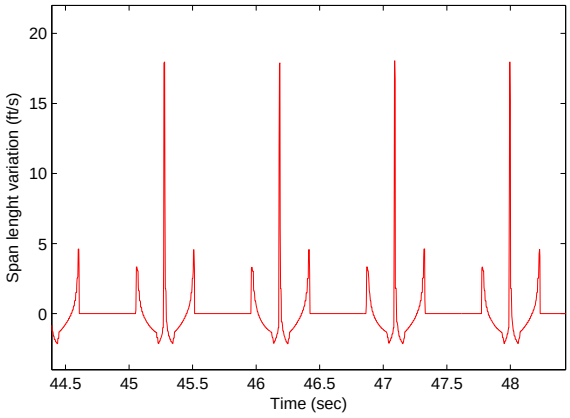

(b) Span length variations.

Figure 4.16: Example of how the use of the peripheral velocity neglects a significant amount of material flow in the case of a roll with a flat spot.

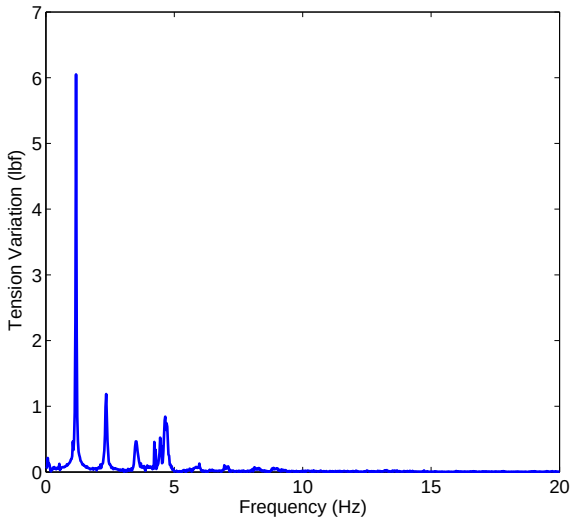

(a) FFT of the experimental data.

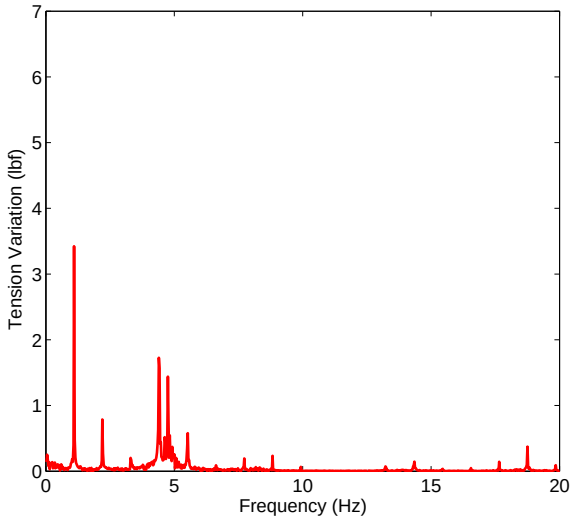

(b) FFT of the simulated data.

Figure 4.17: Comparison between experimental and simulation data at 200 FPM with wooden insert simulating a flat spot using modified governing equation for web tension.

Chapter 5

Control Algorithms for the Attenuation of Tension Oscillations

The previous chapters of this study focused on the development of models for web tension and web velocity in the presence of non-ideal rolls and rollers. This chapter focuses on the design of control algorithms for the attenuation of the tension oscillations which may be due to the presence of the eccentric rollers or out-of-round material rolls.

While designing a controller for an industrial application, in addition to the usual stability and performance issues, there are other aspects to be taken into consideration which limit the choice of the control algorithm. First, the operators of the algorithm will most likely be first level control engineers who seldom have more than a basic knowledge of control theory. Hence, it is preferable to choose a simple control technique that is easy to implement as well as whose development is straight forward. Despite a number of algorithms are available in the literature on compensation of nonlinearities arising from non-ideal behavior of the underlying

system components, many of these approaches are general and not application specific. Moreover they are complicated and require an understanding that is beyond the theoretical background of a first level controls engineer. Further the algorithm has to be implemented on a real time platform and therefore it needs to be executed within one sampling period which is typically of the order of 5 to 10 milliseconds. Also the algorithm must be adequately robust such that it need not be continuously monitored and tuned. These represent the main constraints in the design for a feasible control algorithm.

The choice of specific model based control techniques is not an option given the constraints introduced previously. In fact, as shown in the previous chapters, the models for web tension and web velocity are very complex and often require the use of time consuming numerical algorithms that are not well suited for real time application. For this reason the focus was on the design that include adaptive algorithms.

The compensation of tension oscillations due to eccentric roller was considered first. Eccentricity compensation is a common problem in rotating mechanical systems and therefore, there has been existing work addressing this problem. Some of the algorithms are considered and among those the adaptive feed-forward (AFF) was elected to be the best fit for the eccentricity compensation. Several adjustments to the original algorithm are presented to apply to the web handling machine and to achieve better reduction of the tension oscillations. The second part of this chapter shows how the same algorithm can also be used for attenuation of tension oscillations due to out-of-round rolls. Lastly, the designed algorithm can be used in web line where one is not sure of the source of tension oscillations, that is, this algorithm is not specific to tension oscillations originating from non-ideal rollers.

5.1 Control Algorithms for Eccentricity Compensation

The presence of eccentricity is fairly common in the presence of rotating machines, examples include: engine noise in turboprop aircrafts [18] and automobiles [19], ventilation noise in Heating, Ventilation and Air Conditioning Systems, [20] and many more. Several studies on control algorithms for the compensation of eccentricity can be found in the literature. For example [21] proposes an adaptive algorithm for the compensation of eccentricity. The authors first included in the system an internal model of the eccentricity, designed an observer for the extended system, and then proposed an adaptation law for the estimation of the frequency of the eccentricity. In [22] the authors propose the use of repetitive control for eccentricity compensation in rolling; computer simulations are shown to illustrate the effectiveness of repetitive control in rejecting oscillations but no experimental results are provided. In [23] more details on repetitive control for nonlinear systems can be found, and in [24] the use of repetitive control for state dependant disturbances rejection is discussed. In [25] a nonlinear PI controller for controlling an uncertain system is introduced; one of the applications of the controller presented in the paper is eccentricity compensation. These algorithms are computationally complex and therefore difficult to implement in real time, therefore they cannot be adapted for the use in web lines.

One important aspect in the compensation of eccentricity is that it is a state dependant disturbance and not an exogenous time dependant disturbance. Therefore, even if the resulting effects of eccentricity on the output are periodic oscillations, the techniques available for exogenous disturbance rejection cannot be used. However, under certain circumstances eccentricity appearing in the gov-

erning equation may be approximated by an exogenous disturbance. Consider a simple model for a motor with eccentricity

$$\begin{aligned} \dot{\theta} &= \omega, \\ J\dot{\omega} &= -b\omega - mge\sin(\theta) \end{aligned} \tag{5.1}$$

where J is the inertia of the motor, b is the viscous friction coefficient, m is the mass of the motor, g is the acceleration due to gravity and e is the amount of eccentricity. If the motor speed is regulated at a reference value ω_r, it is possible to define the angular displacement error e_θ by

$$e_\theta = \theta(t) - \omega_r t. \tag{5.2}$$

Using (5.2) the eccentricity term can be written as

$$\begin{aligned} mge\sin(\theta(t)) &= mge\sin(\omega_r t + e_\theta) \\ &= mge(\sin(\omega_r t)\cos(e_\theta(t)) + \cos(\omega_r t)\sin(e_\theta(t))) \\ &\approx mge\sin(\omega_r t) \end{aligned} \tag{5.3}$$

Under the assumption that the regulation error $e_\theta << 1$, the eccentricity term as above may be approximated with an exogenous time dependant disturbance. Clearly, the angular displacement error is a function of several variables, including the amount of eccentricity, the physical properties of the motor and the parameters of the controller. In general one cannot assume that the regulation error is smaller than one. To verify whether the approximation in (5.3) is valid for the EWL, several tests were run at different velocities and the result was that $e_\theta << 1$. Figure 5.1 shows the error e_θ in the S-Wrap Lead roller for one of the experiments, for this experiment $\max(|e_\theta|) = 0.004$.

Since eccentricity can be approximated by an exogenous disturbance in certain cases as discussed above, classical techniques may be considered for disturbance rejection.

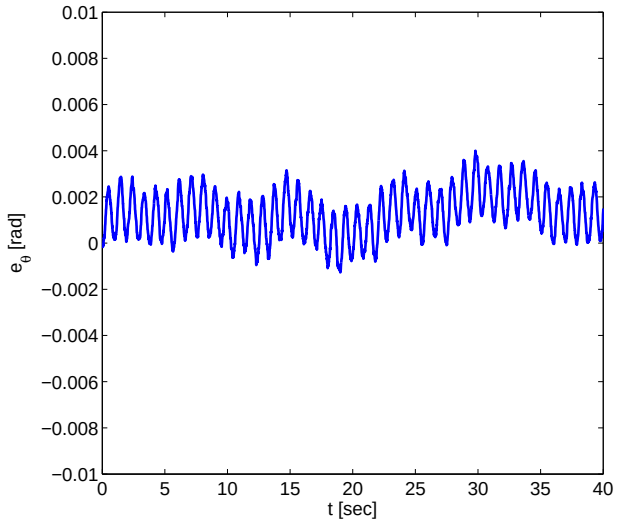

Figure 5.1: Angular displacement error e_θ for the S-wrap Lead roller for web line speed of 200 FPM.

The most established technique for exogenous disturbance rejection is the use of internal model of the disturbance in the controller [26]. The internal model principle states that in order to reject an exogenous disturbance it is sufficient to have a model of the disturbance in the controller under the constraint that the resulting closed loop system is stable. Hence, the rejection of sinusoidal oscillations requires the inclusion of a model of the sinusoidal disturbance in the controller which means adding two complex conjugate poles on the imaginary axis of the complex plane at the frequency of the sinusoidal disturbance. Despite this technique is well known and well understood, it carries a major disadvantage. The addition of marginally stable poles in the controller makes the stability of the overall system more difficult to the point that, if disturbances at multiple frequencies are present, a simple PI might not be enough to stabilize the overall system. For these reasons the adaptive feed-forward was considered instead.

The adaptive feed-forward (AFF) is based on a very simple idea: use an adap-

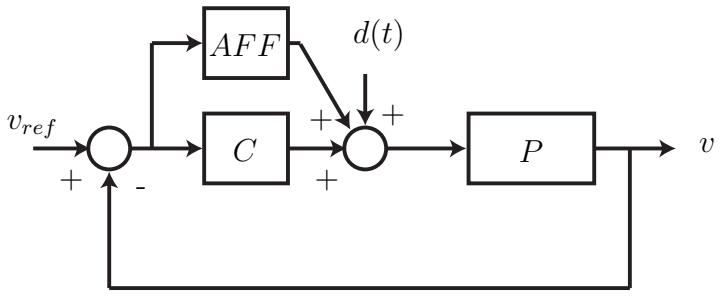

Figure 5.2: Adaptive feed-forward control scheme.

tive algorithm to estimate the amplitude and phase of the disturbance and feed-forward a control action equal and opposite to the estimated disturbance. Early work on the AFF can be found in [27, 28] in which the authors describe stability and robustness of the algorithm. Consider a system such as the one in Fig. 5.2 and assume that the disturbance $d(t)$ is in the form

$$\begin{aligned} d(t) &= A\sin(\omega t + \phi) \\ &= A\sin(\phi)\sin(\omega t) + \cos(\phi)\cos(\omega t) = A_1\sin(\omega t) + A_2\cos(\omega t). \end{aligned} \tag{5.4}$$

The AFF uses the output error to estimate A_1 and A_2. Let the estimates for the parameters A_1 and A_2 be denoted by θ_1 and θ_2, respectively. The adaptation law for the parameters θ_1 and θ_2 is

$$\begin{aligned} \dot{\theta}_1 &= g_1 e(t)\sin(\omega t), \\ \dot{\theta}_2 &= g_1 e(t)\cos(\omega t) \end{aligned} \tag{5.5}$$

where $e(t) = y_r - y(t)$ is the output error and g_1 is the adaptation gain. The feed-forward part of the algorithm is

$$u_{ff} = -\theta_1\sin(\omega t) - \theta_2\cos(\omega t). \tag{5.6}$$

The adaptive algorithm may be explained in the following way. The adaptive parameter θ_1 is initialized to zero. If the output error has a sinusoidal component at the frequency ω, i.e., $e(t) = \bar{e}(t) + e_{A_1}\sin(\omega t)$, the product $e(t)\sin(\omega t)$

will produce a term $e_{A_1}\sin^2(\omega t)$ which is positive and will therefore increase the estimation parameter θ_1. As θ_1 increases the effect of the disturbance starts decreasing until θ_1 reaches the amplitude of the disturbance A_1. At that point the output error will not have any more sinusoidal components at the frequency ω since the disturbance is fully compensated by the term $-\theta_1\sin(\omega t)$ in u_{ff}. With the disturbance compensated, the integral of product $e(t)\sin(\omega t)$ will be zero over a period and hence the estimation parameter θ_1 will remain constant. The same reasoning applies for θ_2.

The control algorithm in (5.5) and (5.6) is the AFF in its simplest form. In [29] the authors introduce a modified version of the AFF algorithm which includes a phase shifter. The phase shifter helps in increasing the stability margin of the AFF and reduces the adaptation time. The implementation of the phase shifter requires the knowledge of the transfer function between the disturbance and the control input or at least the value of the transfer function at the frequency of the disturbance. The algorithm for the modified AFF is

$$\begin{aligned}\dot{\theta}_1 &= g_1 e(t)\sin(\omega t+\phi),\\ \dot{\theta}_2 &= g_1 e(t)\cos(\omega t+\phi)\end{aligned} \tag{5.7}$$

where $\phi = \angle P(j\omega)$ is the phase of the process transfer function at the frequency of the disturbance.

Several versions of the AFF for cases where the frequency of the disturbance is unknown and time varying have also been developed; a complete discussion about these algorithms can be found in [30]. This is not a concern for the web handling application since the frequency of oscillation due to rotating machines is always known. In fact the frequency of the oscillations is equal to the rotational frequency of the machines or it is an integer multiple of this frequency. The

rotational frequency of the machine can be obtained from the velocity feedback for material rolls or computed from the line speed for rollers of known radius.

The AFF algorithm with phase shifter was applied to the web handling case in [31]. In the paper the authors assume that the tension oscillations can be modeled as an input sinusoidal disturbance to the transfer function $G(s)$ from the torque input to the output tension. However, as shown in previous chapters, the tension disturbances in the presence of a non-ideal roll come from different locations. This is important since in order to use the phase shifted version of the AFF, it is necessary to know the exact transfer function from the disturbance to the output, otherwise the benefits of the phase shifter are lost and it could even lead to decreased performance of the AFF. Moreover, the authors apply the AFF to a small testbed where all the parameters in the model are easily identified, whereas in an industrial setup the model parameters are mostly unknown and experiments to obtain the process transfer function might be unpractical. In [32] a version of the AFF with an adaptive phase shifter is presented. In this case the adaptation algorithm not only adapts to the sinusoidal disturbance amplitudes but it also adapts the phase shifter to identify the transfer function from the disturbance to the output. However, the AFF with adaptive phase shifter is a much more complicated algorithm which nullify the main reason for picking the AFF, its simplicity. Hence, the AFF with adaptive phase shifter was not considered as a viable option.

After literature review and a number of experiments on the web handling platform, EWL, using various approaches it is evident that the AFF in its basic form is the best suited control algorithm for the rejection of the oscillations due to eccentricity.

In the EWL both S-wrap lead and follow rollers have eccentricity, see Fig. 2.4.

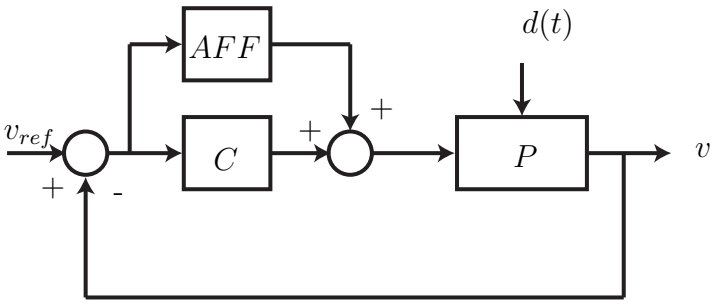

Figure 5.3: Adaptive feed-forward control scheme torque signal implementation.

The initial step was to add the AFF to compensate for the oscillations in the roller velocity. In chapter 3 it was discussed how the oscillations in tension are in part due to the oscillations in velocity, therefore, by reducing the velocity oscillations it is possible that the oscillations in tension would be reduced as well. Moreover, attenuation of oscillations in the velocity signal could be useful for many other applications.

As described in previous the chapters the S-wrap lead and follower rollers are both under pure velocity control. The AFF input is the velocity error and the output is a torque reference signal for the drive, see Fig. 5.3. The equations for the AFF controller are

$$\begin{aligned} \dot{\theta}_1 &= g_1(v_r - v_{Sf})\sin(\omega t), \\ \dot{\theta}_2 &= g_1(v_r - v_{Sf})\cos(\omega t), \\ \tau_{ff} &= -\theta_1 \sin(\omega t) - \theta_2 \cos(\omega t) \end{aligned} \tag{5.8}$$

where v_r is the velocity reference for the line, v_{Sf} is the velocity of the S-wrap follower, ω is the frequency of the disturbance that is being attenuated, τ_{ff} is the feed-forward torque signal generated for the drive, and g_1 is the adaptation gain. The AFF is designed to attenuate the fundamental frequency of the oscillations

which is given by

$$f = \frac{v}{\pi D} \tag{5.9}$$

where v is the web velocity and D is the diameter of the roller.

The tuning procedure for the gain of the AFF is simple and a direct consequence of the stability proof of the AFF algorithm [33, 30]. It is proven that the AFF is stable as long as the underlying process is stable and the adaptation gain is small. Based on that the AFF can be tuned by starting with a very small gain and increasing it until a good performance is achieved.

Figure 5.4 shows the comparison of the FFT of the velocity of the S-wrap follower with and without the AFF and with a reference velocity of 200 FPM. First note that the fundamental frequency of the disturbance is practically eliminated. However a slight increases over the whole spectrum is also shown in the plot. This is because the AFF is generating a torque signal which is input to the motor drive. It is well known in the web handling community that the performance of the motor drive for tracking torque reference is not as good compared to the performance of the same drive when tracking a velocity reference.

To avoid this problem the AFF can be used to generate a velocity reference instead of torque reference, see Fig. 5.5. The equations for this new version of the AFF are

$$\begin{aligned} \dot{\theta}_1 &= g_1(v_r - v_{Sf})\sin(\omega t), \\ \dot{\theta}_2 &= g_1(v_r - v_{Sf})\cos(\omega t), \\ v_{ff} &= -\theta_1 \sin(\omega t) - \theta_2 \cos(\omega t) \end{aligned} \tag{5.10}$$

where the output of the AFF is now a reference velocity correction to the drive. The reason why the AFF is originally used to generate a compensating torque signal is because it is expected directly cancel the effect of the torque due to ec-

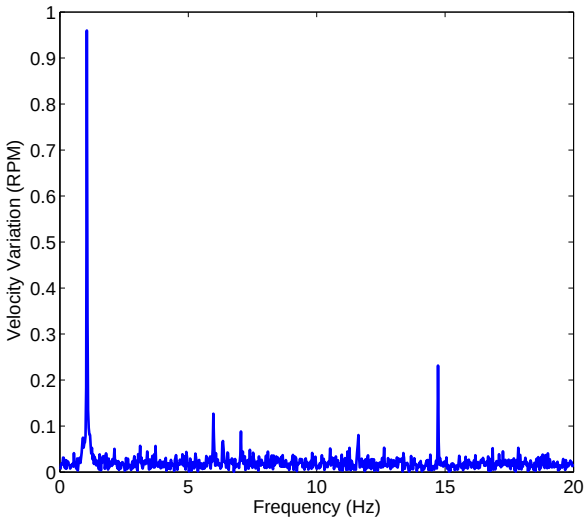

(a) FFT of the S-wrap follower velocity with PI only.

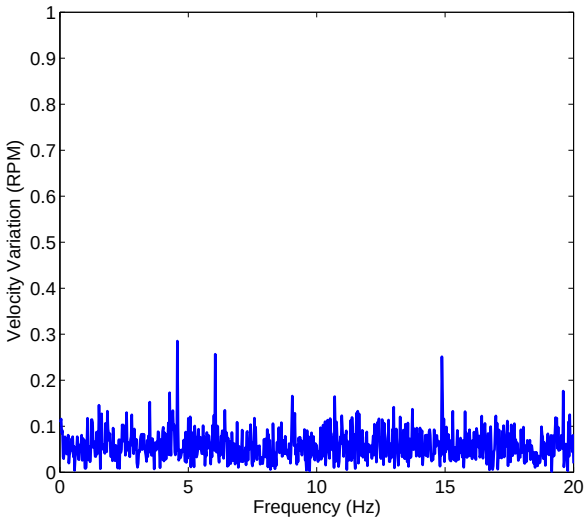

(b) FFT of the S-wrap follower velocity with PI and AFF.

Figure 5.4: Comparison between FFT of S-wrap follower velocity for PI only and PI+AFF.

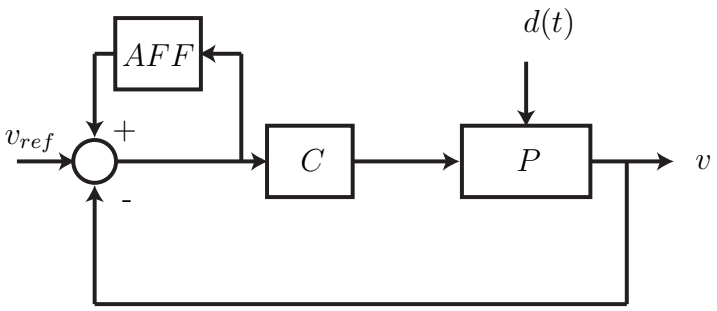

Figure 5.5: Adaptive feed-forward control scheme.

centricity using the torque generated by the drive. However, this is not necessary. Assuming that the torque due to eccentricity τ_e can be approximated by

$$\tau_e = A\sin(\omega t + \phi) \tag{5.11}$$

and the transfer function of the PI controller is $C(s)$, when using the AFF to generate a velocity reference as in Fig. 5.5, the AFF output u_{AFF} will converge to

$$v_{ff} = \frac{1}{|C(j\omega)|} A\sin(j\omega + \phi - \angle C(j\omega)) \tag{5.12}$$

as opposed to $-\tau_e$. The signal v_{ff} in the input to the controller will produce an output equal and opposite to τ_e and hence compensation will be achieved in the same manner as in the previous configuration. Using similar arguments one can state that the AFF can be added at any point in the control loop as long as the path between that point and the entry of the disturbance into the system is composed of linear systems.

Figure 5.6 shows the FFT of the velocity signal with the AFF output as a velocity correction. Comparison of results shown in Fig. 5.6(b) and Fig. 5.4 indicates that in both cases the AFF effectively attenuates the velocity oscillations, but Fig. 5.6(b) shows no increase in the base line oscillations compared to Fig. 5.4(b). Figure 5.7 shows the FFT of the tension signal in the pull-roll section of the

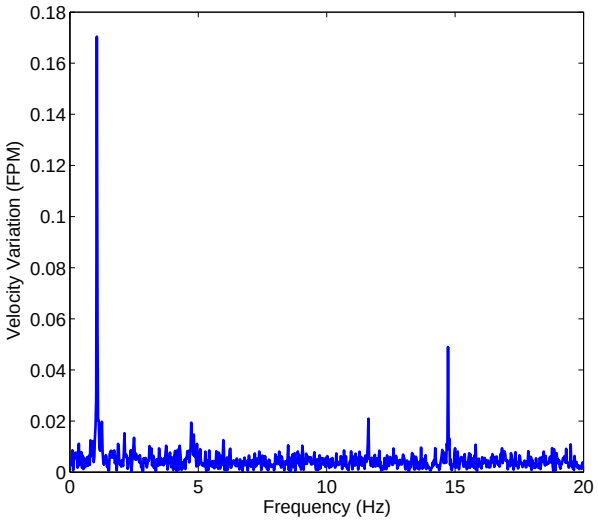

(a) FFT of the S-wrap follower velocity with PI only.

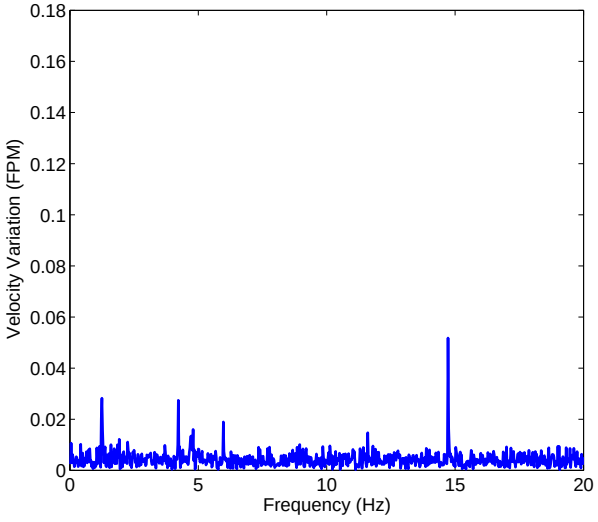

(b) FFT of the S-wrap follower velocity with PI and AFF.

Figure 5.6: Comparison between FFT of S-wrap follower velocity for PI only and PI+AFF with feed-forward signal on velocity reference.

EWL with and without the AFF for the compensation of the eccentricity in the S-wrap follower. The figure shows how the compensation of the eccentricity in the S-wrap has little effect on the tension signal. In fact only the second harmonic is attenuated. Note that the pull-roll section is chosen because in this section tension oscillations are only due to the eccentricity of the S-wrap follower and therefore the effect of the AFF would be more evident compared to the unwind zone where tension oscillations are due to both eccentricity of the S-wrap lead roller and out-of-roundness of the unwind roll.

The addition of the AFF in the velocity loop, despite good attenuation of the oscillations in the velocity signal, did not improve the tension signal as expected. With similar arguments as the ones presented in (5.3) one can assume that the oscillations in tension can also be approximated by an exogenous sinusoidal disturbance. Under this assumption the AFF can be used to attenuate such oscillations. This new configuration of the AFF is shown in Fig. 5.8 and the equations are

$$\begin{aligned} \dot{\theta}_1 &= g_1(t_r - t_{pr})\sin(\omega t), \\ \dot{\theta}_2 &= g_1(t_r - t_{pr})\cos(\omega t), \\ v_{ff} &= -\theta_1 \sin(\omega t) - \theta_2 \cos(\omega t) \end{aligned} \tag{5.13}$$

where t_r is the tension reference and t_{pr} is the tension feedback from the pull roll section. Figure 5.9 shows the comparison of the FFT of the tension with and without the AFF with the line speed of 200 FPM. The figure shows that the AFF achieves very good attenuation at the fundamental frequency and at the second and third harmonics. This further corroborates the model for the eccentric roller developed in Chapter 3. The model shows that the higher order harmonics are generated as a consequence of the interaction between the tension disturbance at the fundamental frequency and the disturbance in web velocity. Therefore, by

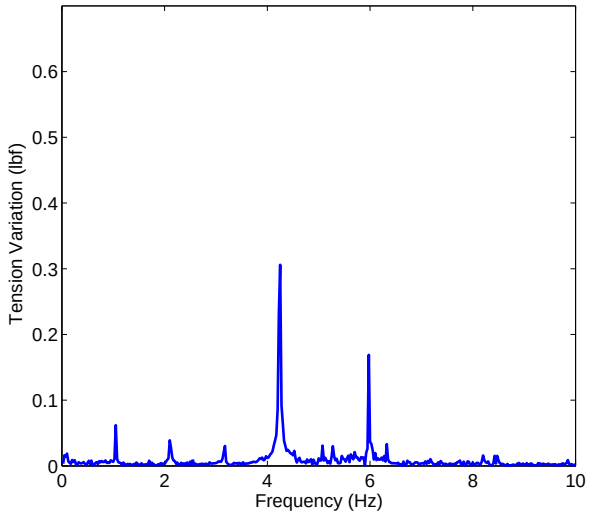

(a) FFT of the tension in the Pull-Roll section with S-wrap follow on PI only.

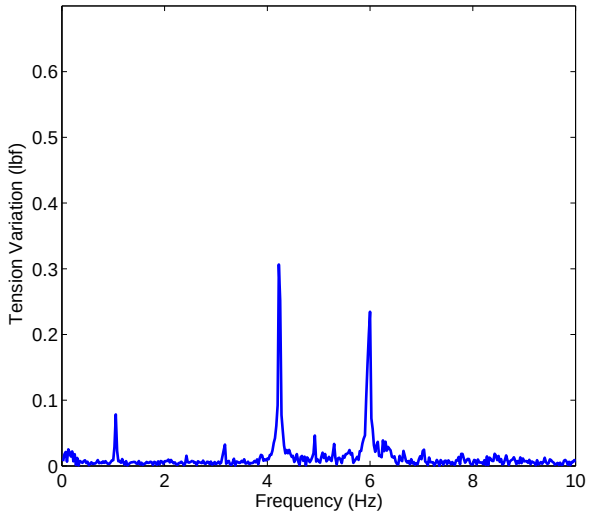

(b) FFT of the tension in the Pull-Roll section with S-wrap follow on PI+AFF.

Figure 5.7: Comparison between FFT of the tension in the Pull-Roll section for S-wrap with PI only and PI+AFF with feed-forward signal on velocity reference.

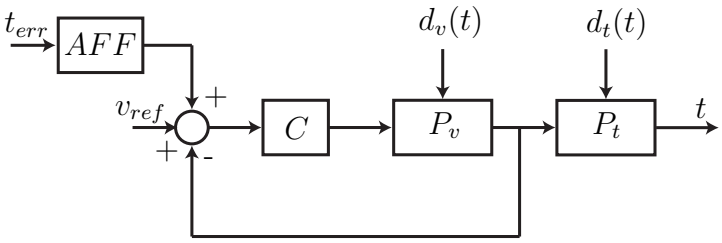

Figure 5.8: Adaptive feed-forward control scheme.

reducing the disturbance at the fundamental frequency, higher order harmonics are attenuated as well.

The AFF satisfies all the constraints described in the introduction and is efficient in compensating tension and velocity oscillations in the case of the presence of an eccentric roller. The following section describes the application of the AFF to the case of an out-of-round material roll.

5.2 Attenuation of Tension Oscillations Due to an Out-of-round Material Roll

The problem of compensating tension oscillations due to the presence of out-of-round material roll is similar to the case of the eccentric roller. However, one major difference is that while the frequency of the disturbance induced by the presence of an eccentric roller remains constant over time, the frequency of the disturbance associated with an out-of-round material roll changes with decrease in roll diameter. The equation used for the computation of the fundamental frequency of the disturbance in (5.9) for the case of the eccentric roller is also applicable to the out-of-round roll, but now the diameter of the roll is time varying making the frequency of the disturbance also time varying.

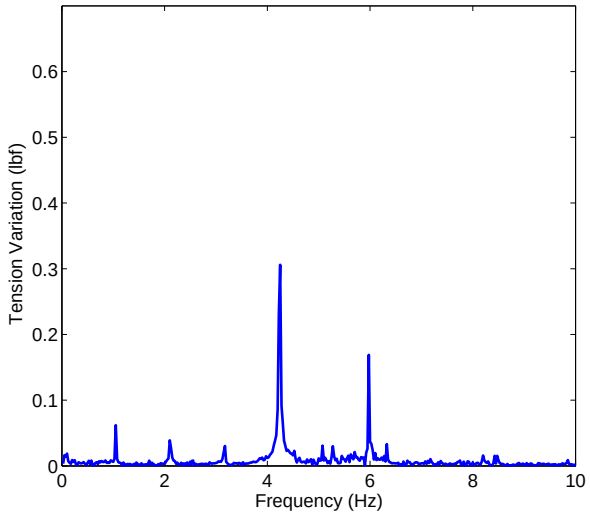

(a) FFT of the tension in the Pull-Roll section with S-wrap follower on PI only.

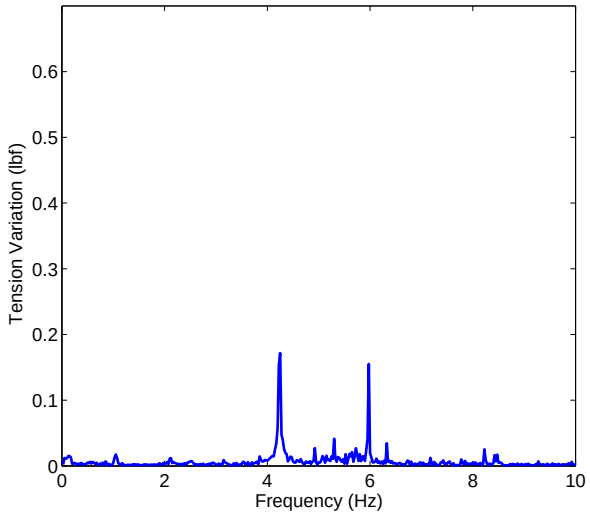

(b) FFT of the tension in the Pull-Roll section with S-wrap follower on PI+AFF.

Figure 5.9: Comparison between FFT of the tension in the Pull-Roll section for S-wrap with PI only and PI+AFF with AFF using tension error.

The AFF algorithm is originally intended for the compensation of sinusoidal disturbances with constant frequency. However, in [30] it is shown that the algorithm can also be used when the frequency is time varying if the rate of change of frequency is small. The frequency of the disturbance generated by an out-of-round roll (5.9) and its rate of change depend on two factors: the line velocity and the diameter of the roll. The frequency of the disturbance is varying slowly if the line speed is slow or if the roll has a large radius, in these cases the AFF can be used for the attenuation of disturbances. This might seem too restrictive but there is another aspect to be considered: disturbances at low frequencies are more critical than the one with high frequency. The system of web spans and idle rollers naturally behave as a low pass filter and reject high frequency disturbances as the web is transported. On the other hand, low frequency disturbances are not attenuated significantly and if no action is taken they can propagate downstream and affect processes downstream. Therefore, the AFF can be used effectively because the disturbance with low frequencies that need to be rejected can only be generated in the presence of rolls with large radii or for web lines with low speed.

The AFF algorithm, similarly to the case of the eccentric roller, has tension error as input and generates a speed reference correction. It is assumed that the tension oscillation can be considered as an exogenous disturbance, as was done previously. The equations describing the AFF algorithm are

$$\begin{aligned} \dot{\theta}_1 &= g_1(t_r - t_{un})\sin(\omega t), \\ \dot{\theta}_2 &= g_1(t_r - t_{un})\cos(\omega t), \\ v_{ff} &= -\theta_1 \sin(\omega t) - \theta_2 \cos(\omega t) \end{aligned} \tag{5.14}$$

Figure 5.10 shows the overall control scheme for the unwind roll with the AFF placed in parallel with the PI controller for tension regulation. In the figure multi-

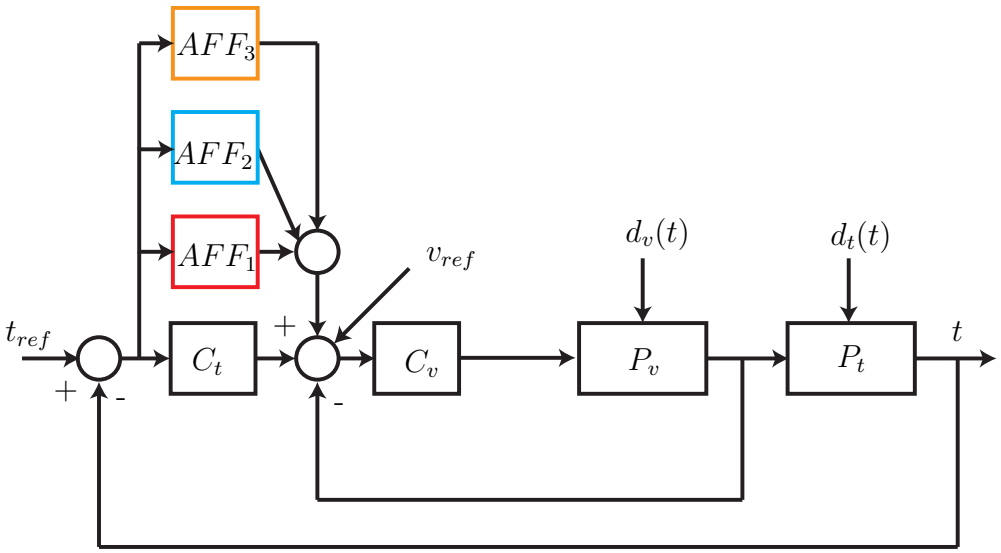

Figure 5.10: Adaptive feed-forward control scheme.

ple AFF blocks are added in parallel. In the presence of an out-of-round material roll, attenuation of the signal component at fundamental frequency does not produce attenuation of higher order harmonics, such as in the case of the eccentric roller. Therefore, it is necessary to add extra AFF blocks for the harmonics that need to be attenuated.

To test the algorithm the unwind roll is made purposely out-of-round by winding the web over a stack of paper; three different shapes of the out-of-round roll are used for testing:

- Shape 1: roll with flattened bulge (Fig. 5.11(a)). This shape is meant to resemble a flat spot
- Shape 2: roll with a bulge (Fig. 5.11(b)). Rolls might bulge due to gravity when they are suspended for extended period of time on mandrels.
- Shape 3: asymmetric profile (Fig. 5.11(c)). This shape was used to test the algorithm when the roll has an asymmetric profile that induces oscillations

with multiple frequencies.

Two different polymer materials are tested: Tyvek, a polymer made by Dupont, and polyethylene. This is done to test the robustness of the algorithm to different configurations, since it is possible to have web lines running different materials and out-of-round rolls can have different shapes. It is important to have a robust algorithm because it would be impractical in a production environment to adjust the AFF gains when the operating conditions change.

All the tests were performed with the web moving at 100 FPM, with material roll radius of 8 in and with the gain of the AFF unchanged. Figures 5.12, 5.13, 5.14, 5.15 show the results of the tests. The plots show that the AFF performed very well on the fundamental and first harmonic of the disturbance in all the scenarios while the performance on the second harmonic is not as good. The reason for this decreased performance for the second harmonic is that its frequency is moving at a faster rate compared to the fundamental frequency and the first harmonic, and hence, the AFF is expected to be less effective.

In conclusion the AFF is a simple and robust solution for attenuation of oscillations due to the presence of non-ideal rolls. It satisfies all the requirements discussed in the introduction. It is a simple algorithm that can be used by a first level control engineer or a line technician; it is not computational intensive so that it can be easily implemented on a real-time platform. It is also shown to be robust to different scenarios without the need for retuning of the adaptation gains with extensive experimentation on a web platform.

(a) Roll with a flattened bulge.

(b) Roll with a bulge.

(c) Asymmetric profile.

Figure 5.11: Roll shapes.

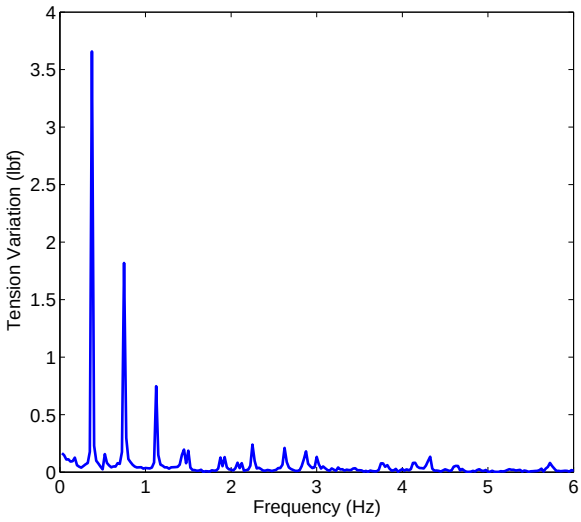

(a) PI only.

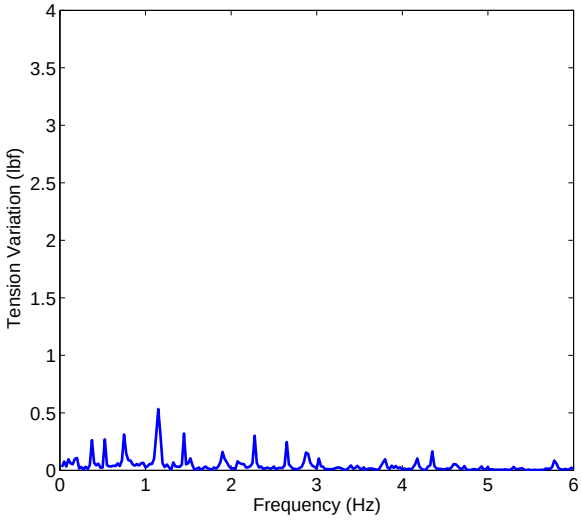

(b) PI+AFF.

Figure 5.12: Comparison between FFT of tension for PI and PI+AFF implementation in the unwind section for roll shape 1.

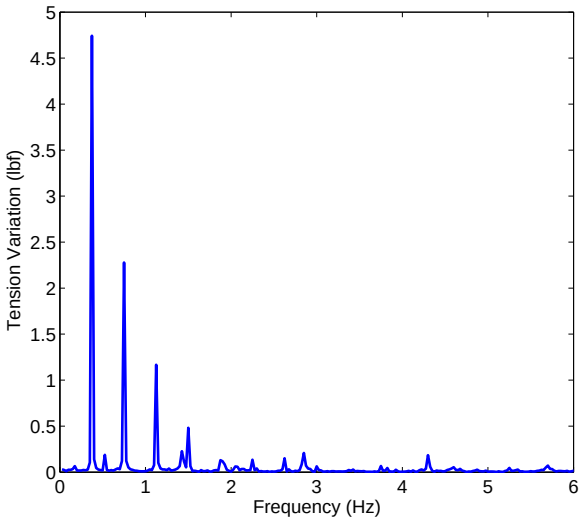

(a) PI only.

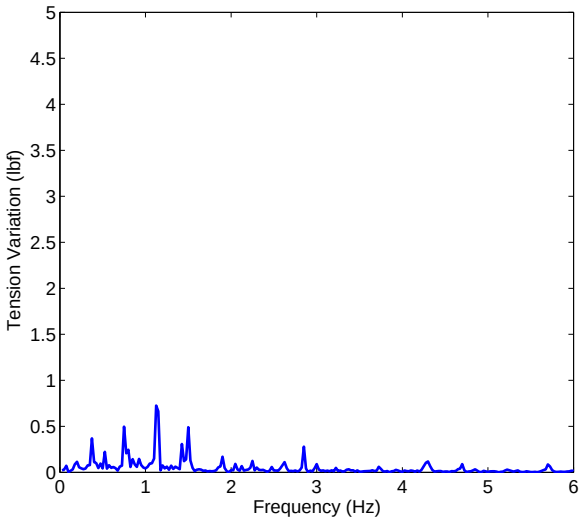

(b) PI+AFF.

Figure 5.13: Comparison between FFT of tension for PI and PI+AFF implementation in the unwind section for roll shape 2.

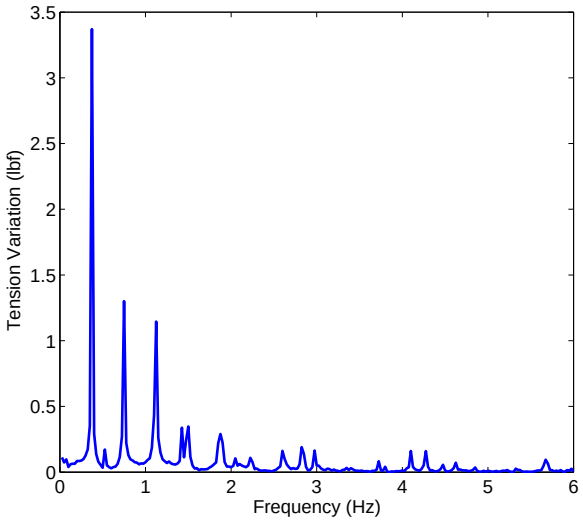

(a) PI only.

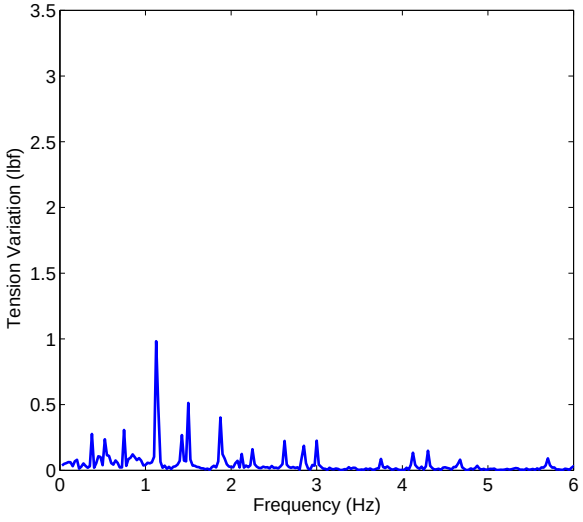

(b) PI+AFF.

Figure 5.14: Comparison between FFT of tension for PI and PI+AFF implementation in the Unwind section for roll shape 3.

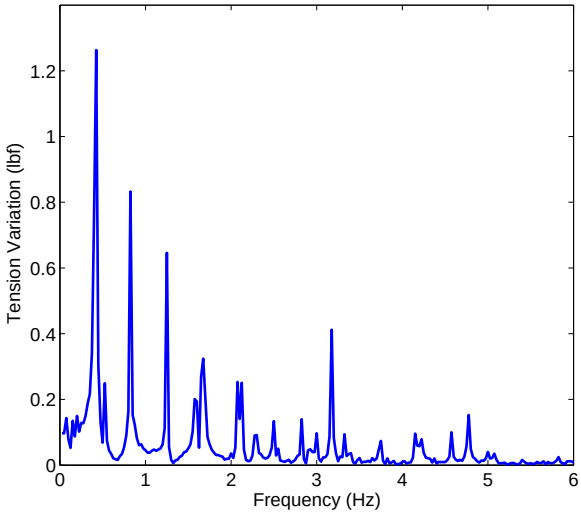

(a) PI only.

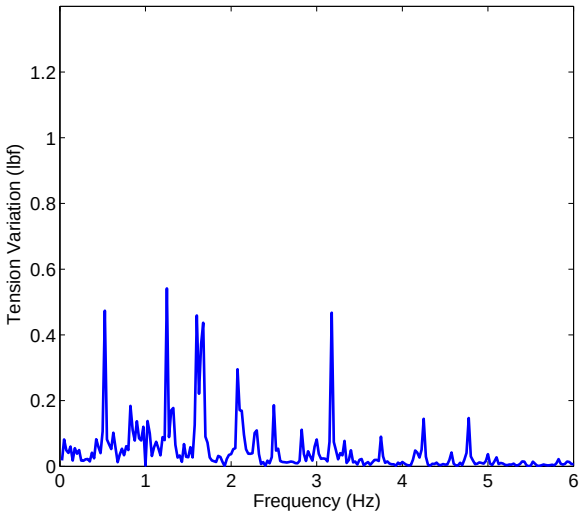

(b) PI+AFF.

Figure 5.15: Comparison between FFT of tension for PI and PI+AFF implementation in the unwind section for roll shape 1 for polyethylene.

Chapter 6

Summary and future work

The research presented in this report focused on modeling and control problems associated with web handling machines in the presence of non-ideal rotating elements. Web processes, also know as roll-to-roll processes, are very common industrial processes, and therefore, the literature contains many articles proposing models for describing the behavior of web (web tension and web velocity) it while is transported on rollers through the machine. Among the proposed models the one which is most widely accepted is based on the concept of primitive elements: every basic element of the web line is modeled independently using a first principles approach and the model for the web line is obtained by combining these basic building blocks. Despite the availability of these primitive element models of web machines, comprehensive experimental validation of the primitive elements was lacking. Therefore, the first objective of this research was to design a set of experiments for the validation of the models available in the literature. Chapter 2 focused on modeling and experimental validation of primitive elements for web handling machines. The results from the model validation show how the models found in the literature are able to reproduce the behavior of the web tension only in an average sense but fail to reproduce the periodic oscillations that are

commonly seen measured signals from web machines. This showed that the first order effects are included in existing primitive element models and highlighted the need to investigate second order effects that could be the cause for oscillations in tension and speed signals.

An extensive set of experiments which show the link between the presence of tension oscillations and rotating elements in the web line are presented in the second part of Chapter 2. Through extensive experimental observations on a large platform, the source of oscillations due to non-ideal rolls is identified. Once the source of the oscillation was identified, it was necessary to include in the models the mechanism that actually produces these oscillations.

Chapter 3 discussed the modeling and validation of the governing equations for web tension and web velocity in the presence of an eccentric roller. First it was observed that the length of the spans adjacent to the eccentric roller is time-varying. One of the assumptions in the derivation of the governing equation for web tension is the time invariance of the web span length. This assumption was relaxed and a new governing equation for web tension in a span was obtained. The new governing equation for tension includes the time-varying span length and its derivative. In order to numerically solve the new governing equation for web tension, expressions for the span length and its derivative are needed. A procedure to obtain a closed form expression for the span length as a function of the roller position was given. The modified equation for web velocity was derived to include the torque due to the eccentricity. The chapter ends with the validation of the proposed model.

The derivation of the governing equations for web tension and roller angular velocity in the presence of an out-of-round material roll were described in Chapter 4. The presence of an out-of-round material roll introduces additional

challenges compared to the case of the eccentric roller. The length of the span adjacent to the out-of-round roll is also time-varying but the computation of the span length as a function of the angular position of the roll is much more involved and a closed form expression for the span length is difficult to obtain. A numerical algorithm was proposed instead. The numerical algorithm is based on formulating the problem of founding the span length as an optimization problem which is employed to search among the family of tangents to the out-of-round roll the one that is also tangent to the downstream idle roller.

Apart from the inclusion of the span length variation in the governing equation of web tension, another aspect had to be considered in the case of the out-of-round material roll. The derivation of the governing equation for web tension is based on the conservation of mass in the control volume encompassing the span. For an ideal roll the material flow rate in the control volume is proportional to the peripheral velocity of the web on the roll; this is not true for an out-of-round material roll. Again, a closed form expression for the material flow rate could not be found, a numerical algorithm was presented.

A new governing equation for the angular velocity is derived including the effect of the out-of-roundness of the roll. The proposed model for the out-of-round roll was validated by comparing the data from model simulations with experimental data from the Euclid Web Line platform.

In summary, the first part of this document showed that the first order effects are well represented by the primitive element models in the literature. However, when non-ideal elements are present in the web line, second order effect must be included in the governing equation of tension and velocity. To identify the second order effects in the governing equation it was necessary reconsider the derivation of the governing equations and verify all the assumptions. By doing so it was

identified the need to include the span length variations and the computation of the material flow rate in the governing equation of tension in the web span. Similar approaches should be used when modeling other non-ideal elements or other processes, such us thermal or hygral effects. For example, if thermal effects have to be included in the the governing equation of web tension what is the right mechanism to consider the span length variations induced by the thermal effect? For example, because of the heating or cooling of the web, the density of the incoming web will be different from the density of the outgoing web which has to be considered when computing the material flow rate.

The last part of this research covered the design of a controller for attenuation of the oscillations generated by an eccentric roller or an out-of-round material roll. There are constraints on the choice of the control algorithm enforced by the fact that the algorithm has to be executed in a real-time platform and in an industrial environment. First, the control algorithm has to be executed within the system sampling time, therefore, there is a constraint on the computational complexity of the algorithm. There is also a constraint on the theoretical complexity of the algorithm. Also to limit the down time of the web line in a production environment, the algorithm should require little or no retuning of the existing control algorithm for tension and velocity regulation and work in parallel to the existing controller.

After a literature review of the available control algorithms for tension attenuation, the adaptive feed-forward was identified as a control algorithm that would satisfy all the constraints. The AFF is based on a simple concept, the amplitude and phase of the disturbance are identified and a feed-forward signal is generated to compensate for those oscillations. Several implementations of the AFF were investigated and tested for different scenarios including different web and different

roll shapes. The AFF implementation in the velocity loop of the control system proved to be effective in reducing the oscillations due to out-of-round material rolls and eccentric rollers.

This work focused on modeling, validation, and tension control in the presence of non-ideal rolls in web handling machines. Other primitive elements are commonly found in roll-to-roll processes such us pendulum dancers, accumulators, etc. Experimental validation of these elements is still lacking and should be considered as future work.

Implementation and testing of more sophisticated versions of the AFF may be considered as part of the future work. Also of interest is the analysis of the effect of the sampling period on the performance of the AFF, it is possible that a faster sampling time might improve the performance of the AFF for disturbances with fast changing frequencies.

The adaptive feed-forward technique was presented as a feasible control scheme for attenuation of tension oscillations. Improvements to the implementation of the controller should be investigated to extend its application to high speed lines. Also, the AFF could be considered for compensation of periodic oscillations generated by other non-ideal components.

BIBLIOGRAPHY

[1] G. Brandenburg, "New mathematical model for web tension and register error," in *Proceedings of the 3rd International IFAC Conference Instrumentation Automation Paper, Rubber Plastic Industry*, pp. 411–438, 1977.

[2] J. J. Shelton, "Dynamics of web tension control with velocity or torque control," in *Proceedings of the American Control Conference*, pp. 1423–1427, 1986.

[3] G. E. Young and K. N. Reid, "Lateral and longitudinal dynamic behavior and control of moving webs," *ASME Transactions, Journal of dynamic systems, measurement, and control*, vol. 115, no. 2, pp. 309–317, 1993.

[4] H. Koc, D. Knittel, M. DeMathelin, and G. Abba, "Modeling and robust control of winding systems for elastic webs," *IEEE Transactions on Control Systems and Technology*, vol. 10, pp. 197–208, March 2002.

[5] P. R. Pagilla, N. B. Siraskar, and R. V. Dwivedula, "Decentralized control of web processing lines," *IEEE Transactions on Control Systems Technology*, vol. 15, pp. 106–116, January 2007.

[6] K. Shin, *Distributed control of tension in multi-span web transport systems.* PhD thesis, Mechanical Aerospace Engineering, Oklahoma State University, Stillwater, 1991.

[7] R. V. Dwivedula, *Modeling the Effects of Belt Compliance, Backlash, and Slip on Web Tension and New Methods for Decentralized Control of Web Processing Lines*. PhD thesis, Mechanical Aerospace Engineering, Oklahoma State University, December 2005.

[8] A. Bowyer and J. R. Woodwark, *A programmer's geometry*. Kent, England: Butterwoths, 1983.

[9] D. Freund, "An interactive procedure for constructing line and circle tangencies," *Computer Graphics and Applications, IEEE*, vol. 6, no. 4, pp. 59 –63, 1986.

[10] L. Parida and P. Koparkar, "A closed form solution to the problem of tangential circles, lines, points with extension to 3d," *Computer & Graphics*, vol. 15, no. 1, pp. 49–55, 1991.

[11] L. Parida and S. Mudur, "Common tangents to planar parametric curves: A geometric solution," *CAD Computer Aided Design*, vol. 27, no. 1, pp. 41 – 47, 1995.

[12] J. Sj*öberg*, Q. Zhang, L. Ljung, A. Benveniste, B. Delyon, P. Y. Glorenned, H. Hjalmarsson, and A. Juditsky, "Nonlinear black-box modeling in system identification: a unified overview," *Automatica*, vol. 31, no. 12, pp. 1691–1724, 1995.

[13] P. Lindskog and L. Ljung, "Tools for semiphysical modeling," *International Journal of Adaptive Control and Signal Processing*, vol. 9, pp. 509–523, Nov. 1995.

[14] Y. Oussar and G. Dreyfus, "How to be a gray box: dynamic semi-physical modeling," *Neural Networks*, vol. 14, no. 9, pp. 1161–1172, 2001.

[15] P. Thomas, *Simulation of Industrial Process for Control Engineers*. Oxford, UK: Butterworth and Heinemann, 1999.

[16] M. H. Butterfield and P. J. Thomas, "Methods of qualitative validation for dynamic simulation model - part 1: Theory," *Transactions of the Institute of Measurement and Control*, vol. 8, pp. 182–200, 1986.

[17] R. G. Cameron, "Model validation by the distortion method: linear state space systems," *IEE Proceedings-D*, vol. 139, pp. 296–300, May 1992.

[18] U. Emborga and C. F. Ross, "Active control in the saab 340," in *Proc. 2nd Conf. Recent Adv. Active Control Sound Vibr.*, pp. S67 –S73, 1993.

[19] R. Shoureshi and T. Knurek, "Automotive applications of a hybrid active noise and vibration control," *IEEE Control Systems*, vol. 16, pp. 72 –78, dec 1996.

[20] L. Eriksson, "A practical system for active attenuation in ducts," *Sound and Vibration*, vol. 22, pp. 30–34, February 1988.

[21] C. de Wit and L. Praly, "Adaptive eccentricity compensation," *IEEE Transactions on Control Systems Technology*, vol. 8, pp. 757 –766, sep 2000.

[22] S. Garimella and K. Srinivasan, "Application of repetitive control to eccentricity compensation in rolling," in *American Control Conference, 1994*, vol. 3, pp. 2904 – 2908 vol.3, june-1 july 1994.

[23] J. Ghosh and B. Paden, "Nonlinear repetitive control," *IEEE Transactions on Automatic Control*, vol. 45, pp. 949 –954, may 2000.

[24] H.-S. Ahn and Y. Chen, "Periodic adaptive learning compensation of state-dependent disturbance," *Control Theory Applications, IET*, vol. 4, pp. 529 –538, april 2010.

[25] R. Ortega, A. Astolfi, and N. E. Barabanov, "Nonlinear pi control of uncertain systems: an alternative to parameter adaptation," *Systems & Control Letters*, vol. 47, no. 3, pp. 259 – 278, 2002.

[26] B. Francis and W. Wonham, "The internal model principle of control theory," *Automatica*, vol. 12, no. 5, pp. 457 – 465, 1976.

[27] D. Chen and B. Paden, "Nonlinear adaptive torque-ripple cancellation for step motors," in *Proceedings of the 29th IEEE Conference on Decision and Control*, pp. 3319 –3324 vol.6, dec 1990.

[28] M. Bodson, A. Sacks, and P. Khosla, "Harmonic generation in adaptive feed-forward cancellation schemes," *IEEE Transactions on Automatic Control*, vol. 39, pp. 1939 –1944, sep 1994.

[29] A. Sacks, M. Bodson, and P. Khosla, "Experimental results of adaptive periodic disturbance cancellation in a high performance magnetic disk drive," *Journal of Dynamic Systems, Measurement, and Control*, vol. 118, no. 3, pp. 416–424, 1996.

[30] M. Bodson, "Rejection of periodic disturbances of unknown and time-varying frequency," *International Journal of Adaptive Control and Signal Processing*, vol. 19, no. 2-3, pp. 67–88, 2005.

[31] Y. Xu, M. de Mathelin, and D. Knittel, "Adaptive rejection of quasi-periodic tension disturbances in the unwinding of a non-circular roll," in *Proceedings of the 2002 American Control Conference*, vol. 5, pp. 4009 – 4014 vol.5, 2002.

[32] S. Pigg and M. Bodson, "Adaptive algorithms for the rejection of sinusoidal disturbances acting on unknown plants," *IEEE Transactions on Control Systems Technology*, vol. 18, pp. 822 –836, july 2010.

[33] M. Bodson, "Effect of the choice of error equation on the robustness property of adaptive control scheme," *International Journal of Adaptive Control and Signal Processing*, vol. 2, pp. 249–257, 1988.

VITA

Carlo Branca

Candidate for the Degree of

Doctor of Philosophy

Thesis: MODELING AND CONTROL OF WEB TRANSPORT IN THE PRESENCE OF NON-IDEAL ROLLERS

Major Field: Mechanical and Aerospace Engineering

Biographical:

Education:

Completed the requirements for the Doctor of Philosophy degree with a major in Mechanical and Aerospace Engineering at Oklahoma State University in May, 2013.

Received the M.S. degree from Oklahoma State University, Stillwater, Oklahoma, USA, 2005, in Electrical Engineering.

Received the Laurea degree from Università degli Studi di Roma "Tor Vergata", Rome, Italy, 2003, in Computer Engineering.

Experience:

Senior Engineer, Bluewater Technology, Stillwater, OK, USA, 2012 to 2013.

Staff Engineer Inter, ARCON Corporation, Waltham, MA, USA, summer 2010.